

REPUBLIQUE ALGERIENNE DEMOCRATIQUE ET POPULAIRE
Ministère de l'Enseignement Supérieur et de la Recherche Scientifique



Université El-Hadj Lakhdar -
BATNA 1



Faculté des Sciences de la
Matière
Département de Physique

Laboratoire d'Etudes Physico-
Chimiques des Matériaux (LEPCM)

THÈSE

En vue de l'obtention du
Diplôme de Doctorat troisième cycle

Présenté par :
Aissam Hidoussi

Thème :

**Calcul Ab-Initio des propriétés thermodynamiques
appliquées à l'établissement des diagrammes de phase à base
de métaux de transition**

Domaine : Sciences de la Matière
Filière : Physique
Spécialité : Physique des matériaux
Intitulé de la Formation : Physique des matériaux métalliques et semi-conducteurs

Soutenue le 18/01/2018

Devant le jury :

Président :	E. Belbacha	Professeur	Université de Batna 1
Rapporteur :	A. Belgacem Bouzida	Professeur	Université de Batna 1
Examineurs :	Y. Djaballah	Professeur	Université de Batna 1
	H. Baaziz	Professeur	Université de M'sila
	Z. Charifi	Professeur	Université de M'sila

PEOPLE'S DEMOCRATIC REPUBLIC OF ALGERIA
Ministry of Higher Education and Scientific Research



University El-Hadj Lakhdar -
BATNA 1



Faculty of Material Sciences

Departement of Physics

Laboratory of Physico-Chemical
Studies of Materials (LEPCM)

THESIS

In order to obtain the
Diploma of Doctorat third cycle

Presented by :

Aissam Hidoussi

Theme :

**Ab-Initio calculation of thermodynamic properties applied
to the assessment of transition metal-based phase diagrams**

Field : Material Sciences
Sector : Physics
Speciality : Materials Physics
Title of Training : Physics of metallic and semiconductor materials

Defended on 01/18/2018

In front of the jury :

President :	E. Belbacha	Professor	University of Batna 1
Supervisor :	A. Belgacem Bouzida	Professor	University of Batna 1
Examiners :	Y. Djaballah	Professor	University of Batna 1
	H. Baaziz	Professor	University of M'sila
	Z. Charifi	Professor	University of M'sila

Abstract

In this thesis, DFT method was used to calculate thermodynamic properties of intermediate phases and compounds in Cd-Sc, Ru-Sc, Os-Th, Os-Y, and Dy-Zn systems which are difficult to be treated experimentally due to high reactivity of its compounds. The PAW method was used to achieve the accuracy of the FP-LAPW method while maintaining the efficiency of the pseudo-potentials. This study was carried out to obtain the structural and energetic properties of the various compounds. The ground state was determined by confirming several phases and discarding others while proposing explanations to several experimental facts. The results obtained are very satisfactory and show very good agreement with the thermodynamic properties obtained from experimental results. Finally, a new CALPHAD modeling is presented taking into account the Ab-Initio results.

ملخص

في هذه الأطروحة، استعملت طريقة المبدأ الأول لحساب الخصائص الترموديناميكية للأطوار الوسيطة و المركبات في الأنظمة Cd-Sc، Ru-Sc، Os-Th، Os-Y، و Dy-Zn التي يصعب دراستها تجريبياً بسبب مركباتها عالية التفاعل. تم استخدام طريقة PAW لتحقيق دقة طريقة FP-LAPW مع الحفاظ على فعالية الكمونات الزائفة. أجريت هذه الدراسة للحصول على الخصائص البنيوية والطاقوية لمختلف المركبات. تم تحديد الحالة الأساسية من خلال تأكيد عدة أطوار وتجاهل البعض الآخر مع اقتراح تفسيرات لعدة حقائق تجريبية. النتائج التي تم الحصول عليها مرضية جداً وتظهر اتفاق جيد جداً مع الخصائص الترموديناميكية التي تم الحصول عليها من النتائج التجريبية. وأخيراً، تم تقديم نمذجة CALPHAD جديدة مع الأخذ بعين الاعتبار لنتائج المبدأ الأول.

Resumé

Dans cette thèse, la méthode DFT a été utilisée pour calculer les propriétés thermodynamiques des phases intermédiaires et des composés dans les systèmes Cd-Sc, Ru-Sc, Os-Th, Os-Y et Dy-Zn qui sont difficiles à traiter expérimentalement en raison de haute réactivité de ses composés. La méthode PAW a été utilisée pour obtenir la précision de la méthode FP-LAPW tout en maintenant l'efficacité des pseudo-potentiels. Cette étude a été réalisée pour obtenir les propriétés structurales et énergétiques des différents composés. L'état fondamental a été déterminé en confirmant plusieurs phases et en rejetant d'autres en proposant des explications à plusieurs faits expérimentaux. Les résultats obtenus sont très satisfaisants et montrent un très bon accord avec les propriétés thermodynamiques obtenues à partir des résultats expérimentaux. Enfin, une nouvelle modélisation CALPHAD est présentée en tenant compte des résultats Ab-Initio.

Keywords: Thermodynamic; Ab-Initio; CdSc; RuSc; Os-Th; Os-Y; Dy-Zn; Phase diagram; CALPHAD;

Publications list

- [1] H. Ghamri, A. B. Bouzida, Y. Djaballah, and A. Hidoussi. Thermodynamic assessment of the ho-te system supported by ab initio calculations. *Journal of Alloys and Compounds*, 552:387 – 391, 2013. doi: 10.1016/j.jallcom.2012.11.084.
- [2] A. Hidoussi, A. B. Belgacem, M. H. Braga, and H. Righi. Theoretical investigation of defect structure in b2 trsc (tr =cd, ru) alloys. *Modern Physics Letters B*, 29(35n36): 1550234, 2015. doi: 10.1142/S0217984915502346.
- [3] Y. Djaballah, A. S. Amer, Ş. Uğur, G. Uğur, A. Hidoussi, and A. B. Bouzida. Thermodynamic description of the bi-cs and bi-tm system supported by first-principles calculations. *Calphad*, 48:72 – 78, 2015. doi: 10.1016/j.calphad.2014.11.002.
- [4] Abdelhak Kerboub, E. Belbacha, A. Hidoussi, Y. Djaballah, and A. B. Belgacem. First-principles calculations of defect structures in b2 alco and gaco. *Journal of Phase Equilibria and Diffusion*, 38(2):143–150, Apr 2017. doi: 10.1007/s11669-017-0526-y.
- [5] A. B. Bouzida, Benhafid R., and A. Hidoussi. Ab-initio calculations and calphad approach for the assessment of the dy-zn system. Poster presented at the 40th conference on phase equilibria JEEP2014, Universite Claude Bernard Lyon 1, Villeurbanne, France, 2014.
- [6] H. Chamri, Y. Djaballah, A. B. Bouzida, and A. Hidoussi. Calphad assessment of the ho-te system focused on non-stoichiometric phase. Poster presented at the World Symposium on Mechatronics Engineering & Applied Physics WSMEAP, Sousse, Tunisia, 2014.
- [7] A. Kerboub, E. Belbacha, A. B. Bouzida, A. Hidoussi, and Y. Djaballah. The effect of excess energy in the simulation of dendritic growth using the phase field model coupled with a calphad database. Poster presented at the 1st International Workshop on the thermodynamics metallic alloys, Batna, Algeria, 2015.
- [8] A. Hidoussi, A. B. Bouzida, F. Tesfaye, and S. Kardellass. Thermodynamic and ab-initio investigations of the os-th and os-y systems. Poster presented at the 145th TMS Annual Meeting & Exhibition, Nashville, TN, USA, 2016.
- [9] A. Hidoussi and A. B. Bouzida. Influence of defects in the formation enthalpy of the intermediate phase rusc from sqs and supercell calculations. Oral presentation at the 3rd International Workshop on the thermodynamics metallic alloys, Batna, Algeria, 2017.

Acknowledgements

All praise is due to Allah, the lord of the worlds. Peace and blessing be upon whom Allah sent as a mercy to the worlds, upon his family, his companions, and his brothers till the day of resurrection. Therefore, I would like to thank God almighty for giving me the strength, knowledge, ability and opportunity to undertake this research study and to persevere and complete it satisfactorily. Without his blessings, this achievement would not have been possible.

First and foremost, I would like to express my sincerest thanks to my supervisor **Mr. Aissa Belgacem Bouzida**, a professor at the University of Batna 1, for his advice and guidance. Without his support and encouragement, it would have been more difficult to complete my research.

I would like to express my profound gratitude to **Mr. Eldjemai Belbacha**, a professor at the University of Batna 1, who accepted the responsibility of being the chairman of the dissertation committee of this thesis.

I also express my gratitude to **Mr. Yassine Djaballah**, a professor at the University of Batna 1, **Mr. Hakim Baaziz**, a professor at the University of M'sila, and **Mme. Zoulikha Charifi**, a professor at the University of M'sila, for accepting the task being reviewers of this thesis.

Finally, I thank all the members of my family, close and distant, who supported me even by an invocation. I would also like to thank all those who contributed to the smooth running of this work.

Contents

Acknowledgements	i
List of Figures	v
List of Tables	vii
Introduction	1
1 From the begining: Ab Initio methods	6
1.1 Ab Initio approach	7
1.1.1 Introduction	7
1.1.2 The many-electron problem	7
1.1.2.1 The Hartree Self Consistent Field (SCF) method	8
1.1.2.2 The Hartree-Fock method	9
1.1.2.3 Slater Determinants	9
1.1.2.4 The Variation Theorem	10
1.1.3 Density Functional Theory (DFT)	12
1.1.3.1 Hohenberg et Kohn Theorem	12
1.1.3.2 Kohn-Sham equation	12
1.1.3.3 Exchange and Correlation Functional	14
1.1.3.4 Local Density Approximation	14
1.1.3.5 Generalized Gradient Approximation	14
1.1.3.6 Calculations in the solid with plane waves	15
1.1.3.7 Stress and Force calculations	16
1.1.4 Utility and physical sense of pseudo-potentials	17
1.1.5 PAW Method	18
1.1.6 Successes and limitations of DFT	20
1.2 Thermodynamic properties from Ab-Initio study	21
1.2.1 Ab-Initio study of thermodynamic properties at absolute temperature	21
1.2.1.1 Formation enthalpy at $0k$	21
1.2.1.2 Special quasi-random structure method (SQS)	21
1.2.1.3 Super-cell method	23
1.2.2 Ab-initio study of thermodynamic properties at finite temperature	23
1.2.2.1 Phonon	23
1.2.2.2 Wagner-Schottky model	24
2 Thermodynamic modelling: CALPHAD method	25
2.1 Thermodynamic modeling of type CALPHAD	26
2.1.1 Introduction	26
2.1.2 Presentation of the CALPHAD method	27

2.1.2.1	Data Selection	29
2.1.2.2	Selection of thermodynamic models	31
2.1.3	Optimization principle	31
2.1.4	Calculation software	31
2.1.5	Procedure for critical evaluation/optimization of systems	34
2.1.6	Conclusion	34
2.2	Thermodynamic models	35
2.2.1	Introduction	35
2.2.2	Thermodynamic description of pure elements	35
2.2.2.1	Magnetic contribution	35
2.2.2.2	Lattice Stability	36
2.2.3	Thermodynamic models used for solutions and compounds	36
2.2.3.1	Gibbs energy Modeling of Gibbs	36
2.2.3.2	Disordered substitutional solutions models	38
2.2.3.3	Ideal Solutions	38
2.2.3.4	Regular and non-regular solutions	39
2.2.3.5	Disordered interstitial solutions models	41
2.2.3.6	Thermodynamic description of stoichiometric compounds	42
2.2.3.7	Ordered phases model; Sublattices model	43
2.2.3.8	Sites fraction defenition	44
2.2.3.9	Molar Gibbs energy	45
2.2.3.10	Special cases	49
2.2.4	Conclusion	49
3	Results and Discussions	50
3.1	Thermodynamics of the intermediate phases in the Tr-Sc systems	51
3.1.1	Introduction	51
3.1.2	Computational methodology	51
3.1.3	Results and discussion	53
3.1.4	Conclusion	58
3.2	The Os-Th and Os-Y systems	60
3.2.1	Introduction	60
3.2.2	Review of literature data	60
3.2.2.1	The binary system Os – Th	60
3.2.2.2	The binary system Os – Y	61
3.2.3	Ab-Initio details	63
3.2.3.1	VASP calculations	63
3.2.3.2	WIEN2k calculations	63
3.2.4	Optimization procedure	64
3.2.5	Results and discussion	64
3.2.6	Conclusion	73
3.3	The Dy-Zn system	74
3.3.1	Introduction	74
3.3.2	Review of literature data	74
3.3.3	Ab initio details	74
3.3.4	Optimization procedure	76
3.3.5	Results and discussion	77
3.3.6	Conclusion	79
	Conclusion	81

Bibliography	83
A List of acronyms	98
B Glossary	100
C List of symbols	101

List of Figures

1	Breakdown of Rare earths (RE) tonnage	4
1.1	Figures (pairs a, triplets b and four sites c)	22
1.2	Representation of a random substitution	22
2.1	Diagram of phases and free energies of Gibbs	27
2.2	Schematic representation of the CALPHAD method	28
2.3	Swedish software usage diagram Thermo-Calc	32
2.4	Gibbs energy of the <i>c.f.</i> reference phase in a A – B binary system.	36
2.5	Molar Gibbs energy of an ideal binary phase α	39
2.6	Molar Gibbs energy of an ideal ternary phase α	40
2.7	Influence of parameter order $\nu L_{A,B}^{\Phi}$ on G.	42
2.8	Centered cubic structure B2 of type <i>CsCl</i>	43
2.9	(figure 2.9a) The space of composition encompassed by the system and (figure 2.9b) the reference Gibbs energy surface described by equation (2.43) from Hillert and Staffansson [100], Hillert [120].	47
3.1	Crystal structures of $Tr_{1-x}Sc_x$	52
3.2	Comparison between first-principles calculated formation enthalpies using supercell and SQS approaches for B2 <i>TrSc</i> as a function of composition[122].	54
3.3	Structural equilibrium of B2 <i>CdSc</i> and <i>RuSc</i> alloys as a function of composition[122].	55
3.4	Equilibrium defect concentrations in B2 <i>CdSc</i> at T = 1428 K as a function of composition[122].	56
3.5	Equilibrium defect concentrations in B2 <i>RuSc</i> at T = 2373 K as a function of composition.	57
3.6	Equilibrium of defect concentration in stoichiometric B2 <i>TrSc</i> as a function of temperature.	59
3.7	Enthalpy of formation of <i>RuSc</i> phase as a function of molar fraction of <i>Sc</i> [122].	59
3.8	Phonon dispersion curves along high symmetry directions and total DOS for Os_2Th	65
3.9	Phonon dispersion curves along high symmetry directions and total DOS for Os_2Y	66
3.10	Phonon dispersion curves along high symmetry directions and total DOS for OsY_3	66
3.11	Calculated phase diagram of the <i>Os–Th</i> system compared with that of Thomson [144], Kleykamp [145].	68
3.12	Calculated phase diagram of the <i>Os–Y</i> system compared with that of Chiotti et al. [153], Savitskii and Polyakova [158].	69
3.13	Standard enthalpies of formation of intermediate phases in the <i>Os–Th</i> system.	70
3.14	Standard enthalpies of formation of intermediate phases in the <i>Os–Y</i> system.	71

3.15 Normalized entropy for the number of moles of atoms for Os_2Th	71
3.16 Normalized entropy for the number of moles of atoms for Os_2Y	72
3.17 Normalized entropy for the number of moles of atoms for OsY_3	72
3.18 Calculated phase diagram of the $Dy-Zn$ system compared with that of Sac- cone et al. [190]	78
3.19 Standard enthalpies of formation of intermediate phases in the $Dy-Zn$ system.	78

List of Tables

3.1	First-principles calculated formation enthalpies of isolated point defects and complex composition-conserving defects in stoichiometric B2 <i>TrSc</i> [122] . . .	53
3.2	The crystal structure data of the <i>Os</i> - <i>Y</i> and <i>Os</i> - <i>Th</i> systems.	62
3.3	The crystal structure data and the enthalpy of formation at 0 K of the Os_2Th_3 compound with the composition 60% at. thorium.	65
3.4	The enthalpies of formation of compounds in the <i>Os</i> - <i>Y</i> and <i>Os</i> - <i>Th</i> systems.	67
3.5	The optimized parameters of <i>Os</i> – <i>Y</i> and <i>Os</i> – <i>Th</i> systems.	68
3.6	The invariant reactions in the <i>Os</i> – <i>Y</i> and <i>Os</i> – <i>Th</i> systems	70
3.7	The crystal structure data of the <i>Dy</i> - <i>Zn</i> system.	75
3.8	The formation enthalpies of the <i>Dy</i> - <i>Zn</i> system compounds.	76
3.9	The optimized parameters of <i>Dy</i> - <i>Zn</i> system.	77
3.10	The invariant reactions in the <i>Dy</i> - <i>Zn</i> systems	79

Introduction

In materials science and many other fields, scientific investigations are carried out according to the two classical axes: (i) theoretical research and (ii) experimental research. Since the appearance of computers and the computing power they offer, a third axis has expanded dramatically; digital modeling allows to describe a real system through mathematical models. The aim is that the description can reproduce the studied properties within the limits of the desired precision, which constitutes a validation of the model. The model which is validated becomes a predictive tool capable of enriching scientific knowledge by providing information that may not be accessible by experience or theory. This enrichment opens the way to other experimental and theoretical investigations that will in turn influence numerical modeling; this indicates the complementarity between the three research axes.

Numerical modeling depends on two limiting factors: the statistical accuracy of the model which makes it possible to judge its domain of reliability, and the efficiency that determines the computing resources required with this model. In other words, the value of a model is determined by the quality of its results and at what price we obtain them.

In the solid state, the origin of the macroscopic properties, in their diversity, lies in the nature of the interactions at the atomic scale, and more precisely, under ordinary conditions, in the behavior of valence electrons. The wavelengths of the order of interatomic distances which imposes a purely quantum processing characterize the wave nature, this is why modeling on this scale will quickly find its limits as long as the problem of electronic structure does not consider the framework of quantum mechanics. So, formally, the electron structure of a system of atomic nuclei with their electrons is obtained by passing through the solution of the Schrödinger equation. Unfortunately, the exact analytical solution is known only for the hydrogen atom with a single electron, and already for helium with two electrons, there is no analytical solution, this is called the n-body problem. Schrödinger equation solution, $\Psi(r_1, r_2, \dots, r_n, t)$ is function of $3n$ variables which represent the coordinates of each electron plus the time variable. If we consider a wave function of a single electron, which is defined over the whole space, we would need, for a mathematical description, a discretization that requires m points. For two electrons the discretization requires m^2 points and for n electrons m^n points, a figure that quickly becomes astronomical, indeed, even a digital solution quickly becomes prohibitive. It is evident that this difficulty is due to the fact that the fundamental magnitude in the Schrödinger equation is the wave function; The framework of the [Density Functional Theory \(DFT\)](#) largely avoid this difficulty, which is a reformulation of quantum mechanics. It is clear that the electron density of the ground state is an equally fundamental quantity as the wave function and whose determination is possible. In principle, to determine all the properties of the studied system, there is no need to find the n-body wave function. We replace the problem by finding the electron density of the ground state which represents a scalar field that can be discretized as a function of only four variables: x , y , z and t ; Which is an obvious advantage from the digital point of view. It is a great simplification of the n-

body problem which has made it possible in our days to make high-quality calculations starting only from the atomic number of a system; This is called [Ab Initio](#).

From a thermodynamic point of view, the topology of a phase diagram is entirely determined by energy considerations. More specifically, when the variables considered are temperature and pressure, the Gibbs, $G = U + PV - TS$ free energy governs the stability of the phase. A stable phase is the result of the minimization of its energy. Therefore, it is the free energy of Gibbs which ultimately determines the phase diagram by process of minimization at constant temperature and pressure. So, the [Ab Initio](#) calculations naturally find their place in the determination of phase diagrams by allowing the evaluation of the free energy of Gibbs under well-defined conditions.

The most straightforward case is where the temperature and pressure are zero with a fixed composition. The internal energy $G = U$ confound with the free energy of Gibbs where it is directly accessible by the [Ab Initio](#) calculations if we neglect the residual vibrations at 0K. In practice, it is possible to obtain the equilibrium volume of a phase by minimizing this energy concerning the volume. The difference between the energies evaluated to the minimum for each phase determines the relative stability of these two phases. The most stable phase is that which ensures the minimum energy. The introduction of the pressure adds the term PV , and G becomes confounded with the enthalpy $G = H = U + PV$. Nature favors the phases which reduce the volume by increasing the pressure, so it becomes possible to reverse the relative stability between two phases by increasing the pressure. The effect of temperature introduces the term $-TS$ which favors the phases that show the most disorder (which have a higher entropy). Among the different forms that disorder can take in a system are the vibrations of atoms that deviate from their positions of equilibrium.

Phase diagrams have always been an essential source of information for the development and design of new materials; this has led to considerable improvements in experimental techniques which have now reached a very high level of accuracy. However, considering the increasing demands of high-tech materials that are very complex, it is crucial that theoretical predictions guide the experimental work. Such a possibility is to apply the principles of physical-chemistry to calculate the polyphase equilibria of multiconstituted systems. Such an approach proves to be very powerful in defining experimentations, which are expensive and can also reduce the number of experiments. The use of numerical modeling is the approach that addresses the current need to characterize complex thermodynamic systems; it has been made possible by developments in computing and by the development of thermodynamic computing software.

Literature Review

Among the materials that have found remarkable development and progress over the last few years are the magnetic materials based on [Transition metal \(TM\)](#). These compounds form a wide range of materials which are used in the field of permanent magnets of high performance.

The origin of these exceptional magnetic properties is due mainly to the coexistence of two parallel types of magnetism: the itinerant magnetic magnetism of the electrons $3d$ of the [TM](#) such as Iron and Nickel and the localized magnetism characteristic of the electrons $4f$ of the [RE](#). In this way, the crystals are strongly anisotropic due to the interactions between their orbital moment and the crystalline field. The $3d$ metals provide high magnetization and a high Curie temperature (higher than 350 – 500°C), thanks to the critical interactions between the elements $3d$. The combination of the two magnetic behaviors

of the elements $3d$ and $4f$ may lead to compounds which exhibit exceptional permanent magnet properties. The atomic radius of the RE elements is much higher than that of the TM which is favorable to the formation of a series of intermetallic compounds of which the most interesting crystallize in a hexagonal or rhombohedral structure and where such magnetic compounds may exhibit exceptional permanent magnet properties [1].

The RE represent the group of lanthanides (Elements with atomic numbers between 57 and 71, lanthanum to lutetium), to which yttrium (Y) and Scandium (Sc) are added due to similar chemical properties (same column of the periodic table). We distinguish the ceric earths (Lanthane (La), Cerium (Ce), praseodymium (Pr), neodymium (Nd) and Samarium (Sm)) and heavier earth (The other RE). The RE forms the largest group of elements with a consistent chemical behavior [2] due to their electronic configuration. Throughout the lanthanide series, from La (atomic number 57) to Lu (atomic number 71), electrons are added to the internal electron layer $4f$ rather than to an outer layer. The electrons $4f$ are thus protected by the electrons in the outer layers $5s$ and $5p$ and consequently, do not participate in the chemical bonds. Because of this shielding, the ionic radius of RE decreases progressively with increasing atomic number (from $102 \mu\text{m}$ for (La) to $86 \mu\text{m}$ for (Lu)), an effect known under Name of "contraction of the lanthanides" [3]. In the last fifteen years, RE have become indispensable to the development of high-tech products that are critical for energy or military applications [4–7]. Initially, they were a tiny market, but the development of clean technologies in the 1990s, initiated by developed countries, led to an explosion of demand (metal alloys for batteries, permanent magnets for wind turbines, Luminophores for low energy lighting) [4, 8–11]. In 2011, China abruptly reduced its export quotas, replacing the Chinese industry with a brutal but rather late stage of China's monopoly position (It provides 97%) [12]. Beijing, which has in fact measured the danger of the environmental damage created by their intensive extraction, also wishes to find external supplies. Also, it wants to take advantage of its organic growth to ensure the supply of the best-finished products in its market, and definitively take a position as a world leader in clean technology products. Such as electric vehicles (magnets NdFeB with composition $\text{Nd}_2\text{Fe}_{14}\text{B}$), hybrid vehicles (Nickel Metal Hydride batteries NiMH), wind turbines (magnets NdFeB), and low energy fluorescent bulbs (Yttrium, Europium, and Terbium). Many other products which contain RE-based components such as jet aircraft, military equipment, pollution control of combustion engines, medical imaging, radiotherapy and other electrical or electronic equipment such as ceramic capacitors, superconductors, computers and smartphones [13–15] (see figure 1).

The compounds RE-TM have found a remarkable and numerous studies, either for a practical purpose such as the improvement of the magnetic properties [17–20], or from a more fundamental point of view such as the determination of the existing compounds, their stability domains and their crystallographic structures in order to deepen the understanding of the magnetism of these compounds [21, 22]. The most studied properties are, for example, the exchange interactions [23–27], the magnetocrystalline anisotropy [28]. These compounds are in particular good candidates for the appearance of a perpendicular anisotropy, highly sought for increasing the storage density in magnetic recording systems.

The recycling of RE metals from permanent magnet waste becomes inevitable to maintain a balance between supply and demand. Since the process of recycling magnetic materials has not established yet, fundamental research on the thermodynamic behavior of RE magnetic materials and on the chemical reactions between magnetic materials and the solvent medium is essential to understand and improve the recycling process of RE.

In this perspective, a modern approach lies in the use of the phase diagram calcula-

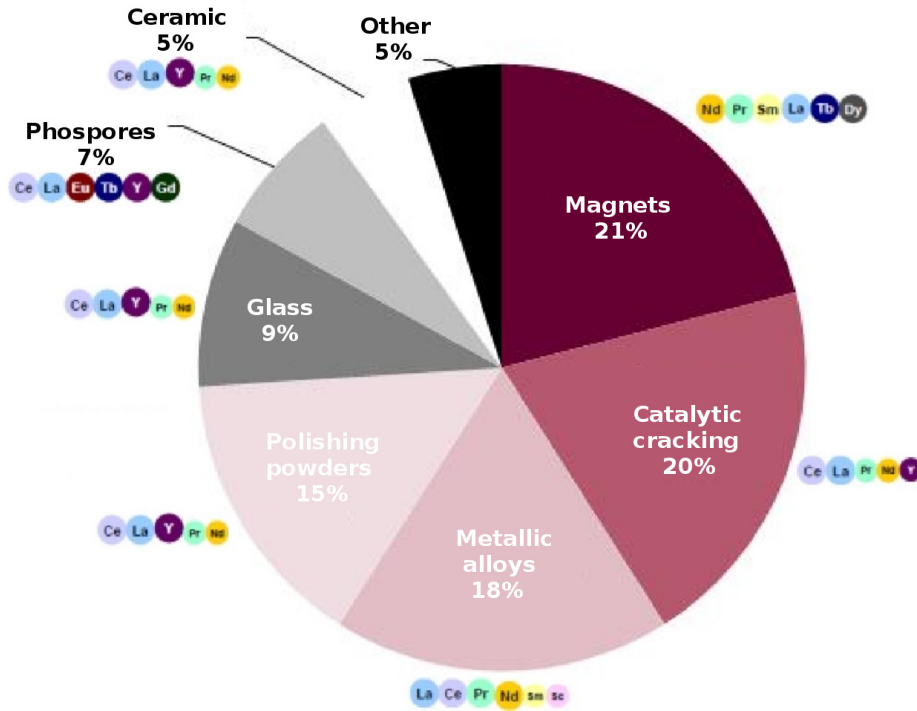


Figure 1 – Breakdown of RE tonnage used in their main applications [16].

tion method [CALPHAD](#) [29]. To design an efficient recycling process for the alloys of RE and TM, we need to develop a thermodynamic database containing the model parameters which describe the thermodynamic properties of the phases involved as a function of temperature and the composition. The thermodynamic database with Gibbs free energy minimization software such as [Thermo-Calc](#) [30] through the [PARROT](#) [31] module will help us in the processing of the phases and the proposed variables, which are otherwise obtained by trial and experiment representing a substantial investment in money and time. The word software suggests that the computation is self-sufficient, whereas the determination of complex equilibria requires constant assistance from a competent thermodynamicist, to avoid this nuance, one speaks of computer-aided computing [32].

Aims and Objectives of the Work

Our work aims at calculating thermodynamic properties for compounds and phases of the five binary systems $Cd - Sc$, $Ru - Sc$, $Os - Y$, $Os - Th$, and $Dy - Zn$ using the [Ab Initio](#) methods. These results and all available thermodynamic data and phase diagrams for the $Os - Y$, $Os - Th$, and $Dy - Zn$ binary systems will be evaluated critically, where Gibbs free energies of all phases will be represented by the appropriate model equations. The parameters of these models will be obtained by an optimization procedure using the Swedish software [Thermo-Calc](#). The prepared database of thermodynamic properties in this work can be integrated with other binary and multi-component systems to provide a complete multi-component database for transition metals.

In this work, structural and thermodynamic properties of alloys of the transition metal system were calculated using the [Special Quasirandom Structure \(SQS\)](#) and the Super-cell approaches along with density functional theory. [Local Density Functional \(LDA\)](#) and [Generalized Gradient Approximation \(GGA\)](#) were also used to investigate formation en-

ergy of transition metal alloys and their vibrational properties. This work was carried out by the assessment of the transition metal phase diagrams using the obtained properties from *Ab Initio* calculations. The primary objectives of performing this study are as follows:

- * To investigate the structural and defect structure and defect formation enthalpy of transition metal alloys using *SQS* and super-cell approaches along with density functional theory (*DFT*) at absolute temperature.

- * To study the structural and defect structure of transition metal alloys using Schottky model.

- * To study the structural, formation energy, and vibrational properties of transition metal alloys using density functional theory (*DFT*).

- * To assess the phase diagrams of transition metal using *CALPHAD* method and obtained results from *Ab Initio* calculations.

Outline of Thesis

In addition to this general introduction which discussed the inspirations and motivations to perform the current study of transition metal materials, the structure of this thesis consists of three chapters, briefly described below, followed by a general conclusion.

The first chapter (1) presents the *DFT* approach, used for the calculations of thermodynamic properties. The presentation of the principles and the calculation software that was used for the calculation of properties of our systems are presented.

The second chapter (2) presents the *CALPHAD* approach, used for the modeling of phase diagrams. The presentation of the principle and the calculation software that was used for the modeling of our systems are presented and gives a detailed account of the different thermodynamic models of which we were interested in during the optimization of the various phases of the considered systems in the framework of this thesis.

Finally, in the third chapter (3) we presented and discussed the results of *Ab Initio* calculations of defects enthalpies of intermetallic compounds in the binary systems based on *Sc*: *Sc-TM* ($TM = Cd, Ru$) using the *SQS* and supercell methods. Also, the third chapter (3) deals in detail with thermodynamic calculations of the phase diagrams of the binary systems: *Os-Y*, *Os-Th*, and *Dy-Zn* based on the realized *Ab Initio* calculations during this work.

The main results proposed in this manuscript are summarized and discussed in conclusion.

Chapter 1

From the beginning: Ab Initio methods

Contents

1.1 Ab Initio approach	7
1.1.1 Introduction	7
1.1.2 The many-electron problem	7
1.1.2.1 The Hartree SCF method	8
1.1.2.2 The Hartree-Fock method	9
1.1.2.3 Slater Determinants	9
1.1.2.4 The Variation Theorem	10
1.1.3 Density Functional Theory (DFT)	12
1.1.3.1 Hohenberg et Kohn Theorem	12
1.1.3.2 Kohn-Sham equation	12
1.1.3.3 Exchange and Correlation Functional	14
1.1.3.4 Local Density Approximation	14
1.1.3.5 Generalized Gradient Approximation	14
1.1.3.6 Calculations in the solid with plane waves	15
1.1.3.7 Stress and Force calculations	16
1.1.4 Utility and physical sense of pseudo-potentials	17
1.1.5 PAW Method	18
1.1.6 Successes and limitations of DFT	20
1.2 Thermodynamic properties from Ab-Initio study	21
1.2.1 Ab-Initio study of thermodynamic properties at absolute temperature	21
1.2.1.1 Formation enthalpy at $0k$	21
1.2.1.2 Special quasi-random structure method (SQS)	21
1.2.1.3 Super-cell method	23
1.2.2 Ab-initio study of thermodynamic properties at finite temperature	23
1.2.2.1 Phonon	23
1.2.2.2 Wagner-Schottky model	24

1.1 Ab Initio approach

1.1.1 Introduction

Classical mechanics failed to predict experiments on atomic and molecular phenomena; black body radiation, the photoelectric effect, radioactivity, relativity, the nuclear atom, the Bohr atom, the wave mechanical atom [33]. Quantum mechanics which incorporates the wave-particle duality can explain previous phenomena and deal with small systems.

The term **Ab Initio** refers to a family of theoretical concepts and computational methods that treat the many-electron problem from the beginning [34]. In other words, **Ab Initio** calculations rest on solving the Schroedinger equation using the principles of quantum mechanics and not using empirical or other extrapolated information, interpolated or transferred from other systems (adjustable variables) [35].

The primary uses of the **Ab Initio** methods are calculations of molecular geometries, energies, vibrational frequencies, spectra, ionization energies, etc. Among these methods, **DFT** is based on the two Hohenberg-Kohn theorems, which state that the electron density determines the ground state properties of a molecule. Nowadays, **DFT** calculations have become one of the leading computational methods in computational physics and physical-chemistry due to their high degree of accuracy without the use of any fitting parameters. Interest has been growing in the engineering disciplines to exploit these properties to predict new materials with desired material properties, significantly accelerate the prototyping of materials over experimental methods with a degree of accuracy which is not available in other computational methods [36–39].

1.1.2 The many-electron problem

The corresponding time-independent **Schrödinger** equation for a non-relativistic many-body of an atomic, molecular or solid system comprising M atoms and N electrons will be:

$$\hat{H}\Psi(\{r\}, \{R\}) = E\Psi(\{r\}, \{R\}) \quad (1.1)$$

$\{r\} = \{r_1, r_2, \dots, r_N\}$ et $\{R\} = \{R_1, R_2, \dots, R_M\}$ are the position vectors of the nuclei and electrons (nuclear and electronic degrees of freedom), respectively; \hat{H} is the exact many-electron Hamiltonian:

$$\hat{H} = \hat{T}_N + \hat{T}_e + \hat{V}_{e-e} + \hat{V}_{N-N} + \hat{V}_{e-N} \quad (1.2)$$

The terms denote (in atomic units):

$$\hat{T}_N = -\frac{1}{2} \sum_i^M \frac{\nabla_i^2}{M_i} \quad \text{kinetic nuclear energies} \quad (1.3)$$

$$\hat{T}_e = -\frac{1}{2} \sum_i^N \nabla_i^2 \quad \text{kinetic electronic energies} \quad (1.4)$$

$$\hat{V}_{e-e} = \frac{1}{2} \sum_{i<j}^N \frac{1}{|r_i - r_j|} \quad \text{electron-electron repulsions} \quad (1.5)$$

$$\hat{V}_{N-N} = \frac{1}{2} \sum_{i<j}^M \frac{Z_i Z_j}{|R_i - R_j|} \quad \text{nucleus-nucleus repulsions} \quad (1.6)$$

$$\hat{V}_{e-N} = - \sum_i^N \sum_j^M \frac{Z_j}{|r_i - R_j|} \quad \text{attractive electron-nucleus interactions} \quad (1.7)$$

Whereas the **Schrödinger** equation for a hydrogen atom can be solved exactly, an exact solution is not possible for any molecule because the simplest molecule consists of three particles (two nuclei and one electron). The nuclei mass exceeds that of electrons by a factor of one thousand or more, and their movements are slow relatively and may be treated as stationary while the electrons move in their field [40]. Therefore, **Born-Oppenheimer** proposed an approximation ([41]) to neglect the coupling between the nuclei and electronic motion. This allows the electronic part to be solved with the nuclear positions as parameters, and the resulting **Potential energy surface (PES)** forms the basis for solving the nuclear motion. The major computational effort is in solving the electronic **Schrödinger** equation for a given set of nuclear coordinates [41], where equations (1.1) and (1.2) become:

$$\hat{H}_e \psi_e(\{r\}) = E_e \psi_e(\{r\}) \quad (1.8)$$

$$\hat{H}_n \Psi(\{R\}) = E \Psi(\{R\}) \quad (1.9)$$

$$\hat{H}_e = \hat{T}_e + \hat{V}_{e-e} + \hat{V}_{N-N} + \hat{V}_{e-N} \quad (1.10)$$

$$\hat{H}_n = \hat{T}_N + E_e(\{R\}) \quad (1.11)$$

In order to determine the corresponding (ground-state) many-electron wave-function $\psi(\{r\}, \{m\})$, where $\{m\} = \{m_1, m_2, \dots, m_N\}$ stands for a set of electronic spin variables, which is the solution of a **Schrödinger** equation with the Hamiltonian of equation (1.8), one usually falls back on a related variational principle [34, 42]:

$$E_0(\{R\}) = \min_{\psi(\{r\}, \{m\})} E(\{R\}) = \min_{\psi(\{r\}, \{m\})} \frac{\langle \psi(\{r\}, \{m\}) | \hat{H}_e | \psi(\{r\}, \{m\}) \rangle}{\langle \psi(\{r\}, \{m\}) | \psi(\{r\}, \{m\}) \rangle} \quad (1.12)$$

In general, the resulting electronic wave-function $\psi(\{r\}, \{m\})$ will be some approximation to the real antisymmetric wave-function of the corresponding many-electron system. The art of **Ab Initio** will simply consist of finding ingenious ways to numerically determine an approximate wave-functions [34].

1.1.2.1 The Hartree SCF method

Hartree's method ([43, 44]) was to write a plausible approximate polyelectronic wave-function for an atom as the product of one-electron wave-functions:

$$\Psi_0(\{r\}) = \prod_i^N \psi_0(r_i) \quad (1.13)$$

This function is called a **Hartree** product. Here $\psi_0(r)$ is a function of the coordinates of all the electrons in the atom, $\psi_0(r_i)$ is a function of the coordinates of electron i . The one-electron functions $\psi_0(r_i)$ where i is a range from 1 to N , are called atomic orbitals (molecular orbitals if we were dealing with a molecule). The initial guess, ψ_0 , is the initial approximation to be refined with the **Hartree** process for k cycles till we have a wave-function ψ_k and/or an energy calculated from ψ_k that are essentially the same (according to some reasonable criterion) as the wave-function and/or energy from the previous cycle. This happens when the new one-electron wave-functions are identical with the old ones, where the the electron-electron potential has (essentially) ceased to change, so the fields of cycle k and previous cycle $k - 1$ are consistent, and so the **Hartree** procedure is called the **SCF** procedure [35].

The problem with **Hartree** product of equation (1.13) is that doesn't respect Pauli exclusion principle; the **Hartree** product is symmetric, where the theory with the results of experiment predictions show that electronic wave-functions are actually antisymmetric with respect to exchange [35, 41]:

$$\Psi(r_1, r_2, \dots, r_j, \dots, r_k, \dots, r_n) = -\Psi(r_1, r_2, \dots, r_k, \dots, r_j, \dots, r_n) \quad (1.14)$$

1.1.2.2 The Hartree-Fock method

The symmetry of the **Hartree** product was corrected by **Pauling** (1928) and **Slater** (1929). **Pauling** and **Slater** showed that as a first approximation at least a wavefunction can be written as a determinant of spin orbitals. Although **Slater's** publication appeared in the year after **Pauling's**, this determinant is called a **Slater** determinant [35].

1.1.2.3 Slater Determinants

The **Hartree** wavefunction is product of one-electron functions called spatial orbitals, where the **Slater** wavefunction is composed of spin orbitals, not just of spatial orbitals. A spin orbital $\psi(\textit{spin})$ is the product of a spatial orbital and a spin function (α or β). Unlike most other functions, α or β have only one eigenvalue, which are $\frac{1}{2}(\hbar/2\pi)$ or $-\frac{1}{2}(\hbar/2\pi)$, respectively, associated with the spin operator \hat{S}_z , and have as their variables a spin coordinate, sometimes denoted ξ or ω , their peculiar property is zero unless $\xi = 1/2$ (α spin function) or $\xi = -1/2$ (β spin function). The delta function is a function that is zero everywhere except at one value of its variable (invented by **Dirac**) [35].

Suppose we wish to write a **Slater** determinant for a N -electron closed-shell system. We need v spatial molecular orbitals ($N = 2 \times v$), since each can hold a maximum of two electrons; each spatial orbital $\psi(\textit{spatial})$ is used to make two spin orbitals, $\psi(\textit{spatial})\alpha$ and $\psi(\textit{spatial})\beta$. Along the first (top) row of a determinant we write successively the first α spin orbital, the first β spin orbital, the second α spin orbital, the second β spin orbital, ... up to, the v -th α spin orbital, and the v -th β spin orbital, using up our occupied spatial (and thus spin) orbitals. Electron one is then assigned to all N spin orbitals of the first row—in a sense it is allowed to roam among these N spin orbitals. The second row of the determinant is the same as the first, except that it refers to electron two rather than electron one; likewise the third, ... and N rows refer to electrons three, ... and N , respectively. The result is the determinant of equation (1.15):

$$\psi_0(\{r\}) = \frac{1}{\sqrt{N!}} \begin{vmatrix} \psi_1(r_1)\alpha(r_1) & \psi_1(r_1)\beta(r_1) & \cdots & \psi_v(r_1)\alpha(r_1) & \psi_v(r_1)\beta(r_1) \\ \psi_1(r_2)\alpha(r_2) & \psi_1(r_2)\beta(r_2) & \cdots & \psi_v(r_2)\alpha(r_2) & \psi_v(r_2)\beta(r_2) \\ \vdots & \vdots & \ddots & \vdots & \vdots \\ \psi_1(r_N)\alpha(r_N) & \psi_1(r_N)\beta(r_N) & \cdots & \psi_v(r_N)\alpha(r_N) & \psi_v(r_N)\beta(r_N) \end{vmatrix} \quad (1.15)$$

The $1/\sqrt{N!}$ factor ensures that the wavefunction is normalized. This **Slater** determinant ensures that there are no more than two electrons in each spatial orbital, since for each spatial orbital there are only two one-electron spin functions, and it ensures that ψ is antisymmetric (equation (1.14)) since switching two electrons amounts to exchanging two rows of the determinant, and this changes its sign. Note that instead of putting the electrons successively to rows, we could have placed them in columns: ψ'_0 of equation (1.16) = ψ_0 of equation (1.15). Some authors use the row format for the electrons, others the column format [35]:

$$\psi'_0(\{r\}) = \frac{1}{\sqrt{N!}} \begin{vmatrix} \psi_1(r_1)\alpha(r_1) & \psi_1(r_2)\alpha(r_2) & \cdots & \psi_1(r_N)\alpha(r_N) \\ \psi_1(r_1)\beta(r_1) & \psi_1(r_2)\beta(r_2) & \cdots & \psi_1(r_N)\beta(r_N) \\ \vdots & \vdots & \ddots & \vdots \\ \psi_v(r_1)\alpha(r_1) & \psi_v(r_2)\alpha(r_2) & \cdots & \psi_v(r_N)\alpha(r_N) \\ \psi_v(r_1)\beta(r_1) & \psi_v(r_2)\beta(r_2) & \cdots & \psi_v(r_N)\beta(r_N) \end{vmatrix} \quad (1.16)$$

1.1.2.4 The Variation Theorem

The molecular energy is expressed by the **Hartree-Fock** in terms of the total wavefunction ψ , and to be minimized with respect to each of spin orbitals $\psi\alpha$ and $\psi\beta$ (equation (1.12)). The derivation of these equations needs considerable algebraic manipulation which have been summarized by A and Beveridge [45], Pople and Nesbet [46], and Lowe [47].

From the **Schrödinger** equation, energy of a system is given by:

$$E = \frac{\int \psi^* \hat{H} \psi d\tau}{\int \psi^* \psi d\tau} = \frac{\langle \psi | \hat{H} | \psi \rangle}{\langle \psi | \psi \rangle} \quad (1.17)$$

ψ^* is the wavefunction complex conjugate, which ensures that E , the energy of the molecule, will be real. If ψ is complex then $\psi^2 d\tau$ will not be a real number, while $\psi^* \psi d\tau = |\psi|^2 d\tau$ will. Integration is with respect to spatial and spin coordinates ($d\tau = dx dy dz d\xi$). Using a normalized wavefunction, equation (1.17) can be written as:

$$E = \int \psi^* \hat{H} \psi d\tau = \langle \psi | \hat{H} | \psi \rangle \quad (1.18)$$

Substituting **Slater** determinant in equation (1.15) for ψ (and ψ^*) and explicit expression for the electronic Hamiltonian into equation (1.18), using a closed-shell system with $N = 2 \times v$ electrons and M atomic nuclei (the M th nucleus has charge Z_M) gives:

$$E = 2 \sum_{i=1}^v H_{ii} + \sum_{i=1}^v \sum_{j=1}^v (2J_{ij} - K_{ij}) \quad (1.19)$$

for the electronic energy of a N -electron molecule. The terms in equation (1.19) have these meanings:

$$H_{ii} = \int \psi_i^*(r) \hat{H}^{core}(r) \psi_i(r) dr \quad (1.20)$$

where

$$\hat{H}^{core}(r) = -\frac{1}{2}\nabla_r^2 - \sum_{j=1}^M \frac{Z_j}{|r - R_j|} \quad (1.21)$$

The operator \hat{H}^{core} is so called because it leads to H_{ii} , the electronic energy of a single electron (r) moving simply under the attraction of a nuclear "core", with all the other electrons stripped away. $\hat{H}^{core}(r)$ represents the kinetic energy of electron (r) plus the potential energy of attraction of that electron to each of the nuclei M . The integration in equation (1.20) is respect to spatial coordinates only ($dr = dx dy dz$, not $d\tau$) [35].

$$J_{ij} = \int \psi_i^*(r_1)\psi_i(r_1) \left(\frac{1}{|r_1 - r_2|} \right) \psi_j^*(r_2)\psi_j(r_2) dr_1 dr_2 \quad (1.22)$$

J is called a Coulomb integral; it represents the electrostatic repulsion between an electron in ψ_i and one in ψ_j ; J and K integrals allow each electron to experience the average electrostatic repulsion of a charge cloud due to all the other electrons [35].

$$K_{ij} = \int \psi_i^*(r_1)\psi_j^*(r_2) \left(\frac{1}{|r_1 - r_2|} \right) \psi_i(r_2)\psi_j(r_1) dr_1 dr_2 \quad (1.23)$$

K is called an exchange integral; mathematically, it arises from Slater determinant expansion terms that differ only in exchange of electrons. The K integral can be regarded as a kind of correction to J [35].

The energy calculated from equation (1.18) is the expectation value of the energy operator \hat{H} . Of course, this energy will be the exact (true energy of the molecule) only if the wavefunction ψ and the Hamiltonian \hat{H} are exact; unfortunately, they are not. The variation theorem states that:

Theorem 1 *The energy calculated from equation (1.18) must be greater than or equal to the true ground-state energy of the molecule [35].*

The variation theorem assures us that any ground state energy we calculate "variationally" must be greater than or equal to the real energy of the molecule (the lower, the better).

The variational principle, again, allows us to obtain the equations of Hartree-Fock:

$$\left[-\frac{1}{2}\nabla_i^2 - \sum_j \frac{Z_j}{|r_i - R_j|} + \sum_{\mu} \int |\psi_{\mu}(r_j)|^2 \frac{dr_j}{|r_i - r_j|} \right] \psi_{\lambda}(r_i) - \sum_{\mu} \left[\int \psi_{\mu}^*(r_j) \frac{1}{|r_i - r_j|} \psi_{\lambda}(r_j) dr_j \right] \psi_{\mu}(r_i) = E \psi_{\lambda}(r_i) \quad (1.24)$$

We can see a term (third term) similar to the term obtained in the formulation of Hartree which represents the electrostatic interaction of the electron with the mean field of electron density. The fourth term is a new purely quantum term that stems directly from the antisymmetry constraint (Pauli's exclusion principle). A final term, however, remains missing in this approximation: it is the correlation between the electrons. Indeed, in this description, the free electron which feels only the average electrostatic field of the other electrons misses the correlation between the electrons which makes each electron tend to remain as far as possible from the other electrons individually. Noting, finally, that the method of Hartree-Fock quickly becomes prohibitive when the number of electrons increases which limits its use in physics of the solid.

1.1.3 Density Functional Theory (DFT)

1.1.3.1 Hohenberg et Kohn Theorem

The Hohenberg-Kohn [48] theorems relate to any system consisting of N electrons moving under the influence of an external potential v_{ext} . Stated simply they are as follows:

Theorem 2 *The external potential v_{ext} , and hence the total energy, is a unique functional of the electron density $n_0(r)$.*

The energy functional $E[n(\mathbf{r})]$ alluded to in the first Hohenberg-Kohn theorem can be written in terms of the external potential $n_0(r)$ in the following way,

$$\begin{aligned} E[n(r)] &= \langle \Psi | \hat{H} | \Psi \rangle \\ &= \langle \Psi | \hat{T}_e + \hat{V}_{e-e} + v_{ext} | \Psi \rangle \\ &= F[n(r)] + \int v_{ext} n(r) dr \end{aligned} \quad (1.25)$$

$$F[n(r)] = \langle \Psi | \hat{T}_e + \hat{V}_{e-e} | \Psi \rangle \quad (1.26)$$

where \hat{H} is the system hamiltonien, $F[n(r)]$ is the electronic Hamiltonian consisting of a kinetic energy operator \hat{T}_e and an interaction operator \hat{V}_{e-e} ,

The electron operator $F[n(r)]$ is the same for all N -electron systems, so \hat{H} is completely defined by the number of electrons N , and the external potential v_{ext} . The ground-state density uniquely determines the external potential v_{ext} , to within an additive constant. Stated simply, the electrons determine the positions of the nuclei in a system, and also all ground state electronic properties, because as mentioned earlier, v_{ext} and N completely define \hat{H} .

Theorem 3 *The ground state energy can be obtained variationally: the density that minimises the total energy is the exact groundstate density.*

Any density $n(r)$ that is not that of the ground state will always give an energy greater than the energy corresponding to the density of the ground state:

$$E[n(r)] > E[n_0(r)] \quad (1.27)$$

The Hohenberg-Kohn theorems do not offer a way of solving the Schrödinger equation. About one year after the original DFT paper by Hohenberg and Kohn, Kohn and Sham [49] devised a simple method for carrying-out DFT calculations, which retains the exact nature of DFT. The next section describes this technique.

1.1.3.2 Kohn-Sham equation

So far the theory is formally exact, the only problem is that the universal functional is unknown; to try to exploit these two theorems, Kohn and Sham [49] proposed to replace the external electrons-potential system by another system of fictitious electrons which are free electrons under the action of a potential of Kohn-Sham. The condition being that the charge density of the ground state of the new system must be the same as that of the real system. The main feature of the Kohn-Sham equation is that the electrons are independent, and the electron-electron interaction of the real system is replaced by

an effective potential. For this, the universal functional in Kohn-Sham system can be decomposed as follows:

$$\begin{aligned}
 F[n(r)] &= T[n(r)] + E_H[n(r)] + E_{xc}[n(r)] \\
 &= \sum_{i=1}^N -\frac{1}{2} \int \Psi_i^*(r) \nabla_i^2 \Psi_i(r) dr + \frac{1}{2} \int \int \frac{n(r_1)n(r_2)}{|r_1-r_2|} dr_1 dr_2 + E_{xc}[n(r)] \quad (1.28)
 \end{aligned}$$

The first term $T[n(r)]$ is the kinetic energy of the Kohn-Sham electrons. The second term is the classic Colombian contribution which is the sum of the Coulomb interactions of the charge density of the infinitesimal volume at the point r_1 and the charge density at the point r_2 , It is the energy of Hartree E_H . These two contributions can be calculated exactly for the Kohn-Sham electrons which are independent. The last contribution in this functional is $E_{xc}[n(r)]$ remains unknown and should be processed approximately. It encompasses all the complexity of the n-body problem. It counts the energy of exchange and correlation and another part which is the difference between the kinetic energy of the real system and that of the free electrons. The interesting point is that it is relatively small compared to the other terms, which means that much of the physics of the system is already taken into account in the first terms which explain the great success of this approach.

The second theorem gives us a variational principle to minimize the functional energy (equation (1.28)) under the constraint of a determined number of electrons. The Lagrange multiplier method gives:

$$\begin{aligned}
 &\delta \left[E[n(r)] - \epsilon \left(\int n(r) dr - N \right) \right] = 0 \\
 \Rightarrow &\delta \left[F[n(r)] + \int v_{ext} n(r) dr - \epsilon \left(\int n(r) dr - N \right) \right] = 0 \quad (1.29) \\
 \Rightarrow &\frac{\delta F[n(r)]}{\delta n(r)} + v_{ext}(r) = \frac{\delta T[n(r)]}{\delta n(r)} + v_{KS}(r) = \epsilon
 \end{aligned}$$

where $v_{KS}(r)$ is the Kohn-Sham potential which takes the following form:

$$v_{KS}(r) = v_{ext}(r) + \int \frac{n(r')}{|r-r'|} dr' + v_{xc}(r) \quad v_{xc}(r) = \frac{\delta E_{xc}[n(r)]}{\delta n(r)} \quad (1.30)$$

This result is identical to the equation obtained for an electron in an effective potential $v_{eff}(r)$:

$$\frac{\delta T[n(r)]}{\delta n(r)} + v_{eff}(r) = \epsilon \quad (1.31)$$

The problem is reduced to solving N equations similar to the Schrödinger equation of an electron in an effective Kohn-Sham potential:

$$\left[-\frac{1}{2} \nabla_i^2 + v_{KS}(r) \right] \Psi^{(i)}(r) = \epsilon_i \Psi^{(i)}(r) \quad \text{et} \quad n(r) = \sum_i \left| \Psi^{(i)}(r) \right|^2 \quad (1.32)$$

As in the Hartree approach, the $\Psi^{(j)}(r)$ solution for the j particle depends on the effective potential $v_{KS}(r)$ which depends on the density of this $\Psi^{(j)}(r)$ orbit and all other $\Psi^{(i)}(r)$ orbitals at the same time. The solution depends on the actual potential, and the effective potential depends on the solution. It is a self-consistent problem in which, once

solved, the effective potential used to solve the equations is equal to the effective potential obtained by the solution. In practice, the solution is obtained after several iterations, starting with an initial density which is modified during the iterations until the self-consistency is reached.

1.1.3.3 Exchange and Correlation Functional

To do the computation, we now need an approximation for the $V_{xc}(r)$ exchange and correlation term, is the last term for which we do not know any expression as a function of density or orbital. Finding the precise approximation for the exchange and correlation is still valid, and we present here only the standard functionals, which have already been widely used [39].

1.1.3.4 Local Density Approximation

The most common approximation to calculate the term of exchange and correlation is **LDA**. This approximation assumes that the density fluctuates quite slowly. It replaces the potential of exchange and correlation at each point of space by that of a regular gas of interacting electrons. The electron gas is taken at the same density as the density at the calculated position; this makes it possible to give an exact expression by interpolating Monte-Carlo calculations, and it was done at the beginning of the 80 [50]. The **LDA** is often an efficient approximation, even when the density fluctuates non-negligibly. However, there are some particular disadvantages, such as a systematic underestimation of the cohesion energy of the solids and the mesh parameters [51, 52]. The error on the structural parameters is often low (on the order of 1 to 2 %), but can become significant when Van der Waals type bindings are in account [39].

The system energy is the sum of the energies of these calculated points of space:

$$E_{xc}^{\text{LDA}}[n(r)] = \int n(r) \epsilon_{xc}(r) dr \quad (1.33)$$

$\epsilon_{xc}(r)$ Being the exchange and correlation energy of a free electron gas whose density is equal to the charge density $n(r)$ on point r .

The approximation of the local density **LDA** is the most important and indeed most used approximation to solve the problem of the functional correlation exchange. The approximation **LDA** completely ignores the exchange-correlation corrections to be performed when the electronic density is no longer locally homogeneous. However, the **LDA** is particularly useful and its application to atoms and molecules is justified by the success of these digital applications [53].

1.1.3.5 Generalized Gradient Approximation

The most natural way to improve **LDA** is to take into account the inhomogeneity of the electron density by introducing terms which depend on the gradient of the density into the exchange and correlation energy. The **GGA** [54] introduces a combination of local terms and gradient-dependent terms. It gives good results and makes it possible to improve the cohesive energies and the mesh parameters. However, the improvement over **LDA** is not always systematic because **GGA** sometimes overcorrects the **LDA** [55, 56]. Therefore, in the results section of this thesis, we have systematically compared the relative stabilities of the phases as well as the elastic constants obtained in **GGA** and **LDA** [39].

The energy is calculated by considering the gradient of the density:

$$E_{xc}^{GGA}[n(r)] = \int f_{xc}(n(r), \nabla n(r)) dr \quad (1.34)$$

1.1.3.6 Calculations in the solid with plane waves

We have an approximation allowing us to calculate the total energy of a system using the Kohn and Sham approach of the DFT and note that the Kohn-Sham Hamiltonian has the network periodicity of Bravais lattice. The Bloch theorem then allows us to look for the eigenvectors in the form of a plane wave multiplied by a function which has the periodicity of the Bravais lattice:

$$\psi_k(r) = e^{ik \cdot r} u_k(r) \quad \text{avec} \quad u_k(r + R) = u_k(r) \quad (1.35)$$

If one replaces this form of the wave equation in one of the Kohn-Sham equation (1.32), an equation for the periodic part is obtained for each vector Of wave k [57]:

$$\left[-\frac{1}{2} (\nabla_i + ik)^2 + v_{KS}(r) \right] u_k(r) = \epsilon_k u_k(r) \quad (1.36)$$

This last equation is an eigenvalue equation but with the advantage that $u_k(r)$ has the network periodicity and it becomes possible to restrict the study on a mesh instead of working on the whole crystal. This periodicity constraint allows us to expect a quantization of the eigenvalues ϵ_{nk} . In the equation (1.36), it can be seen that the wave vector k occurs parametrically; a continuous variation of k should produce continuous variation of the energies ϵ_{nk} to give a set of functions $\epsilon_n(k)$, each of which describes the variation of an energetic level as a function of k . This spreading of each energy level constitutes a band of energy.

Strictly, the vector k is a continuous variable and takes all possible values in C^3 . However, the mathematical trick of periodic boundary conditions gives us the possibility of discretizing this variable and constraining it to real values. The periodic boundary conditions consist in imposing on the eigenvectors to be periodic on a crystal composed of N_1, N_2 and N_3 meshes in the directions of the vectors of the primitive mesh a_1, a_2 and a_3 respectively. This is written:

$$\psi_{nk}(r + N_i a_i) = \psi_{nk}(r) \quad (1.37)$$

By replacing equation (1.35) in this last equation we find:

$$e^{iN_i k \cdot a_i} = 1 \quad (1.38)$$

The projection of k on the vectors of the primitive lattice of the reciprocal lattice b_i allows us to write $k = \sum_i x_i b_i$, knowing that $b_i \cdot a_i = 2\pi \delta_{ij}$, we obtain:

$$e^{2\pi i N_i x_i} = 1 \quad (1.39)$$

This requires:

$$x_i = \frac{m_i}{N_i} \quad \text{avec} \quad m_i \quad \text{entier} \quad (1.40)$$

The wave vector k will then have real and discrete components and take the form:

$$k = \sum_i \frac{m_i}{N_i} b_i \quad (1.41)$$

This result shows that each vector k corresponds to a volume in the reciprocal space:

$$\delta V = \frac{1}{N} b_1 \cdot (b_2 \times b_3) \quad (1.42)$$

$N = N_1 N_2 N_3$ is the number of meshes in the crystal and $b_1 \cdot (b_2 \times b_3)$ is the volume of the primitive cell in the reciprocal lattice; this means that the number of vectors k in the primitive mesh of the reciprocal lattice is the number of meshes in the crystal. By increasing the size of the crystal, the discrete values of the components of k become increasingly close to one another. They tend to the limit of the continuous values when the crystal size tends to the ideal crystal (which is infinite); this means that the choice of periodic boundary conditions should not matter when the crystal is large enough.

While the wave vector k can take an infinity of values in \mathbb{R}^3 , under the constraint (equation (1.42)), it is possible to restrict the study to the first zone of Brillouin which is the mesh of Wigner-Seitz in the reciprocal network. Indeed, any vector k' which is not in the first Brillouin zone can always be written as the sum of a vector G of the reciprocal lattice and a vector k in the first Brillouin zone $k' = k + G$. We can then write:

$$\psi_{k'}(r) = e^{i(k+G)\cdot r} u_{k'}(r) = e^{ik\cdot r} \left[e^{iG\cdot r} u_{k'}(r) \right] \quad (1.43)$$

But $u(r) = e^{iG\cdot r} u_{k'}(r)$ has the periodicity of the Bravais lattice, exploiting the relation-ship which define The reciprocal lattice $e^{iG\cdot R} = 1$, one can write:

$$u(r + R) = e^{iG\cdot(r+R)} u_{k'}(r + R) = e^{iG\cdot R} u(r + R) = u(r) \quad (1.44)$$

The wave function corresponding to k' can always be brought to a wave function with the wave vector k by multiplying the part which has the periodicity of the Bravais lattice by the factor $e^{iG\cdot r}$. So all the information is already present in the first zone of Brillouin, and it is sufficient to restrict the problem to this zone. In practice, the wave vectors in the first Brillouin zone are discretized according to a given sampling scheme with a given point density. The higher the dot density is, the closer it gets to the ideal crystal and the more accurate the results. A convergence study is then necessary to obtain the best possible compromise between points density in the Brillouin zone and the precision of the calculation, or the standard way to choose the plane wave base is to consider all plane waves, Kinetic energy is less than a certain limit, the cut-off energy:

$$K^2 + G^2 \leq E_{cutoff} \quad (1.45)$$

So to get a complete base, it is enough to increase E_{cutoff} ; this is one of the great forces of wave-plane methods because it allows us to reduce the study of the convergence of the base to the variation of a single parameter [39].

1.1.3.7 Stress and Force calculations

With energy, we have access to an essential set of physical properties, such as equilibrium mesh parameters, which minimize energy, equations of state, or relative energy between different phases.

The stress tensor and the forces exerted on the atoms are also deduced from the total energy by:

$$\sigma_{ij} = \frac{1}{V_0} \left(\frac{\partial E}{\partial \epsilon_{ij}} \right) \quad (1.46)$$

$$F_i^\alpha = \frac{\partial E}{\partial \omega_i^\alpha} \quad (1.47)$$

Where i and j are the cartesian indices, σ_{ij} is a component of the stress tensor, ϵ_{ij} is a component of the strain tensor, F_i^α is a component of the vector of the force exerted on the atom α , and ω_i^α a component of the vector of the position of the atom α ; definitions are extended in section 1.2.

1.1.4 Utility and physical sense of pseudo-potentials

The idea of using pseudopotentials stems first from the observation that the free electron models (Drude) give mostly reasonably good descriptions of the metal properties [58]. Even if the potential being affected by electrons in metal consists of a superposition of atomic potentials; which assume large values in the vicinity of the nucleus. The real potential is therefore very far from the practically constant potential implied by the Drude model. This paradox is solved by introducing the concept of valence electrons and electrons. Core electrons closely related to the nucleus are barely affected by the chemical environment of the atom and describe very efficiently the potential created by the nucleus. This concept is not limited to metals but is generalized to all materials. The minerals also have the additional feature that the description of the valence electrons of the nucleus and the core electrons is very efficient, so the valence electrons have a much less kinetic attraction.

Therefore, it is the valence electrons that mainly determine the properties of materials by forming chemical bonds and by delocalizing in the solid. The interaction of the valence electrons with the set nucleus and core electrons can then be described by an effective potential, much less attractive than the potential created by the nucleus. This effective potential is in our case approached by a pseudopotential.

Since valence electrons behave practically as free electrons, at least in metal, and a solid is modeled by a periodic arrangement of atoms, the natural basis for making the numerical calculations is the plane wave base [58]. However, in the region near the nucleus, the valence states cannot be close to a plane wave. Indeed, the valence states are orthogonal to the core states and therefore have many zeros also called nodes. These fast oscillations require a massive number of plane waves to be able correctly represented and consequently a very long computation time.

To avoid this problem, the valence wave functions and the potential are then softened in the region near the nucleus. The model then loses its relevance in this area. However, an astute construction of the pseudopotential makes it possible to conserve the more significant part of the information as soon as one moves away from the region of core [59].

For the pseudopotential to be interesting to use, it must be transferable. That is, once created in a given chemical environment, usually the isolated atom, it must be able to provide accurate calculations for other chemical environments, such as the solid. Thus, the pseudopotential can be generated in a simple configuration and then transferring it into much more complex arrangements. The pseudopotential makes it possible to reduce the number of electrons to be taken into account in the calculation and also to reduce the number of plane waves necessary for describing the wave functions of the solid.

1.1.5 PAW Method

Projected-Augmented Wave (PAW) is a very practical and very popular approach to solving the Kohn-Sham equations is to express the wave functions $|\psi\rangle$ as a linear combination of waves Planes $|\phi_n\rangle$:

$$|\psi\rangle = \sum_n C_n |\phi_n\rangle \quad (1.48)$$

This choice is based in the fact that the wave functions in a solid are delocalized, and their decomposition in plane waves is perfectly adapted, in the sense that a delocalized function requires only a very restricted number of waves Planes to be expressed with great precision. Another advantage is the simplicity of the analytical calculation with plane waves (for example the Laplacian and gradient evaluation). Thus, the Kohn-Sham equation is written:

$$\sum_n C_n \hat{H} |\phi_n\rangle = \sum_n E C_n |\phi_n\rangle \quad (1.49)$$

By multiplying the equation by $\langle\phi_m|$ and exploiting the orthogonality of plane waves, the Kohn-Sham equation becomes:

$$\sum_n C_n \langle\phi_m | \hat{H} | \phi_n\rangle = E C_m \quad (1.50)$$

$\langle\phi_m | \hat{H} | \phi_n\rangle$ matrix elements being known, the problem is reduced to solve a simple linear equation system where solution determines the coefficients c_n .

On the other hand, on the other hand, the difficulty facing the plane waves is that the wave functions of the valence electrons in a solid have a completely different signature in the zone where the chemical bond is formed and the zone Surrounding the core. In the chemical bonding zone the wave function is delocalized, but around the nucleus, it oscillates strongly to ensure orthogonality with the wave functions of the core electrons that are localized. The description of these strong variations around the nucleus requires a large number of plane waves; this is a major disadvantage. To solve this problem, the PAW method proposed by Blöchl [60] defines a spherical augmentation region around the ions in which plane waves are augmented by localized functions. These augmented functions allow us to define a linear inversion T which connects the real wave function $|\psi\rangle$ to a wave pseudo-function $|\tilde{\psi}\rangle$:

$$|\psi\rangle = T |\tilde{\psi}\rangle \quad (1.51)$$

An important property is that the pseudo-function $|\tilde{\psi}\rangle$ does not have the expensive oscillations inside the spherical augmentations, it is a soft function. But externally it is identical to $|\psi\rangle$. It is then possible to make less costly calculations with the $|\tilde{\psi}\rangle$ function and to go back to the real wave function through the transformation T. This transformation must modify $|\tilde{\psi}\rangle$ only within the spherical augmentations, which leads us to express it as an $|\tilde{\psi}\rangle$ and $|\psi\rangle$ being identical outside the spheres) plus a sum of localized contributions in the spheres:

$$T = I + \sum_R S_R \quad (1.52)$$

Where S_R is a local term defined for each sphere R which adds to $|\tilde{\psi}\rangle$ the contribution necessary to get $|\psi\rangle$. Inside each sphere we define a base composed of the partial functions $|\phi_i\rangle$, these functions are generally chosen as the solution of the equation

of [Schrödinger](#) of isolated atom. For each partial function, partial pseudo-functions are defined $|\tilde{\phi}_i\rangle$ which must be soft but join the partial functions $|\phi_i\rangle$ to the limit of the spherical augmentation. If we define the operator S_R in a sphere R :

$$S_R |\tilde{\phi}_i\rangle = |\phi_i\rangle - |\tilde{\phi}_i\rangle \quad (1.53)$$

We can then write:

$$\begin{aligned} |\phi_i\rangle &= |\tilde{\phi}_i\rangle + |\phi_i\rangle - |\tilde{\phi}_i\rangle \\ &= |\tilde{\phi}_i\rangle + S_R |\tilde{\phi}_i\rangle \\ &= (I + S_R) |\tilde{\phi}_i\rangle \end{aligned} \quad (1.54)$$

On the other hand, if the base $|\tilde{\phi}_i\rangle$ is complete, we can write in each sphere:

$$|\tilde{\psi}\rangle = \sum_i c_i |\tilde{\phi}_i\rangle \quad (1.55)$$

The coefficients c_i can be determined by defining the projector functions $|\tilde{p}_i\rangle$ which satisfy $\langle \tilde{p}_i | \tilde{\phi}_i \rangle = \delta_{ij}$ which gives $I = \sum_i |\tilde{\phi}_i\rangle \langle \tilde{p}_i|$ and let us write:

$$\begin{aligned} |\tilde{\psi}\rangle &= \sum_i |\tilde{\phi}_i\rangle \langle \tilde{p}_i | \tilde{\psi} \rangle \\ S_R |\tilde{\psi}\rangle &= \sum_i S_R |\tilde{\phi}_i\rangle \langle \tilde{p}_i | \tilde{\psi} \rangle \\ &= \sum_i (|\phi_i\rangle - |\tilde{\phi}_i\rangle) \langle \tilde{p}_i | \tilde{\psi} \rangle \end{aligned} \quad (1.56)$$

The index i notes the functions in the same sphere. The equations (1.52) and (1.56) give us the transformation T as follows:

$$T = I + \sum_i (|\phi_i\rangle - |\tilde{\phi}_i\rangle) \langle \tilde{p}_i| \quad (1.57)$$

And the real function $|\psi\rangle$ is obtained from the pseudo-function $|\tilde{\psi}\rangle$ by:

$$|\psi\rangle = |\tilde{\psi}\rangle + \sum_i (|\phi_i\rangle - |\tilde{\phi}_i\rangle) \langle \tilde{p}_i | \tilde{\psi} \rangle \quad (1.58)$$

The i index traces the functions in all spheres. The other approximation used in the [PAW](#) method is frozen core approximation [61]. In this approximation, it is considered that the configuration of the core electrons, strongly linked to the nucleus, is independent of the environment of the atom and remains frozen when passing from a free atom to a solid, for example. The electronic structure is rearranged essentially at the level of the valence electrons. The wave functions of the electrons of the core are very localized, in contrast to the wave functions of the valence electrons which are extended. In the passage from a free atom to a solid, the overlap between the wave functions of the valence electrons is considerable while it is negligible for the electrons of the core, which leaves them practically unchanged. As a consequence, the electron energy and electron density of the core in the solid and the isolated atom can be expected to be identical; this greatly reduces the computing effort that focuses on valence electrons.

1.1.6 Successes and limitations of DFT

DFT is often able to obtain, at lower cost, results with a precision close to that obtained from the post *Hartree-Fock* calculations. Also, it can be used to study relatively large systems, contain up to several hundred electrons, which the post-*Hartree-Fock* calculations can not process; this explains why DFT is now widely used to study the properties of molecular or even biological systems, sometimes in combination with conventional methods.

Many works carried out in the last few years show that the DFT calculations give good results on very diverse systems (metallic, ionic, organometallic, etc.) for many properties (molecular structures, vibration frequencies, Ionization, etc.).

However, these methods still suffer from several defects. On the other hand, the good or bad results of the DFT on some systems are not always understood and there are no real criteria to chose a functional rather than another. It is also challenging to find approaches to improve a given functional, which sometimes makes the use of DFT difficult.

1.2 Thermodynamic properties from Ab-Initio study

1.2.1 Ab-Initio study of thermodynamic properties at absolute temperature

1.2.1.1 Formation enthalpy at 0K

The energy of formation at $T = 0K$ (which also corresponds to the enthalpy of formation) for the binary compound A_xB_y is obtained by the equation:

$$\Delta E(A_xB_y) = E(A_xB_y) - xE(A) - yE(B) \quad (1.59)$$

where $E(A_xB_y)$, $E(A)$, and $E(B)$ are the total energy for A_xB_y , pure elements at [Stable Element Reference \(SER\)](#) (A and B) at $T = 0K$, respectively.

1.2.1.2 Special quasi-random structure method (SQS)

The random structures of an alloy $A_{1-x}B_x$ are usually generated by random pulling. Each lattice site has the probability $1 - x$ to be occupied by an atom A and x to be held by an atom B. There is a method for generating structures closer to the utterly random structures [62]. To do this, we need to define correlation functions.

A σ configuration is discretized into interactions figures $f = (k, m)$ of k neighboring m^e sites. On each site i , the occupancy variable \hat{S}_i takes the value $-1(+1)$ if the site is occupied by the species A(B). For a perfectly random $A_{1-x}B_x$ solid solution, the correlation function for the f figure is:

$$\langle \overline{\Pi}_f \rangle_{aléatoire} = \langle \overline{\Pi}_{k,m} \rangle_{aléatoire} \quad (1.60)$$

$$= \langle \hat{S}_i \rangle^k \quad (1.61)$$

$$= [(+1)(x) + (-1)(1-x)]^k \quad (1.62)$$

$$= (2x - 1)^k \quad (1.63)$$

The principle of [SQS](#) is to construct a configuration such that its $\langle \overline{\Pi}_{k,m} \rangle_{SQS}$ correlation function tends to the correlation function of the perfect random solution $\langle \overline{\Pi}_{k,m} \rangle_{aléatoire}$ for the maximum number of figures f :

$$\langle \overline{\Pi}_{k,m} \rangle_{SQS} \cong \langle \overline{\Pi}_{k,m} \rangle_{aléatoire} \quad (1.64)$$

Practically, we generate a large number of concentration structures x where their correlation functions $\overline{\Pi}_{k,m}$ are calculated. The arrangement with the correlation functions closest to the correlation function in the equation (1.63) of an entirely random solid solution is then selected.

To analyze the substitutional disorder of an alloy $AB_{1-x}C_x$ it is necessary to construct a super-cell which naturally includes the random alloy statistic. Such a supercell must contain all the first neighboring polyhedra according to their percentages of occurrence. The large size required for such a cell does not make it possible to be treated by [DFT Ab Initio](#). To avoid this pitfall, Zunger et al. [62], Wei et al. [63], Lu et al. [64, 65] and Ruban et al. [66] proposed a super-cell determination method that simulates the statistical characteristics of a random alloy with controlled accuracy. The method is called [SQS](#).

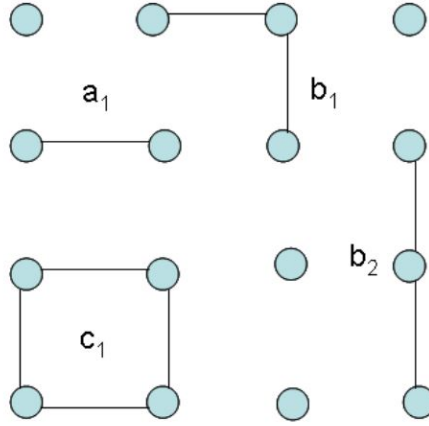


Figure 1.1 – Figures (pairs a, triplets b and four sites c) in a two-dimensional lattice.

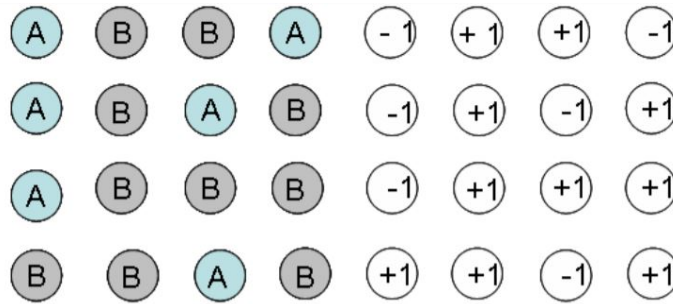


Figure 1.2 – Representation of a random substitution of an alloy A_xB_{1-x} .

In the SQS method we define geometrical figures that connect the sites of the occupation of the atoms. The figures are associated with the occupation sites according to their symmetry ranging from the simplest figures formed by a single site, a pair of atoms, a three-body figure to the polyhedra defined by a growing number of sites (see figure 1.1). The figures are defined by two indices: an index k which represents the number of sites in the figure and an index m which specifies the distance between the sites (or bodies). Each site i is assigned a pseudo-variable of spin S_i : example $S_i = -1(+1)$ if an atom A(B) occupies the site i - see the figure 1.2.

One type of figure $F(k, m)$ is characterized by its correlation function $\prod_{k,m}$ obtained by taking the product of the spin variables on all the sites of the figure and averaging on All the figures of equivalent symmetry. For a perfect random alloy, the pair and multisite functions satisfy the relation [62–65]:

$$\left\langle \prod_k \right\rangle \approx \left(\prod_{k,m} \right)_{\text{SQS}} \quad (1.65)$$

$(\prod_{k,m})_{\text{SQS}}$ Represents the correlation function associated with the $F(k, m)$ figures of the supercell. When an alloy is described by super-cells of finite size which repeat periodically; non-existent or erroneous correlations are introduced beyond a certain distance. However, since interactions between close neighbors are more important than those between more distant neighbors, we can construct SQS structures that exactly reproduce the functions of a random alloy between the nearest neighbors. It is trivial that the smaller the number of atoms minus the correlation functions that correspond to the perfect alloy.

1.2.1.3 Super-cell method

The supercell approach has been widely used in the literature to study defects in materials [67, 68]. Such an approach is usually carried out by introducing one defect in a given supercell to study the point defects regarding first-principles calculations. In the present work, we have used two supercells; a 16-atom $2 \times 2 \times 2$ cubic B2 and a 32-atom one [69], each one contains one single point defect (*Tr* vacancy, *Sc* vacancy, *Tr* anti-site, or *Sc* anti-site) per supercell. In the 16-atom supercell, the periodically arranged point defects form a simple-cubic SC lattice with a lattice parameter of $2a$, while the point defects in the 32-atom supercell form a face-centred-cubic FCC lattice with a lattice parameter of $4a$, where a is the B2 lattice parameter.

The formation enthalpies of point defects in the supercell approach are obtained by means of finite differencing, as follows [70]:

$$H_d = \frac{\partial H_d}{\partial v_d} \approx \frac{\Delta H_d - \Delta H_{TrSc}}{v_d} \quad (1.66)$$

where ΔH_d is the formation enthalpy per atom of a 16-atom (32-atom) B2 *TrSc* supercell containing one point defect of type d and ΔH_{TrSc} is the formation enthalpy of ordered B2 *TrSc* ($Tr = Cd, Ru$), and v_d is the atomic concentration of defect d . For the 16-atom supercell, we have $v_d = 1/16$ for anti-sites and $v_d = 1/15$ for vacancies, and for the 32-atom supercell, we have $v_d = 1/32$ for anti-sites and $v_d = 1/31$ for vacancies.

1.2.2 Ab-initio study of thermodynamic properties at finite temperature

1.2.2.1 Phonon

In the harmonic approximation, phonons are considered as independent of each other. However, the vibrations of a real crystal are not purely harmonic, meaning that the concept of independent phonons breaks down. This section covers the ab initio methods to calculate the phonon characteristics. The partition functions of statistical physics enable calculation of the Gibbs energy of the system. The harmonic approximation is used in the evaluation of the vibrational Gibbs energy.

The total potential of the crystal can be written concerning the inter-atomic potentials assuming multi-body interactions over the sums of two-body terms. Here we will consider two-body interactions only. If an atom whose equilibrium position at lattice site R moves a small distance $u(R)$, its new position is given by:

$$r(R) = R + u(R) \quad (1.67)$$

If the contribution to the total potential of the crystal, U , from two atoms at position R and is given by the potential can be written as [58];

$$U = \frac{1}{2} \sum_{RR'} \phi(R - R' + u(R) - u(R')) \quad (1.68)$$

Expanding the above relation about the equilibrium position as a three-dimensional Taylor series we get:

$$U_{harm} = \frac{1}{2} \sum_{\substack{RR' \\ \mu\nu}} u_{\mu}(R) f_{\mu\nu}(R - R') u_{\nu}(R') \quad (1.69)$$

Where $f_{\mu\nu}$ is the force constant matrix which, for pair potentials, can be written as:

$$f_{\mu\nu}(\mathbf{R} - \mathbf{R}') = \delta_{\mathbf{R}\mathbf{R}'} \sum_{\mathbf{R}''} [\phi_{\mu\nu}(\mathbf{R} - \mathbf{R}'') - \phi_{\mu\nu}(\mathbf{R} - \mathbf{R}')] \quad (1.70)$$

The finite displacement phonon calculations were carried out to calculate the vibrational properties of optimized structures [71] after performing the geometry optimization. In a finite displacement calculation, each atom is displaced by a small amount along the Cartesian direction; then a self-consistent field calculation is carried out to evaluate the forces on the perturbed system. Both positive and negative displacements are applied in each direction so that corresponding force constants can be calculated using the central force differences. Using the harmonic approximation; vibrational frequencies can be evaluated from the force constants. The number of computed spectra is $3N$, where N is the number of atoms in the unit cell. As, there is three center of mass translations along the x , y and z directions, there are, in total, $3N-3$ modes of vibration.

To construct the dynamical matrix, set of rules should be fulfilled [72]. The force constants can be used in Equation 1.69 to get the potential energy.

The displacement of atoms to calculate the force constant destroys the periodic boundary conditions. To treat this problem in practical terms; a supercell is chosen, which consists of a considerable number of primitive cells such that interaction of an atom outside this cell with the displaced atom in the primitive central cell can be regarded as being negligible. The accuracy of phonon calculation depends upon the size of the supercell. By using a massive supercell in force calculations, we can include more inter-atomic interactions and reduce the error in this interaction cut-off approximation.

1.2.2.2 Wagner-Schottky model

Thermodynamic models used to calculate equilibrium point defect concentrations in oxide materials, in general, are often based on the law of mass action. In this formalism, originally developed by Wagner and Schottky [73] using the Kröger and Vink formalism [74], the mass-action type equations describing equilibria between electronic and ionic defects are written under the assumption that defects are noninteracting and infinitely diluted. With this approximation defect activities are simply expressed regarding defect concentrations. To complete the model; electroneutrality and site conservation equations on both sublattices are added. The success of this theory is however mitigated by some important shortcomings [75, 76]:

- The mass action law assumes defects as non-interacting species. However in oxide systems defects are usually charged and as a result subject to long-range Coulomb interactions.
- Because the mass action law generally assumes infinite dilution, the configurational entropy contribution of the different defects in the Gibbs Gibbs energy of the system reduces to site fractions (i.e., the probability that an anion or cation site is occupied by a defect of a particular anionic or cationic type). However, for high defect concentrations, defects are no longer statistically uncorrelated because the presence of a defect excludes others from sharing the same region in the lattice; this is known as the site exclusion effect and becomes increasingly relevant as the defect concentration in the material rises (high deviations from stoichiometry).

Chapter 2

Thermodynamic modelling: CALPHAD method

Contents

2.1 Thermodynamic modeling of type CALPHAD	26
2.1.1 Introduction	26
2.1.2 Presentation of the CALPHAD method	27
2.1.2.1 Data Selection	29
2.1.2.2 Selection of thermodynamic models	31
2.1.3 Optimization principle	31
2.1.4 Calculation software	31
2.1.5 Procedure for critical evaluation/optimization of systems	34
2.1.6 Conclusion	34
2.2 Thermodynamic models	35
2.2.1 Introduction	35
2.2.2 Thermodynamic description of pure elements	35
2.2.2.1 Magnetic contribution	35
2.2.2.2 Lattice Stability	36
2.2.3 Thermodynamic models used for solutions and compounds	36
2.2.3.1 Gibbs energy Modeling of Gibbs	36
2.2.3.2 Disordered substitutional solutions models	38
2.2.3.3 Ideal Solutions	38
2.2.3.4 Regular and non-regular solutions	39
2.2.3.5 Disordered interstitial solutions models	41
2.2.3.6 Thermodynamic description of stoichiometric compounds	42
2.2.3.7 Ordered phases model; Sublattices model	43
2.2.3.8 Sites fraction defenition	44
2.2.3.9 Molar Gibbs energy	45
2.2.3.10 Special cases	49
2.2.4 Conclusion	49

2.1 Thermodynamic modeling of type CALPHAD

2.1.1 Introduction

The term **CALPHAD** is an acronym for "CALculation of PHase Diagram". The abbreviation **CALPHAD** also designates a scientific journal and an annual international conference to optimize software and databases to improve understanding of several thermodynamic-dependent physical system characteristics (species distribution, geochemistry, Cement, etc.). **CALPHAD** is a method for obtaining a mathematical description of a phase diagram and the thermodynamic data that are related to this diagram. This modeling focuses on the evaluation of the fundamental quantity which is the Gibbs energy of Gibbs G of the different phases of a system (pure element, binary system, ternary system, ...) and its evolution as a function of temperature, concentration, and pressure.

From a thermodynamic point of view, the topology of a phase diagram is completely determined by energy considerations. More specifically, when the variables considered are temperature and pressure, it is the Gibbs energy of Gibbs, $G = U + P \times V - T \times S$, which governs the stability of a phase. A stable phase is the result of the minimization of this energy. It is, therefore, the Gibbs energy of Gibbs which completely determines the phase diagram by process of minimization at constant temperature and pressure. Once the Gibbs free energies are determined, it is possible to know the phases present in the system and their proportions under the desired conditions by minimizing the Gibbs energy of the system. The minimization of Gibbs free energy is a considerable advantage since a good description makes it possible to obtain, by interpolation or extrapolation, essential information which can be very difficult or impossible to obtain experimentally; this is particularly true when it comes to the complex systems commonly found in the industry that can easily contain a dozen elements.

In practice, to describe the Gibbs energy of Gibbs G , a mathematical parametric model is assigned to each of the phases in the system. The parameters of each model are then optimized to reproduce the phase diagram and the thermodynamic data of the system by minimizing the Gibbs energy of Gibbs of the whole system. The calculation then consists in conducting a least squares fit which reduces the quadratic errors concerning the available data. In this case, the **CALPHAD** method is a semi-empirical method. It offers numerous advantages such as the rationalization of an experimental plan (limitation of the number of experiments and their costs), the study of multi-constituted systems by extrapolation of simple subsystems, but also the simplicity of calculating isothermal or isopleths sections. The outcome of the optimization gives us a set of mutually consistent data.

The **CALPHAD** method, which prevails in this field and is used in the laboratory, was introduced by Kaufman and Bernstein [29]. It is very well described in many books such as Saunders and Miodownik [77] and Lukas et al. [78]. In this paper, there is a lot of information about this, from the basics of thermodynamics to a concrete example of modeling. Note that the history of the **CALPHAD** method is published by Spencer [79] in a recent article.

The aim of this chapter is not to establish a state of the art of this method but rather to give the principle and to present the software of calculation that was used for the modeling of our systems.

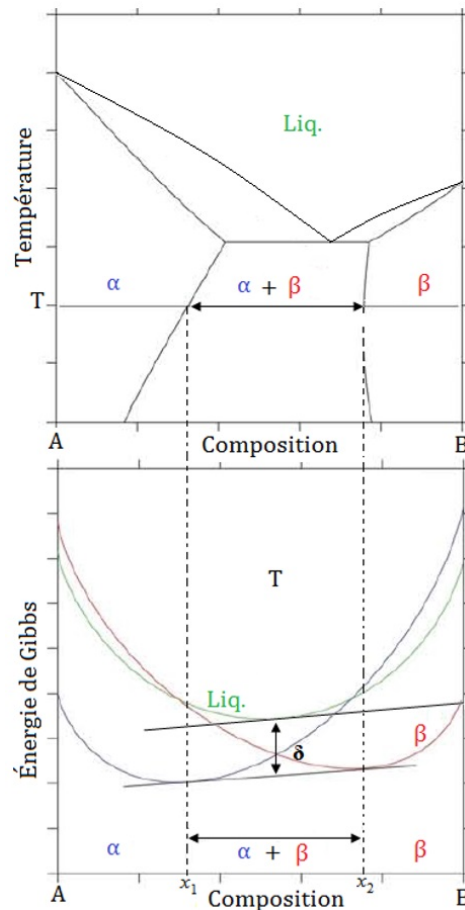


Figure 2.1 – Phase diagram (with eutectic reaction) and Gibbs free energies.

2.1.2 Presentation of the CALPHAD method

The thermodynamic characterization of a system comes down to the study of potential functions of the different phases of this system. The free enthalpy G is the essential thermodynamic function in thermochemistry since it plays the role of potential when the pressure (P), the temperature (T), and the composition (number of moles n_i of each constituent i) are the control variables of the system. The determination of the equilibria between phases is done by minimizing the free enthalpy of the polyphase system as illustrated by Figure 2.1.

At the temperature T , the primary solid solution α is stable at 0 at. % B up to composition x_1 . Then, the two phases α and β are in equilibrium up to x_2 . Beyond x_2 , the primary solid solution β is stable. These stability domains are due to the minimization of the free enthalpy of the system on the composition domain at the temperature T . In each rich zone in A or B, it is respectively the free enthalpy of the α or β phase which is the lowest which corresponds to the stability of the relevant primary solid solution. In the central zone, the minimization of the free enthalpy G leads to establishing the tangent common to the two enthalpic functions. The two points of tangency delimit the composition interval for which the equilibrium between α and β is observed.

The notion of **Driving force per mole component (DGM)** is vital to understand the relation between the stability of a phase and its free enthalpy. The **DGM** is the affinity that a chemical species has to react to an internal process. According to the second law of thermodynamics, this internal process tends to approach equilibrium. For a phase, the **DGM** is the shortest distance between the Gibbs energy surface of the phase and the plane

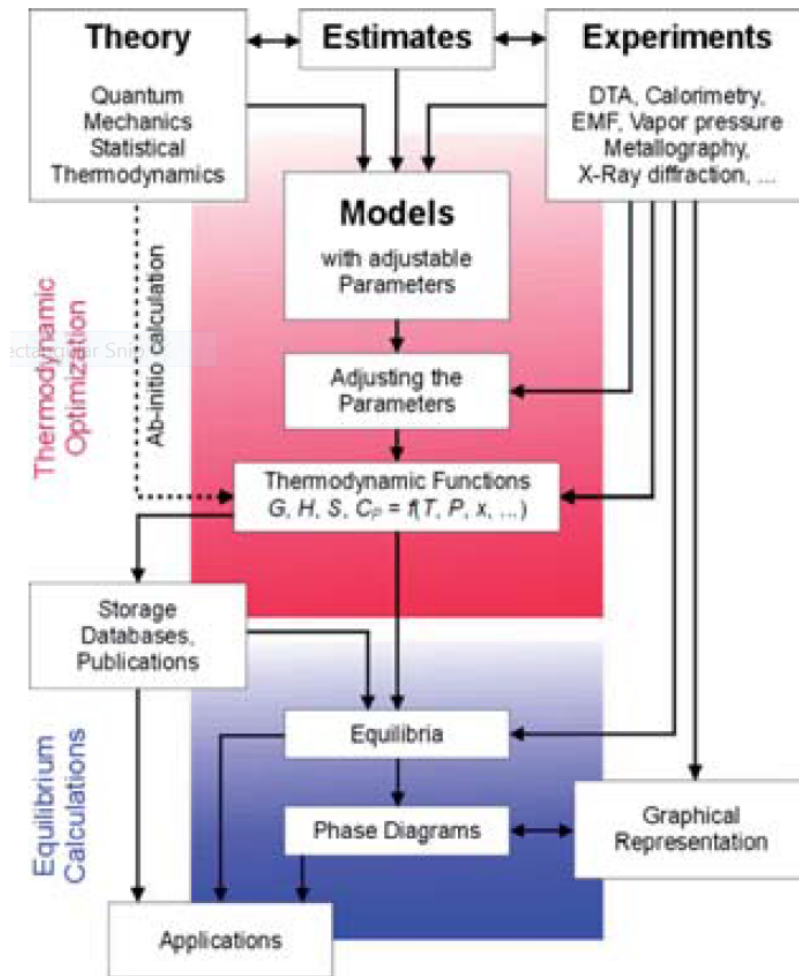


Figure 2.2 – Schematic representation of the CALPHAD method including the different iterative schemes [80].

joining the chemical potentials of the system components at steady state. This plane is called the plane of the common tangents because it is the plane tangent to the surfaces of the free energies of Gibbs of the stable phases. The DGM of a stable phase is zero. For an unstable phase, it is more negative as the phase is unstable.

This concept is illustrated on Figure 2.1, for which we consider a binary system A – B including a eutectic reaction.

A software can, therefore, follow the evolution of this quantity as a function of the temperature and the composition and plot the phase boundaries in all the space defined by the user.

The thermodynamic description of a system is not limited to its phase diagram, which is only a mapping of the equilibria occurring there. The complete characterization of the system is established only with the description of all its thermodynamic quantities; this is possible from its modeling because it consists precisely in describing, for all its phases, the Gibbs energy of Gibbs G which contains all the thermodynamic information.

According to the CALPHAD method, it is performed using mathematical formalisms with adjustable coefficients determined from experimental information (and sometimes from *Ab Initio*) calculations such as transformation temperatures, solubility limits, Enthalpies of formation or calorific capacities. The modeling is carried out by optimizing these parameters to obtain the best possible reproduction of all the experimental inform-

ation (phase diagram and thermodynamic data) taken into account in the calculation. The results of the modeling are then described by a data bank which contains, for all the phases considered, the declaration of the model used as well as the numerical values obtained for the different coefficients. The simplified flowchart of [Figure 2.2](#) describes the various steps of this method [80].

It is possible to distinguish two types of use of the CALPHAD method. The first is to create thermodynamic databases from experimental data; this is called optimization of phase diagrams. The second purpose is on the side of people who use databases to calculate the balances that take place within a system. To figure a phase diagram, it is necessary to use reliable experimental data and to model each phase with the appropriate model. We shall discuss the parameters involved in the choice of experimental data and selection of thermodynamic models, which will help to understand the modeling.

2.1.2.1 Data Selection

Thermodynamic modeling of a system requires information on the presence of different phases in the system. Moreover, CALPHAD is a semi-empirical method that requires experimental input data for the optimization of variables appearing in Gibbs G Gibbs energy models of constituent phases. Also, documentary research is the first step in the thermodynamic modeling of a system.

The experimental determination of a system can go through many characterizations, the nature of which depends mainly on the system. They depend, for example, on the physical state of the elements or compounds of interest (solid, liquid, gas) in the temperature or pressure range of interest, but also on the refractory or volatile nature of the elements, etc.

Experimental information that may be useful for thermodynamic modeling of a system can be divided into the following categories:

a) Phase Diagram Data

They include data on phase balances in a system; Such as the temperatures of the invariant reactions, the gas phase, the liquidus, the solidus, solubility limits, as well as invariant compositions, conjugation lines or tie-lines, pressure, etc.

The experimental techniques used are numerous. The most frequently encountered are:

- The thermal analysis measurements ([Simple Thermal Analysis \(STA\)](#), [Thermo-mechanical Analysis \(TMA\)](#), ...);
- Measurements of resistivity and dilatometry ([Scanning Optical Microscopy \(SOM\)](#), [Scanning Electron Microscopy \(SEM\)](#), [Transmission Electron Microscopy \(TEM\)](#));
- [Electron Probe Micro Analysis \(EPMA\)](#);
- structural analysis (X-ray, neutrons, ...), ...

The experimental techniques used to characterize the equilibrium between phases in a multicomponent system and the fundamental calculations have been detailed in a book published by Lukas et al. [78]. The values of the Gibbs G Gibbs energy's adjustable parameters are optimal when the computation of the different equilibria of a system best reproduces the diagrammatic data.

b) Thermodynamic data

They contain thermodynamic information such as integral enthalpy of mixture, enthalpy of transformation, enthalpy of formation H , partial enthalpy H_p , activity a_i , the chemical potential μ_i , the calorific capacity C_p , and so on. This type of data has the advantage of being connected directly to the quantities that are modeled; The Gibbs energy of Gibbs G or its enthalpic component H .

These data can be obtained either by potentiometric techniques [Electromotive Force Measurements \(EMF\)](#). Also, calorimetry can be used to get information on formation enthalpy or of reaction as well as of specific heat.

c) Crystallographic data

The related information to the crystal structure of the constitutive phases such as the space group, the site's occupation, ... etc. are very important in selecting the appropriate thermodynamic models for each phase.

d) Physical measurements

These are related data to specific heat or magnetism.

e) Calculated data

Information such as the enthalpy of formation or the enthalpy of mixing of the various stable and meta-stable constituents can also be obtained through theoretical calculations of the first-principle type [Ab Initio](#), of electronic structure in the framework of the [DFT](#) (see [section 1.1](#)), or the Miedema approach [81]. They are instrumental in the thermodynamic modeling of a system. The [DFT](#) is used to quickly and accurately calculate the electronic and magnetic properties of various compounds when coupled with a pseudo-potential approach and with the use of plane wave function bases. As far as the phase boundaries are concerned, fundamental calculations such as the [Cluster Variation Method \(CVM\)](#) method can be used as a guide for the form of meta-stable phase boundaries [82–85]. Using [CVM](#) method, Kikuchi [85] treated order-disorder transition phenomena. Also, [CVM](#) method and the Monte Carlo method in combination with [Ab Initio](#) calculations have been used [86].

The detailed examination of the literature gives a good overview of the system to be studied. However, it is not surprising that we can find contradictions between the different experimental studies concerning the temperatures of the invariant reactions, the solubility limits of the different phases, the presence of intermetallic phases in a binary or ternary system, etc. In this case, these data must be chosen according to their credibility:

- a purity of the starting used components. Sometimes a tiny amount of impurities can significantly alter the results (or stabilizing a non-equilibrium phase or create a nucleation barrier to the precipitation of an equilibrium phase);
- The technique of preparation of the sample, the time and the annealing temperatures, it means reaching the thermodynamic equilibrium, the characterization techniques, the type of used equipment, the experimental conditions;
- The standard deviation of the results obtained by the same research group;
- The agreement between the data obtained from different research groups.

Initial optimization trials can also help detect conflicting information and select appropriate data for optimization. Depending on the accuracy and reliability of the experimental data, different weights can be assigned to varying measurements during optimization. Experimental data that are larger and reliable may have higher weights, while less reliable data may have a lower weight, which in some cases may be zero.

Once the experimental dataset has been selected, it is advisable to choose the thermodynamic models adapted to the phases to be modeled.

2.1.2.2 Selection of thermodynamic models

Proper optimization of a system is synonymous with a choice of coherent models with the physics associated with them. For this, first of all, it is necessary to know the nature of the phase to be modeled, like its crystallographic data, the fact that it is stoichiometric, ordered, etc. Then, it is essential to associate the right model. We will detail, in [section 2.2](#), the different models available to model a phase according to its nature. It is also useful, when optimizing a system, to be interested in the compatibility of this system with other optimizations involving common elements and phases; this allows the pooling of optimizations and consequently the construction of databases allowing to extrapolate balances in multi-constituted systems. The selected models have adjustable parameters, and the role of optimization is to determine the values of these parameters.

2.1.3 Optimization principle

The optimization consists in adjusting the parameters of the models by a method of least squares. It is a question of determining the values of the interaction terms and of the energies of formation of the compounds from the experimental data. Optimization of a system (and / or execution of calculations) is done through specialized software modules such as [Thermo-Calc \[30\]](#), [Pandat \[87, 88\]](#), [Factsage \[89\]](#) or [MTDATA \[90\]](#), ... etc.

Proper optimization is based on numerous experimental data of good accuracy of the system under consideration. On the choice of appropriate models, there is an infinite number of optimizations of a system, these being dependent, among other things, on the chosen experimental data set and the weight given to the different measurements, but also on the selected models and their number of parameters. It is agreed that correct optimization involves the minimum of parameters. It is considered that the optimization is completed when all the experimentally selected data has been successfully described with the minimum of parameters. The optimization methodology has been described in detail by Kumar and Wollants [91] and more recently by Schmid-Fetzer et al. [92].

2.1.4 Calculation software

With the increasing needs to analyze the thermodynamic behavior of systems, to predict the relationships between phases or to evaluate thermodynamic properties for well-defined compositions and temperatures, many computational software packages are available that cover several aspects for specific applications [93].

- ① to the tabulation of the thermodynamic properties of the substances, their calorific capacity, their enthalpies, their free enthalpies of formation or transformation, equilibrium constants, partial pressures, ..., as a function of temperature and pressure and their compositions;

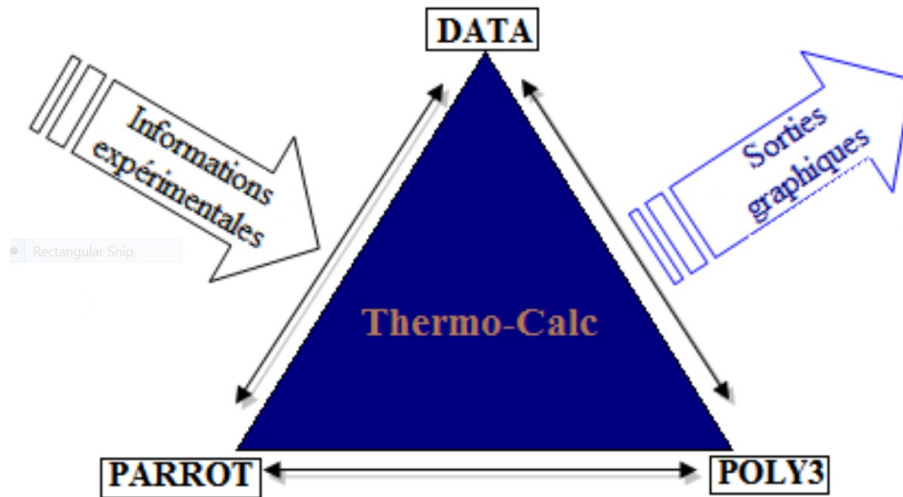


Figure 2.3 – Swedish software usage scheme **Thermo-Calc** [30].

- ② to calculate the thermodynamic properties of metal mixtures, oxides, salts, semiconductor compounds, etc., such as activity, chemical potentials, partial pressures of the various constituents as a function of temperature and pressure and composition;
- ③ For poly-constituted and polyphase systems, to calculate the equilibrium phase compositions, the phase fractions or the volume fractions, as a function of temperature;
- ④ To applications such as solidification paths, isotherms, isopleths or fraction of phases during solidification.

Among these softwares are **Thermo-Calc** (including Parrot) [30], **Pandat** (PanOptimizer) [87, 88], **Factsage** (OptiSage) [89]. The **Thermo-Calc**, **Pandat** and **Factsage** programs have been described in detail in a special issue of the Journal *CALPHAD Volume 26, Issue 2, Pages 141-312 (June 2002)*. For this work, the **Thermo-Calc** program was mainly used.

Thermo-Calc [30] is a powerful and flexible software for a variety of thermodynamic calculations and phase diagrams based on a powerful Gibbs energy minimization of Gibbs G . It has earned the reputation of being one of the best software for these calculations. The software **Thermo-Calc** was originally developed by the Swedes in 1981 notably by Professor Bo Sundman of the **Royal Institute of Technology in Stockholm (KTH)**. In all the continents of the world (except the Antarctic) a large number of researchers uses it (several hundred). It is designed for the optimization of multicomponent solutions that can contain up to 20 elements. The solutions may be metallic, aqueous, molten salts, amorphous or gas. **Thermo-Calc** [30] can use several different thermodynamic databases, especially those developed by **Scientific Group Thermodata Europe (SGTE)** [94].

The user of the Swedish software **Thermo-Calc** can develop its database by optimizing the thermodynamic parameters. The use of the program is based on three main modules as indicated by the **Figure 2.3**.

In **Thermo-Calc** [30], the part needed for modeling **Gibbs Energy System (GES)** is separated from the part that handles the calculation of the equilibria, this leaves the freedom to the user to choose one of the models already incorporated in **Thermo-Calc**, or to introduce a new adequate formalism to the problem to be treated.

The interactive side of **Thermo-Calc** also resides in the explanation of all the instructions to which the user can access by typing "Help".

Thermo-Calc [30] consists of several modules for specific purposes and different tasks that the user might be interested in performing them. The **Thermo DataBase (TDB)** module is used to retrieve databases or data files. The **GES** module is used to enter system information and thermodynamic data. The **Equilibrium Calculations (POLY)** module can compute various complex heterogeneous equilibria by fixing the conditions (T, P, n_i, \dots) which reduce the optimization to the variance 1. It also allows the calculation of the thermodynamic quantities (H, S, G, \dots) under the same imposed conditions. While the **Processing of various phase diagrams (POST)** module is used to draw diagrams, phase diagrams, thermodynamic quantities as a function of temperature and pressure, or to develop post-script files with *.ps* extension. The **PARROT** module provides a powerful and flexible tool for data optimization and evaluation of experimental data, from which Gibbs G Gibbs energy functions can be calculated by optimizing the experimental data by the least squares method. The user has the choice of axes system, given the choice of two linked quantities.

The Swedish software **Thermo-Calc** has several models to handle as many solutions as possible. Among them, there are those based on a theoretical foundation and those that use geometric or polynomial developments:

- Model of the ideal substitution solution,
- Model of the regular solution,
- Association model [95],
- Inden model [96] for ordered magnetic solutions,
- Model of Pitzer [97] for aqueous solutions,
- Kappor-Frohberg model [98] for the amorphous,
- Temkin sub-lattice model [99] generalized by Hillert and Staffansson [100],
- Muggianu geometric weightin [101],
- Geometric weighting of Kohler [102],
- Expansion polynomial of Redlich and Kister [103].

The choice of models to be used by the operator depends on several factors which are:

- The pure constituents of the system;
- The experimental phase diagram;
- Experimental thermodynamic data.

The best approach for optimization with the **PARROT** module is to create a "set-up" file containing all the phase information, with the variables of the model parameters that will be calculated. This is a text file with a *.tcm* extension and is executed with the "macro" command in **Thermo-Calc** [30]. Additional information can be entered in this file for future reference; thermodynamic model changes may also be indicated.

For the construction of the "set-up" file, it is important to have at the beginning a realistic description of the unknown phases (substitution mode, number of sub-lattices) to obtain the most satisfactory results possible with *Thermo-Calc*, and the closest to the experimental field. The experimental data are summarized in the file with *.pop* extension [78]. The data is entered in "Equilibrium" blocks. Each block has its own set of data associated with it. All necessary data to optimize the phases have also been added.

2.1.5 Procedure for critical evaluation/optimization of systems

In the present work, the majority of the experimental information mentioned along with the [section 2.2](#) is selected. For all systems, the optimization of the various thermodynamic parameters was carried out in the same way in three steps, taking into account or not the magnetism of the different phases, as follows:

- ① Obtain a set of model parameters for all present phases in the studied system in a single operation, assuming first that the non-stoichiometric phase as a stoichiometric compound;
- ② Once all equilibria were successfully calculated, the stoichiometric phase model was then changed to a non-stoichiometric model with the appropriate sub-lattices, with the parameters of the other phases being fixed;
- ③ An optimization of all the thermodynamic parameters of all the phases was carried out simultaneously taking into account all the data selected to ensure the correct fit.

Two types of calculation are possible:

- I Calculation of the equilibria between phases, by choosing a good initialization point, this choice is made by fixing equilibrium conditions (T , P , n_i , ...) until the degree of freedom is zero;
- II Calculation of thermodynamic quantities: these calculations are done in the *POLY* module and can be saved in several files with the extension *.PL3*.

In order to avoid the appearance of an inverted miscibility gap in the liquid phase during the calculation of our systems, thermodynamic constraints are imposed during optimization: with the Redlich and Kister [103] formalism, the curvature of Liquidus is positive [91, 104] by imposing an additional constraint $d^2G/d^2x \geq 0$ in the composition domain $0 \leq x(X) \leq 1$ ($X = Os, Th, Y, Cd, Ru$ ou Sc) and every fifty degreesm From the temperature of the liquidus to the temperature of 6000K, and with the recent model of Kaptay [105, 106, 107], enthalpy and entropy must be of the same sign.

2.1.6 Conclusion

The *CALPHAD* method is a powerful tool for describing the thermodynamic properties of the equilibria of multicomponent systems. It allows to determine and propose models to explain the different phases of equilibrium in a system from experimental and theoretical work. A database is then generated to store the parameters of these models for each system. These databases can be used with different thermodynamic calculation software (*Thermo-Calc*, *Pandat*, *MTDATA*, etc.) to plot phases diagrams and calculate the thermodynamic properties of these systems and explore them for higher order systems.

2.2 Thermodynamic models

2.2.1 Introduction

The choice of thermodynamic formalisms [108, 109] used for the description of a phase depends essentially on structural considerations. We present in this chapter, with the notations adopted by Thermo-Calc [30], the Ansara et al. [110] models retained for the characterization of different phases of our systems.

2.2.2 Thermodynamic description of pure elements

In the absence of any absolute scale of enthalpy, unlike entropy, it is important that a state of reference is defined in the description of the Gibbs energy of Gibbs G . The one commonly used comes from formalism developed by the SGTE which lists and compiles the thermodynamic descriptions of the pure components referred to the enthalpy of its stable state SER at 298.15K in databases such as Dinsdale [111] that was adopted in this study. According to the SGTE, the Gibbs energy of a pure element i (Os, Th, Y, Cd, Ru or Sc) ${}^0G_i^{\text{SER}}(T)$, referring to the enthalpy of its stable state SER at 298.15K, ${}^0H_i^{\text{SER}}(T)$ is symbolized in $G_i^{\Phi}(T)$. This quantity is given as a function of the temperature by the equation:

$$\begin{aligned} G_i^{\Phi}(T) &= {}^0G_i^{\text{SER}}(T) - {}^0H_i^{\text{SER}}(298.15\text{K}) \\ &= f(T) \\ &= a + b \times T + c \times T \times \ln T + d \times T^2 + e \times T^3 + f \times T^{-1} + g \times T^7 + h \times T^{-9} \end{aligned} \quad (2.1)$$

The state SER is the state of the element in its stable crystallographic structure at a temperature of 298.15K under a pressure of 10^5Pa . The coefficients a, b, c et d, \dots etc. in this expression were taken from the database [111]. There are also additional contributions taking into account the pressure [112] or the magnetic effects [113–115]. The pressure dependence of condensed phases is ignored.

2.2.2.1 Magnetic contribution

Previous works of Inden [114, 115] have led Hillert and Jarl [113] to the definition of the magnetic contribution to the Gibbs energy of Gibbs molar in the following way:

$${}^{\text{mag}}G^{\Phi} = R \times T \times \ln(\beta_0 + 1) \times g(\tau) \quad (2.2)$$

In this expression:

β_0 : The average magnetic moment per atom expressed in magnetron of Bohr μ_B .

$g(\tau)$: Calculated from the fraction of the total magnetic enthalpy from the short-range order of the spins of the atoms, $\tau = T/T^*$ with T^* Being the critical magnetic temperature, it means:

- Curie temperature T_C For ferromagnetic materials: it is the transition from the ordered magnetic state (ferromagnetic) to the disordered (paramagnetic) state. It represents the direct measurement of the interactions of exchange between the magnetic atoms; these interactions depend mainly on the inter-atomic distances;
- At Néel temperature T_N For antiferromagnetic materials: temperature above which an antiferromagnetic or ferrimagnetic material becomes paramagnetic. Above this

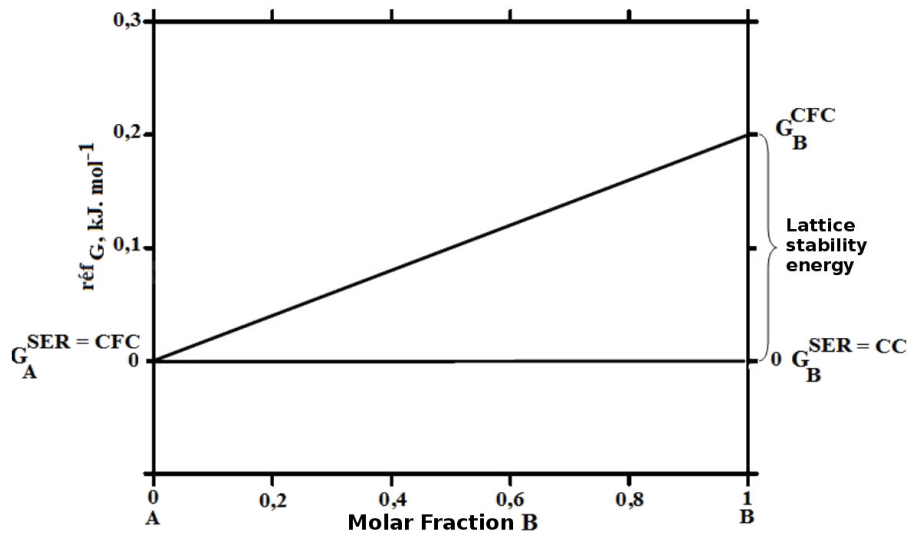


Figure 2.4 – Gibbs energy of the *c.f.* reference phase in a A – B binary system in the case where the two elements A and B have different **SERs**. This diagram introduces the notion of the lattice stability of the energy.

temperature, thermal energy is sufficient to break the microscopic magnetic order of material.

2.2.2.2 Lattice Stability

We will see later that it is also necessary to describe the pure elements in common structures where they are unstable or metastable, it means the changes of reference state. The Figure 2.4 illustrates the example where the B element would crystallize in a state other than A in the state **SER** (eg *c.c.*). In this case, the Gibbs energy of Gibbs of B in form *c.f.c* is higher and the difference between this energy and that in the state **SER** is called the lattice stability of the energy. This energy can be expressed by an equation of the same type as Equation 2.1.

2.2.3 Thermodynamic models used for solutions and compounds

In the **CALPHAD** approach, the different phases are described by using different thermodynamic models. This part is intended to represent the applied mathematical formalism for phases description.

2.2.3.1 Gibbs energy Modeling of Gibbs

The computation of the equilibrium between phases in a multi-constituted system requires the minimization of the Gibbs energy G of all phases that exist in this equilibrium:

$$G = \sum_{i=1}^{n_p} n_i \times G_i^\Phi = \text{minimum} \quad (2.3)$$

Where n_p represents the total number of system phases, n_i is the number of moles, and G_i^Φ is the partial Gibbs energy of component i in the phase Φ .

Thermodynamic description of a system requires the assignment of thermodynamic functions for each phase Φ . Contributions to Gibbs energy G^Φ of a phase can be written as:

$$G^{\Phi} = G_T^{\Phi}(T, x) + G_P^{\Phi}(P, T, x) + G_m^{\Phi}(T_C, \beta_0, T, x) \quad (2.4)$$

- $G_T^{\Phi}(T, x)$: Contribution of temperature and composition,
- $G_P^{\Phi}(P, T, x)$: Contribution of pressure,
- $G_m^{\Phi}(T_C, \beta_0, T, x)$: A magnetic contribution that involves an expression using the Curie T_C (or Neel T_N) temperature and the Bohr number β_0 that represents the average magnetic moment per atom.

The temperature dependence in the term $G_T^{\Phi}(T, x)$ is usually expressed as a power series of T :

$$G_T^{\Phi}(T, x) = a + b \times T + c \times T \times \ln(T) + \sum_n d_n \times T^n \quad (2.5)$$

a , b , c , and d_n Are coefficients, and n is an integer taking generally the values 2, 3, -1 and 7 or -9 . The absolute entropy as well as the calorific capacity are obtained respectively from the first and second derivatives of $G_T^{\Phi}(T, x)$ relative to the temperature.

The optimization of the experimental values of the measurements of C_p determines the coefficients c , d_n ($d_n = d, e, f$ and g or h). This expression is valid for a fixed temperature range. The equations of the following models which describe the concentration dependence, the coefficients of G can have such a temperature dependence. In general, the first two terms are sufficient to describe the thermodynamic evolution of the system when no data on calorific capacity is available [116]. Pressure dependence is generally ignored.

The dependence of the Gibbs energy of a phase Φ is expressed by:

$$G_T^{\Phi}(T, x) = {}^{ref}G^{\Phi} + {}^{id}G^{\Phi} + {}^{ex}G^{\Phi} \quad (2.6)$$

With:

- ${}^{ref}G^{\Phi}$: Free enthalpy of phase reference Φ , This free enthalpy designates the sum of the free enthalpies of the different pure components i representing the situation before mixing. For a ternary system, the sum is made on A, B, and C.
- ${}^{id}G^{\Phi}$: Free Enthalpy of the ideal mixture which denotes an absence of energetic interactions between the constituents i . The unique contribution is then the entropy of configuration the corresponding to the maximum disorder. For a ternary system, the sum is made on A, B, and C.
- ${}^{ex}G^{\Phi}$: Excess free enthalpy of the mixture. This term defines the deviation of the free mixing enthalpy from the ideal mixture. It takes into account the repulsive energy interactions (mixing enthalpy $H_{mél} > 0$) or attractive (mixing enthalpy $H_{mél} < 0$) between the different constituents. Also, it obviously considers the different entropic contributions from the entropy of ideal configuration.

While the first two terms, ${}^{ref}G^{\Phi}$ and ${}^{id}G^{\Phi}$, are perfectly defined according to the type of solution, the excess term, ${}^{ex}G^{\Phi}$, can be described by different models that involve a thermodynamic formalism as well as a determination of the appropriate adjustable coefficients. Since Hildebrand [117] has presented its "regular solution" model to describe

the interactions of different elements in a random solution, several models have been proposed for the phases that deviate from this regularity to describe the Gibbs energy of excess Gibbs energy. So, we show how to model the dependence in temperature and composition of different phases (substitutional solutions, interstitial solutions, stoichiometric compounds, ...).

2.2.3.2 Disordered substitutional solutions models

The disordered substitutional model (the sites of the structure have the same occupancy rates) is used for phases such as the gaseous phase or the liquid phase and the substitutional solid solutions where the constituents can randomly mix on any Site in the phase [77].

2.2.3.3 Ideal Solutions

The most straightforward description of the solution behavior is the ideal solution model. The central assumptions of this model are: (a) the mixed components have the same crystal structure, (b) the mixture is purely random, (c) the mixing energy (of interactions) is nil.

The entropy due to the configuration can be easily calculated and it is related to the probability of exchanges of the components. The entropy of configuration S^{conf} is given by:

$$S^{conf} = \beta_0 \times \ln(\omega_p) \quad (2.7)$$

Where β_0 is the Boltzmann constant and ω_p is the number of configurations in which the constituents can be arranged for a given state. For a multi-constituent system, it is equal to the number of permutations given by:

$$\omega_p = \frac{N!}{\prod_{i=1}^e n_i!} \quad (2.8)$$

where

$$N = \sum_{i=1}^e n_i \quad (2.9)$$

n_i is the number of constituents of i ($i = 1, 2, \dots, e$), And N is the total number of constituents in the Φ phase. For one mole of elements, N is equal to the number of Avogadro. Using the Stirling formula, S^{conf} is now equal to:

$$S^{conf} = k_B \times \sum_{i=1}^e n \times \ln\left(\frac{n_i}{N}\right) \quad (2.10)$$

The ideal molar entropy of the mixture of the phase Φ is given by:

$${}^{ed}S^{\Phi} = -N \times k_B \times \sum_{i=1}^e x_i^{\Phi} \times \ln x_i^{\Phi} \quad (2.11)$$

Where x_i is the molar fraction of the constituent i and e is the number of chemical species. With the hypothesis that the interaction energy is zero, it is possible to substitute the atoms without modifying the energy of this state and ${}^{id}G^{\Phi}$ is given by:

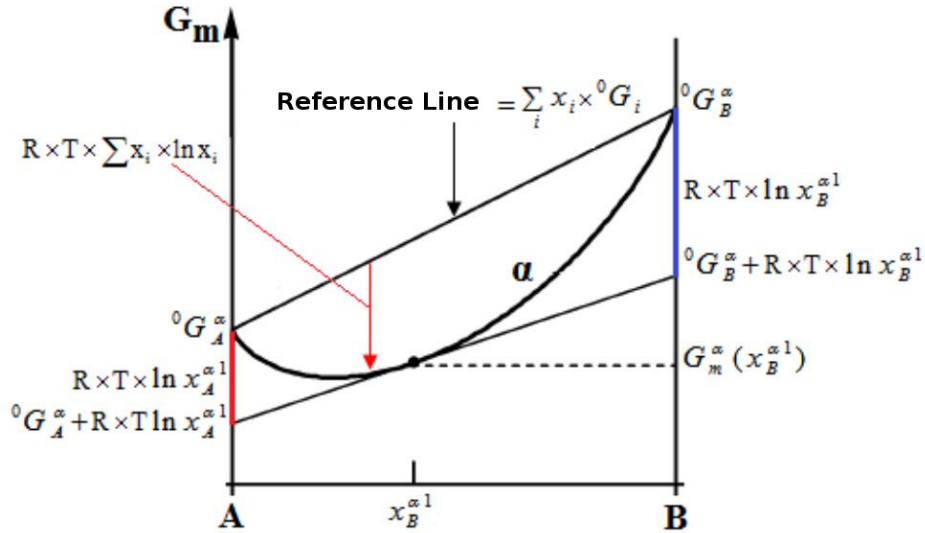


Figure 2.5 – Molar Gibbs energy of an ideal binary phase α , illustrating the reference line.

$${}^{id}G^m = -T \times {}^{id}S^\Phi = R \times T \times \sum_{i=1}^e x_i^\Phi \times \ln x_i^\Phi \quad (2.12)$$

Where R is the perfect gases constant. The molar Gibbs energy of an ideal solution Φ will be:

$$G_m^\Phi = \sum_{i=1}^e x_i^\Phi \times {}^0G_i^\Phi + R \times T \times \sum_{i=1}^e x_i^\Phi \times \ln x_i^\Phi \quad (2.13)$$

With ${}^0G_i^\Phi$ defining the Gibbs energy of the pure elements i in the studied crystal structure Φ .

The first summation of the terms in the Equation 2.13 represents the average of the references for the constituents, and this summation can be considered as the reference frame for the mixture. For a binary solution, it can be viewed as a reference line. This is illustrated on the Figure 2.5.

Second summation terms are negative because all molar fractions are less than unity. They represent the distance between the G^m curve and the reference line. The Figure 2.6 demonstrates the same situation for an ideal ternary solution. The triangle represents the reference plane $\sum_{i=1}^e x_i^\Phi \times {}^0G_i^\Phi$.

For gases case, the ideal mixture is often assumed, and this assumption can often be quite reasonable. However, in the condensed phases, there is always some interaction between the constituents.

2.2.3.4 Regular and non-regular solutions

The simplest non-ideal solution model is the regular solution model. The hypotheses for this model are; (a) random distribution of atoms, (b) the number of nearest neighbors (coordination) is equal to z for all constituents, (c) only interactions between closest neighbors are taken (D) the binding energy E_{ij} is independent of composition and temperature [104].

Under these assumptions, the total energy E_{tot} of a solution in a binary system A – B is equal to:

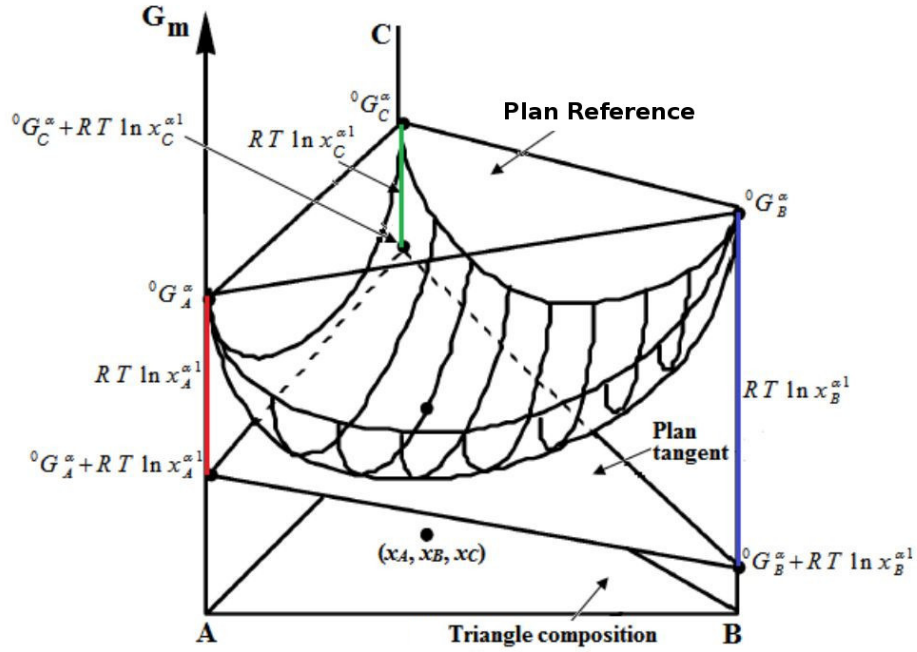


Figure 2.6 – Gibbs energy of an ideal ternary phase α , illustrating the reference plane.

$$E_{tot} = \omega_{AA} \times E_{AA} + \omega_{BB} \times E_{BB} + \omega_{AB} \times E_{AB} \quad (2.14)$$

Where ω_{AA} , ω_{BB} and ω_{AB} are the number of bonds of the type A – A, B – B and A – B, E_{AA} , E_{BB} and E_{AB} , are the corresponding binding energies.

With the assumption of the random distribution of the atoms and the coordination number of the solution which is equal to z for all constituents, the number of each bond type can be calculated as follows:

$$\begin{aligned} \omega_{AA} &= \frac{1}{2} \times N \times z \times x_A^2 \\ \omega_{BB} &= \frac{1}{2} \times N \times z \times x_B^2 \\ \omega_{AB} &= \frac{1}{2} \times N \times z \times x_A \times x_B \end{aligned} \quad (2.15)$$

Where x_A , x_B are the molar fractions of A and B, and N is the total number of particles in the solution. From the equations (2.14) and (2.15), the mixing enthalpy $H^{mél}$ can be calculated as follows:

$$H^{mél} = x_A \times x_B \times \Omega \quad (2.16)$$

Where:

$$\Omega = \frac{N \times z}{2} \times (2 \times E_{AB} - E_{AA} - E_{BB}) \quad (2.17)$$

Ω is called the regular solution parameter. For a mole of atoms, this parameter is obtained for $N = N_{av}$. If the energy of the bonds depends on the temperature, there will also be an excess entropy of mixing. The excess Gibbs energy of mixing can be written as:

$$^{ex}G^m = x_A \times x_B \times \Omega \quad (2.18)$$

Where Ω is a temperature-dependent interaction parameter, usually expressed as: $(a + b \times T)$. Ω in this case is not a regular solution parameter. Generally this excess energy, for a multi-constituent system, is added to the ideal energy in the equation (2.12), the total molar Gibbs energy of the solution is obtained by:

$$G_m^\Phi = \sum_{i=1}^e x_i^\Phi \times {}^0G_i^\Phi + R \times T \times \sum_{i=1}^e x_i^\Phi \times \ln x_i^\Phi + \sum_{i=1}^e \sum_{j>i} x_i^\Phi \times x_j^\Phi \times \Omega_{ij} \quad (2.19)$$

Although it is very simple and straightforward, the regular solution model can be used to obtain a better understanding of the general topological features of phase diagrams.

In the regular solution model, binding energy is assumed to be independent of the composition. This hypothesis is too basic when modeling real systems. This led to the development of the sub-regular solution model [29], where the interaction energies are assumed to be linearly modified with the composition. This leads to the following expression for the molarexcess Gibbs energy of mixture ${}^{ex}G_m^\Phi$:

$${}^{ex}G_m^\Phi = x_i^\Phi \times x_j^\Phi \times \left(\Omega_{ij}^i \times x_i^\Phi + \Omega_{ij}^j \times x_j^\Phi \right) \quad (2.20)$$

A more complex composition dependency of Ω can also be used. Generally this is done using series development for Ω . The most common method is based on the Redlich and Kister [103] polynomials and the equation (2.19) then becomes:

$$G_m^\Phi = \sum_{i=1}^e x_i^\Phi \times {}^0G_i^\Phi + R \times T \times \sum_{i=1}^e x_i^\Phi \times \ln x_i^\Phi + \sum_{i=1}^e \sum_{j>i} x_i^\Phi \times x_j^\Phi \times \sum_{i=1}^e L_{i,j}^\nu \times \left(x_i^\Phi - x_j^\Phi \right)^\nu \quad (2.21)$$

$L_{i,j}^\nu$ is a binary interaction parameter as a function of the value of ν . Since Ω_{ij} can be temperature-dependent and can be written as $(a + b \times T)$ with a and b which are adjustable coefficients of optimization development, using the available experimental data. The equation (2.21) becomes equal to the regular solution model, equation (2.19), when $\nu = 0$ and to the sub-regular model when $\nu = 1$. By modifying the order of development of the parameter ν , it is possible to modify the contribution of the excess Gibbs energy term according to the figure 2.7.

2.2.3.5 Disordered interstitial solutions models

The difference between substitutional and insertional solution models lies in the entropy of disorder. In an insertional solution the large atoms are interchanged, but the small ones swap their positions with vacancy spaces. Such a solution is saturated with interstitial atoms when $x = 0.5$. If we consider that in the solution there is n_B insertional atoms in the lattice of atoms A, then $n_A - n_B$ empty interstitial sites exist, the number of permutations of the atoms B with the vacancy sites is:

$$\frac{(n_B + n_A - n_B)!}{n_B! \times (n_A - n_B)!} = \frac{n_A!}{n_B! \times (n_A - n_B)!} \quad (2.22)$$

The entropy of disorder is written in the form:

$$S = k_B \times \ln \left(\frac{n_A!}{n_B! \times (n_A - n_B)!} \right) \quad (2.23)$$

Using the Stirling approximation we obtain:

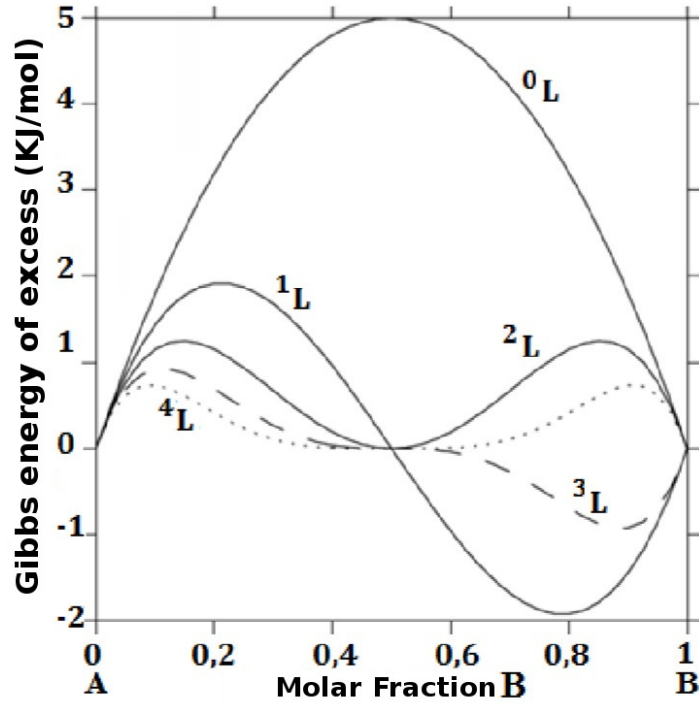


Figure 2.7 – Influence of parameter order ${}^vL_{A,B}^{\Phi}$ on the Gibbs energy term G .

$$S = k_B \times (n_A \times \ln n_A - n_B \times \ln n_B - (n_A - n_B) \times \ln (n_A - n_B)) \quad (2.24)$$

This formula is written using the molar fraction x of the constituent B:

$$S = -R \times \left(x \times \ln \left(\frac{x}{1-2x} \right) - (1-x) \times \ln \left(\frac{1-x}{1-2x} \right) \right) \quad (2.25)$$

2.2.3.6 Thermodynamic description of stoichiometric compounds

Like the pure elements, the free enthalpy of stoichiometric compounds is only temperature dependent. Using the hypothesis of Kopp-Neumann [116], the heat capacity of a compound is the weighted sum of the calorific values of the pure elements: $C_p = \sum_i a_i \times C_{pi}$, molar free enthalpy (per mole of atoms) of a compound ${}^0G_{comp}(T)$ is defined as follows:

$${}^0G_{comp}(T) - {}^0H_{comp}^{SER}(298.15K) = a + b \times T + \sum_i a_i \times G_i^{SER}(T) \quad (2.26)$$

With

$${}^0H_{comp}^{SER}(298.15K) = \sum_i a_i \times {}^0H_i^{SER}(T) \quad (2.27)$$

Where a_i is the mole fraction of the element i in one mole of compound denoted $comp$ and ${}^0H_i^{SER}(T_0)$ is the enthalpy of a mixture of pure elements in their state **SER** to obtain the composition of the given compound at $T_0 = 298.15K$.

In this description, $a + b \times T$ is the free enthalpy of formation of the compound $comp$ formed from the pure elements in their state **SER**. a represents the formation enthalpy of the compound $comp$ and the meaning of the parameter b is described in ???. In this work, the Gibbs energy of the various binary stoichiometric compounds with the formulation

A_pB_q present in the various binary systems, denoted by ${}^0G_{A_pB_q}(T)$, was expressed as a linear function of temperature:

$${}^0G_{A_pB_q} = \frac{p}{p+q} \times {}^0G_A + \frac{q}{p+q} \times {}^0G_B + a + b \times T + {}^{mag}G_{A_pB_q} \quad (2.28)$$

In the case of a ternary system A – B–C, the Gibbs energy of ternary stoichiometric compounds with the formulation $A_pB_qC_r$, denoted by ${}^0G_{A_pB_qC_r}(T)$, is given by the following formula:

$${}^0G_{A_pB_qC_r} = \frac{p}{p+q+r} \times {}^0G_A + \frac{q}{p+q+r} \times {}^0G_B + \frac{r}{p+q+r} \times {}^0G_C + a + b \times T + {}^{mag}G_{A_pB_qC_r} \quad (2.29)$$

Where 0G_A , 0G_B and 0G_C are the Gibbs free energies of pure components; a and b are parameters to be determined. ${}^{mag}G_{A_pB_qC_r}$ is the magnetic contribution to the Gibbs energy described by equation (2.2).

2.2.3.7 Ordered phases model; Sublattices model

The model of disordered solutions is probably the simplest model to describe the thermodynamic behavior of a solution. The Gibbs energy of the reference states in this model is based on the assumption of random mixing of constituents on the simple lattice, which is not appropriate to apply this model for solutions that show an important order, such as intermetallic or ionic compounds and ionic liquids. The different elements constituting preferentially these phases adopt different crystallographic sites. They are usually processed by the sublattice model. This model is based on the fact that each crystallographic site from the structure must be described with a sub-lattice (figure 2.8). So, it is possible to use the regular solutions model which assumes the random mixing within each sublattice. The idea of the sublattice model comes from Temkin [99] for ionic solutions, assuming that two sublattices exist in the ionic crystal. The configuration entropy is described for cations and anions separately. The model was then used for metal systems by Hillert and Staffansson [100], Hillert and Waldenström [118] and adapted for several sub-lattices by Sundman and Ågren [119].

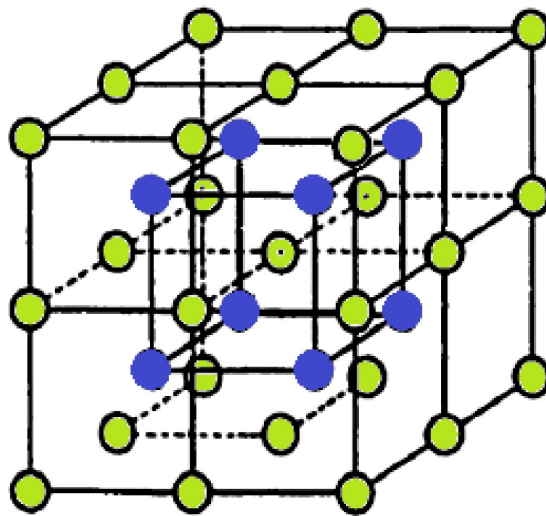
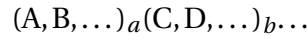


Figure 2.8 – Centered cubic structure B2 of type $CsCl$, Representing the interpenetration of two simple cubic lattices.

An intermetallic phase is often non-stoichiometric (existence of a domain of homogeneity), it can present a domain of composition well extended. Consider such a phase $A_{1-d}B_{1+d}$. Sublattices normally occupied by the A and B atoms will be called the A sublattice and the B sublattice, respectively. The deviation at the stoichiometry (where $d = 0$) can occur by the formation of defects such as antisite atoms (the A atoms occupy the B and the reverse sites), vacancies occupying interstitial sites, etc. One type of defects will predominate for solutions with an excess of A and another type will predominate for solutions having an excess of B.

The power of the sublattice model lies in the fact that most other models, such as the substitutional model, are individual cases of the model. On the other hand, the model can be applied more specifically to a complex ordered crystal structure, such as the sigma phase, or used to describe disorder-order relationships between similar phases. Therefore, it treats many different phases with different structures. Which facilitates the development of software and databases; because many types of solutions can be interpreted as cases of a general formalism.



A pair of parentheses symbolizes each sublattice. They contain, for each sub-lattice, the present species on the crystallographic site associated with the sub-lattice. These species may be atoms, charges (ions, etc.) or vacancies; Depending on the type of concerned phase. The first sublattice contains the species A, B, ..., while the second sublattice contains the species C, D, ..., and so on. a, b, \dots represents the number of sites per unit cell on the first and second sublattices, etc.

2.2.3.8 Sites fraction defenition

The molar fractions in a phase are generally defined by the following relationship:

$$x_i = \frac{n_i}{\sum_{j=1}^c n_j} = \frac{n_i}{n} \quad (2.30)$$

Where n_i and n_j are the moles of the elements i and j , respectively, and n is the total number of moles in the phase. The number of species is c . It is convenient to introduce a variable of similar composition for each sub-lattice if the phase is composed of two or more sub-lattices:

$$y_i^s = \frac{n_i^s}{n^s} \quad (2.31)$$

The exponent s denotes the sub-lattice considered, y_i^s represents the fraction of sites of the species i of the s , n_i^s sublattice, The number of i of the s and n^s sublattice is the total number of sites in the s sublattice. Each sublattice s has the condition: $\sum_i y_i^s = 1$ This can be generalized by including vacancy sites that are important to consider in interstitial phases or interstitial defects in the phase which are important, equation (2.31) becomes:

$$y_i^s = \frac{n_i^s}{n_{Va}^s + \sum_i n_i^s} \quad (2.32)$$

Where n_{Va}^s is the total number of vacancy sites in the s sublattice. One can then define the fraction of vacancy sites and obtain the relation:

$$y_{Va}^s = 1 - \sum_i y_i^s \quad (2.33)$$

It is often convenient to consider vacancy sites in a sublattice as a constituent and include them in the sum for the sub-lattice in the equation (2.32), but not in the sum for the entire phase in the equation (2.30). We also define a^s , the site fraction corresponding to the s sublattice by:

$$a^s = \frac{n^s}{n} \quad (2.34)$$

Where the a^s are given by the number of sites in the elementary mesh, so: $\sum_{s=1}^q a^s = 1$. Q is the number of sublattices and n is the total number of sites. The fractions of sites can be arranged in a $q \times c$ matrix if there exist q sublattices and c constituents:

$$\begin{pmatrix} y_1^1 & y_2^1 & y_3^1 & \cdots & y_c^1 \\ y_1^2 & y_2^2 & y_3^2 & \cdots & y_c^2 \\ \vdots & \vdots & \vdots & \ddots & \vdots \\ y_1^q & y_2^q & y_3^q & \cdots & y_c^q \end{pmatrix} \quad (2.35)$$

Each row represents a sublattice and each column is a constituent. Since most components do not enter all sublattices, many components are null. The overall composition of the phase thus described is related to the site fractions (from a given matrix y) as follows:

$$x_i^\Phi = \frac{n_i}{\sum_{i \neq Va} n_i} = \frac{\sum_{s=1}^q a^s \times y_i^s}{\sum_{s=1}^q a^s \times (1 - y_{Va}^s)} \quad (2.36)$$

Where x_i^Φ is the mole fraction of the i element in the Φ phase with $\sum_{i \neq Va} x_i^\Phi = 1$.

2.2.3.9 Molar Gibbs energy

The sublattice model defines the Gibbs energy of one mole of sites in the Φ , ${}^0G_{ms}^\Phi$ phase by an equation similar to that used for substitutional solutions:

$${}^0G_{ms}^\Phi = {}^{ref}G^\Phi + {}^{id}G^\Phi + {}^{ex}G^\Phi \quad (2.37)$$

① Entropy ideal mixing

To calculate the ideal mixing entropy S of a phase with the sublattices model, we can apply the hypothesis of random mixing of the elements on each sub-lattice and the contributions of the different sub-lattices are added. Indeed, the number of possible arrangements of the species present on the s sublattice is:

$$\frac{n^s!}{\prod_{i=1}^{e^s} n_i^s!} \quad (2.38)$$

Hence the total number of possible arrangements on all sites:

$$\omega_p = \prod_{s=1}^q \frac{n^s!}{\prod_{i=1}^{e^s} n_i^s!} \quad (2.39)$$

The entropy of configuration is equal to $S = k_b \times \ln(\omega_p)$, with k_b the Boltzmann constant.

$$S = -k_b \times \sum_{s=1}^q \sum_{i=1}^{e^s} [\ln(n_i^s!) - \ln(n^s!)] \quad (2.40)$$

The replacement of n_i^s and n^s by $y_i^s \times a^s \times n$ and the use of the Stirling approximation: $\ln a! = a \ln a - a$, lead to:

$$S = -k_b \times n \times \sum_{s=1}^q a^s \times \sum_{i=1}^{e^s} y_i^s \times \ln(y_i^s) \quad (2.41)$$

${}^{id}G^{\Phi}$ is related to the ideal entropy S by the relation: ${}^{id}G^{\Phi} = -T \times S$, so:

$${}^{id}G^{\Phi} = R \times T \times \sum_{s=1}^q a^s \times \sum_{i=1}^{e^s} y_i^s \times \ln(y_i^s) \quad (2.42)$$

② Gibbs Energy Reference States

The end-members effectively define the Gibbs energy of reference states ${}^{réf}G^{\Phi}$. Consider the simplest case, proposed by Hillert and Staffansson [100], a sublattice (1) containing the elements A and B; it is represented by $(A, B)_m$, where m is the multiplicity of the sublattice. If we consider two sub-lattices, we can write $(A, B)_m(C, D)_n$, the elements C and D being on the second sub-lattice (2) of multiplicity n . It is a quaternary phase, but it's composition can only be varied with two degrees of freedom instead of three because of stoichiometric constraints ($y_A + y_B = 1$ et $y_C + y_D = 1$). All possible compositions can therefore be represented on a plane as well as a ternary system.

As shown by the figure 2.9a, a square pattern is the natural shape and each corner is an end-member. End-members are defined compounds formed when each sublattice is occupied by a single element type. They can be either real or hypothetical. Perpendicular to this plane, we can trace the Gibbs energy of Gibbs G .

The figure 2.9b represents the reference surface as a function of the distribution on the sites for particular values of the formation energies of the end-members defined by the model. However, for any values of the Gibbs free energies of the end-members, this surface is not plane [77]. The surface in the figure 2.9b can be represented by the equation:

$${}^{réf}G^{\Phi} = y_A \times y_C \times {}^0G_{A:C} + y_B \times y_C \times {}^0G_{B:C} + y_A \times y_D \times {}^0G_{A:D} + y_B \times y_D \times {}^0G_{B:D} \quad (2.43)$$

Where ${}^0G_{A:C}$ represents the Gibbs energy of the end-member AC and the other quantities have an equivalent definition.

An alternative notation of these quantities would be ${}^0G_{ij}^{st}$, where i is the constituent on the sub-lattice s and j the constituent on the sub-lattice t . In this way, more sublattices can easily be added.

When the equation (2.43) is generalized, the principle suggested by Hillert and Staffansson [100] makes it necessary to consider each possible compound and multiply it's Gibbs energy by the fraction of this compound, i.e., the product of the corresponding site fractions, for example $y_i^s y_j^t$ in the case of two sublattices. Alternatively, the

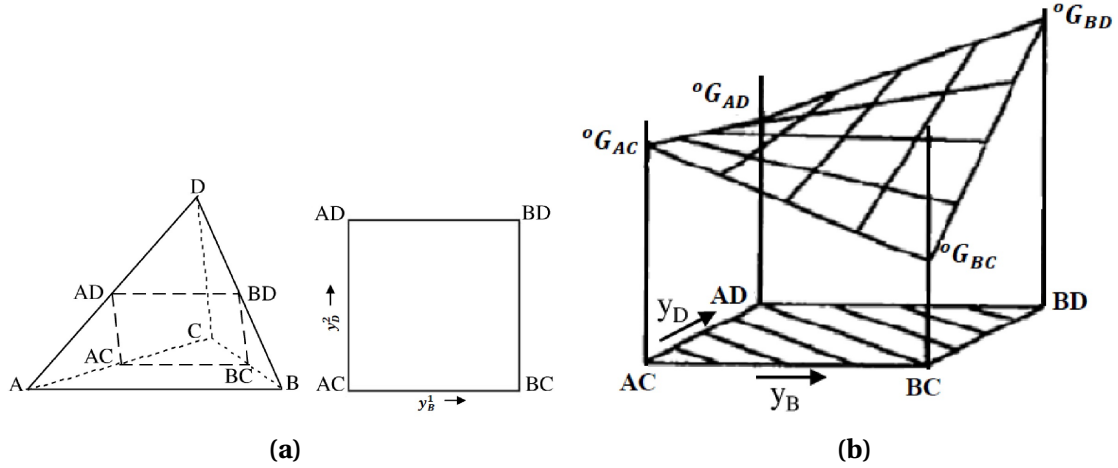


Figure 2.9 – (figure 2.9a) The space of composition encompassed by the system and (figure 2.9b) the reference Gibbs energy surface described by equation (2.43) from Hillert and Staffansson [100], Hillert [120].

information contained in the exponent and the index can be represented by a row (or site occupation) i , which defines a constituent for each sublattice.

Using this notation, we can write the equation (2.43) in the following general form:

$${}^{ref}G^{\Phi} = \sum_I P_I(Y) \times {}^0G_I \quad (2.44)$$

Where 0G_I represents the Gibbs energy of the compound defined by i which can of course depend on temperature and pressure, and $P_I(Y)$ denotes the corresponding product of fractions of sites from The matrix Y .

③ Excess Gibbs energy

The method for describing the excess Gibbs energy can again be better demonstrated by using a two-subarray system $(A, B)_1(C, D)_1$ before generalization to a multi-constituent system. In this alloy, the interactions $A - C$, $A - D$, $B - C$ et $B - D$ are controlled by the Gibbs energy of Gibbs of the compounds AC , AD , BC and BD .

The mixture on the sub-lattices controls the interactions $A - B$ and $C - D$ and the simplest form of interaction is the regular solution format such that:

$${}^{ex}G^{\Phi} = y_A^1 \times y_B^1 \times L_{A,B:*}^0 + y_C^2 \times y_D^2 \times L_{C,D:*}^0 \quad (2.45)$$

Where $L_{A,B:*}^0$ and $L_{C,D:*}^0$ denote the regular solution parameters for mixing on the sublattices, sites of the other sublattice.

A sub-regular model can be introduced to describe the dependence of the composition of the interaction parameters, taking into account the occupation of the site of the other sub-lattice:

$${}^{ex}G^{\Phi} = y_A^1 \times y_B^1 \times y_C^2 \times L_{A,B:C}^0 + y_A^1 \times y_B^1 \times y_D^2 \times L_{A,B:D}^0 + y_A^1 \times y_C^2 \times y_D^2 \times L_{A:C,D}^0 + y_B^1 \times y_C^2 \times y_D^2 \times L_{B:C,D}^0 \quad (2.46)$$

With the polynomial development of the Redlich and Kister [103] type, using fractions of sites, these parameters can be added such as:

$$\begin{aligned}
 L_{A,B:C}^0 &= \sum_{\nu} L_{A,B:C}^{\nu} \times (y_A^1 - y_B^1)^{\nu} \\
 L_{A,B:D}^0 &= \sum_{\nu} L_{A,B:D}^{\nu} \times (y_A^1 - y_B^1)^{\nu} \\
 L_{A:C,D}^0 &= \sum_{\nu} L_{A:C,D}^{\nu} \times (y_C^2 - y_D^2)^{\nu} \\
 L_{B:C,D}^0 &= \sum_{\nu} L_{B:C,D}^{\nu} \times (y_C^2 - y_D^2)^{\nu}
 \end{aligned} \tag{2.47}$$

It is clear that this can be extended to any number of sublattices and constituents and the equation (2.37) can be generalized using the notation of equation (2.44):

$${}^{ex}G^{\Phi} = \sum_{I1} P_{I1}(Y) \times {}^0L_{I1} \tag{2.48}$$

Where (I1) represents a first-order row, where a single sub-lattice contains two constituents, while the remaining sub-lattices are occupied by a single constituent. The summation is taken on all the different (I1). The row type that was introduced in the equation (2.44) can be written I0 and considered of order zero. The equation (2.45) is general in the case of regular solutions, but can be extended to include higher order interactions, as in equation (2.47), by introducing the IZ rows But with an additional restriction that the array must not contain any of the constituents more than once in each sub-lattice [77]. In this way, excess Gibbs energy can be written as:

$${}^{ex}G^{\Phi} = \sum_{Z>0} \sum_{IZ} P_{IZ}(Y) \times L_{IZ} \tag{2.49}$$

${}^{ex}G^{\Phi}$ represents the excess free enthalpy of Φ phase. It reveals terms of interactions between elements for a given occupation of sublattices. This occupation is indicated by the index of interactions terms L_{IZ} .

The total molar Gibbs energy of the phase including, free reference energy, The ideal entropy and the excess terms becomes:

$${}^0G_{ms}^{\Phi} = \sum_{I0} P_{I0}(Y) \times {}^0G_{I0} + R \times T \times \sum_{s=1}^q a^s \times \sum_{i=1}^{e^s} y_i^s \times \ln(y_i^s) + \sum_{Z>0} \sum_{IZ} P_{IZ}(Y) \times L_{IZ} \tag{2.50}$$

This free enthalpy is related to the atomic molar free enthalpy ${}^0G_{ms}^{\Phi}$ by the following relation:

$${}^0G_{ma}^{\Phi} = \frac{{}^0G_{ms}^{\Phi}}{\sum_{s=1}^q a^s \times (1 - y_{Va}^s)} \tag{2.51}$$

If the description of the phase Φ does not involve vacancies ${}^0G_{ma}^{\Phi} = {}^0G_{ms}^{\Phi}$ **Notations**

As usual, the notation used to indicate the occupation of the sublattices is as follows: the two (:) points separate the elements that are not in the same sublattice while the comma (,) Separates two elements interacting on the same sublattice. For

example, $G_{A,B:C}$ denotes the Gibbs energy of a phase modeled by two sublattices whose elements A, B occupy the first sublattice, C occupies the second. An asterisk "*" instead of an element name means that the sublattice can be filled by any element in the system.

2.2.3.10 Special cases

① Case of a defined compound

One of the limiting cases described by the sub-lattice model is that where each sublattice is occupied by a single element. This case corresponds to that of a stoichiometric compound. The terms ${}^{ref}G^\Phi$ and ${}^{id}G^\Phi$ are then zero, and the total molar free enthalpy is equal to the free molar enthalpy of the compound under consideration.

② Case of a substitutional solution

The other limiting case is to consider only one sublattice. It corresponds to the substitution. The fractions of sites of the single sub-lattice are equal to the molar fractions. The Gibbs free energies of the end-members of a solid solution are those of the pure elements. The equations obtained are identical to the equations of the substitutional solutions.

2.2.4 Conclusion

Using associated models with CALPHAD method requires knowledge of the crystallographic and experimental data of each phase taken into account in the calculation. This chapter enabled us to introduce the various useful models for the thermodynamic description of the studied systems during the thesis and to understand the relation between the thermodynamic stability of a phase and its free enthalpy.

Chapter 3

Results and Discussions

Contents

3.1 Thermodynamics of the intermediate phases in the Tr-Sc systems	51
3.1.1 Introduction	51
3.1.2 Computational methodology	51
3.1.3 Results and discussion	53
3.1.4 Conclusion	58
3.2 The Os-Th and Os-Y systems	60
3.2.1 Introduction	60
3.2.2 Review of literature data	60
3.2.2.1 The binary system Os – Th	60
3.2.2.2 The binary system Os – Y	61
3.2.3 Ab-Initio details	63
3.2.3.1 VASP calculations	63
3.2.3.2 WIEN2k calculations	63
3.2.4 Optimization procedure	64
3.2.5 Results and discussion	64
3.2.6 Conclusion	73
3.3 The Dy-Zn system	74
3.3.1 Introduction	74
3.3.2 Review of literature data	74
3.3.3 Ab initio details	74
3.3.4 Optimization procedure	76
3.3.5 Results and discussion	77
3.3.6 Conclusion	79

3.1 Thermodynamics of the intermediate phases in the Tr-Sc ($Tr=Cd, Ru$) systems

3.1.1 Introduction

Ordered intermetallics have already been established as an essential class of high temperature structural materials. The crystal structure of the B2 (*CsCl*) type is one of the simplest and most common ordered structures. B2-type intermetallics exhibit some of the most exciting and diverse physical phenomena in alloys. One outstanding example is the physical, chemical, and mechanical properties of B2 (*CsCl*)-type aluminides [121], where a large number of theoretical investigations of the electronic structure, the optical properties, the nature of interatomic interactions, and the energetics of defects in the crystal structure of these compounds have been performed in the last 20 years [70, 122].

Scandium presents somewhat similar chemical properties to those of aluminum and has an oxidation number of +3 in almost all of its compounds [123]. Among these compounds, the $TrSc$ ($Tr = Cd, Ru$) have homogeneity range in the central part of the $Tr - Sc$ phase diagrams [124, 125], with a strongly ordered B2 (*CsCl*-type) structure that remain ordered up to their melting points. The B2 structure consists of two interpenetrating simple cubic sublattices, with each sublattice having an equal number of lattice sites (see Fig. 3.1a). In its perfectly ordered state at the stoichiometric composition, one sublattice is entirely occupied by Tr and the other entirely by Sc atoms.

Deviations from the ideal stoichiometry are accommodated by the formation of constitutional (structural) point defects. The existence of these point defects has profound effects on essential properties of B2 alloys as mechanical properties and diffusion mechanisms [126]. Moreover, at finite temperatures, thermal and constitutional defects will be activated due to entropy.

Over the last decade, first principles-based methods (ab initio methods) have now become the most powerful tools for the investigation of a remarkable number of physical and chemical properties for atoms, molecules, and solids. These methods are very predictive since only atomic numbers, and crystal structure information is needed as inputs. The goal of the present paper is to use; supercell and SQS approaches to investigate the constitutional defect structure of $TrSc$ compounds, Wagner-Schottky model to provide insight in thermal defect structure of $TrSc$, where the defect structure of these compounds had not been studied before.

3.1.2 Computational methodology

The special quasi-random structure (SQS) specially designs small-unit-cell periodic structure with only a few (8-32) atoms per unit cell, which closely mimic the most relevant local pair and multi-site correlation functions of the random substitutional alloys [127], [62] [128]. In this work we have used SQS-4 ($A_{0.5}B_{0.5}C$, see Fig. 3.1b) and SQS-16 ($A_{0.75}B_{0.25}C$, see Fig. 3.1c) proposed by Jiang et al. [127], where the generated structures are: Sc anti-site ($Tr_{0.5}Sc_{0.5}Sc$), Tr vacuum ($Tr_{0.5}Va_{0.5}Sc$), Tr anti-site ($Sc_{0.5}Tr_{0.5}Tr$), and Sc vacuum ($Sc_{0.5}Va_{0.5}Tr$) in the SQS-4 structure. Sc anti-site ($Tr_{0.75}Sc_{0.25}Sc$), Tr vacuum ($Tr_{0.75}Va_{0.25}Sc$), Tr anti-site ($Sc_{0.75}Tr_{0.25}Tr$), and Sc vacuum ($Sc_{0.75}Va_{0.25}Tr$) in the SQS-16 structure.

The formation enthalpies of $Tr_{1-x}Sc_x$ alloys can be calculated from the following equation:

$$\Delta H(Tr_{1-x}Sc_x) = E(Tr_{1-x}Sc_x) - (1-x)E(Tr) - xE(Sc) \quad (3.1)$$

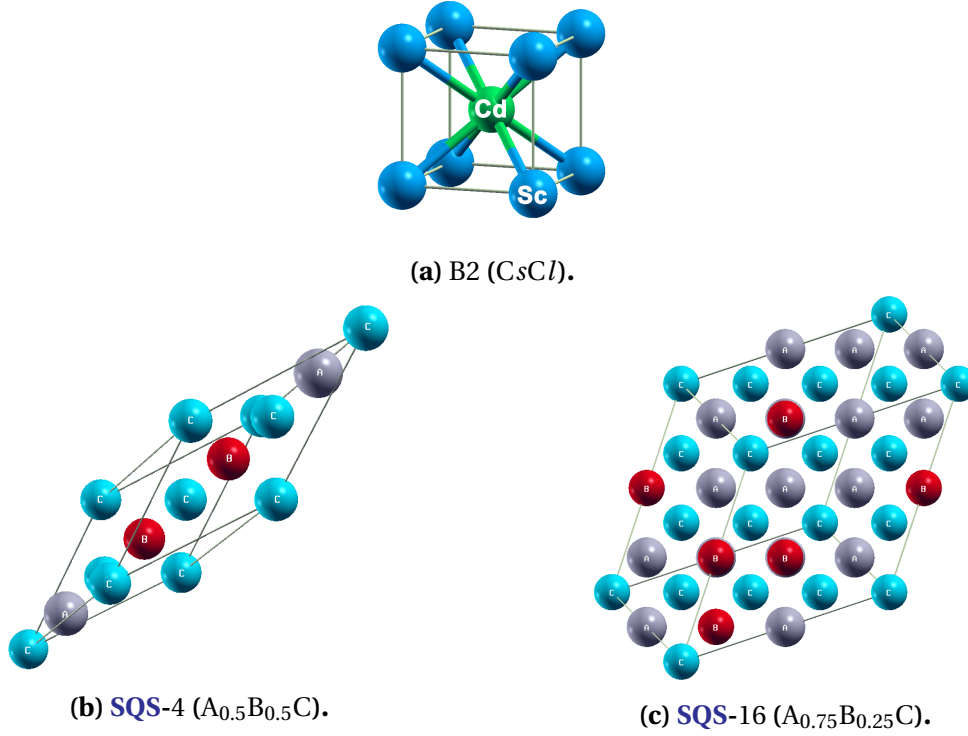


Figure 3.1 – Crystal structures of $Tr_{1-x}Sc_x$.

where $E(Tr)$, $E(Sc)$ and $E(Tr_{1-x}Sc_x)$ are the first-principle calculated total energies per atom of the pure elements Tr ($Tr = Cd, Ru$), Sc and the corresponding alloy, respectively. Here x is the molar composition of Sc in the alloy. Hexagonal close-packed (HCP_A3) Cd , Ru and Sc were used as reference states in Eq. (3.1).

In the SQS approach, for each of the four branches in Fig. 3.2a and 3.2b, formation enthalpies of isolated point defects in stoichiometric B2 $TrSc$ are obtained by fitting the calculated formation enthalpies to a quadratic function of alloy composition in the following form [127]:

$$\Delta H(\chi) = \Delta H_{TrSc} + c_1\chi + c_2\chi^2 \quad (3.2)$$

where $\chi = |x_{Sc} - 0.5|$ is the absolute deviation from stoichiometry and ΔH_{TrSc} is the formation enthalpy of the ordered stoichiometric B2 $TrSc$, which is a linear function of the composition, where the coefficient c_1 represents the tangent and is directly related to the defect formation enthalpies H_d ; since the atomic concentration of defect d is χ for anti-sites and 2χ for vacancies, we have $H_d = c_1$ for anti-sites and $H_d = c_1/2$ for vacancies.

The interactions between point defects of the same type were considered in the SQS calculations, as indicated by the nonlinear quadratic term in Eq. 3.2. The physical means of c_2 coefficient is that two branches in Fig. 3.2a and 3.2b may cross each other at certain composition; in that case, a reversal of the stable constitutional point defects may occur [127]. Such a case is theoretical since the crossover composition is outside of the stable composition range of B2 $TrSc$.

In the present work, calculations were performed using the Projected Augmented Wave (PAW) pseudo-potentials [129, 130] with the generalized gradient approximation as implemented by Perdew, Burke and Erzenfest (GGA-PBE) [54]. A plane wave cutoff energy of 274.265 eV is used. K-point meshes are compiled using the fully automatic scheme [131], which generates centered Monkhorst-Pack [132] grids, where the numbers of subdivisions N_1 , N_2 and N_3 along reciprocal lattice vectors \vec{b}_1 , \vec{b}_2 and \vec{b}_3 , respectively, are

given by:

$$N_i = \max\left(1, l \left| \vec{b}_i \right| + 0.5\right), i = 1, 2, 3 \quad (3.3)$$

Where $\left| \vec{b}_i \right|$ is the norm of the reciprocal lattice vector \vec{b}_i . According to Kresse et al. [131], useful values for the length l vary between 10 (large gap insulators) and 100 (d-metals). In this work, it was found that $l = 50$ is sufficient to achieve convergence to a precision less than 1 *meV/atom* for the B2 TrSc ($Tr = Cd, Ru$). In addition to Monkhorst-Pack k-point meshes, Brillouin-zone integrations are performed using the Methfessel-Paxton technique with the smearing parameter of 0.1 *eV*. All calculations were performed using the ‘‘Accurate’’ setting within VASP, and all the degrees of crystal structures freedom were allowed to relax, including cell shape, volume and atom positions with a preconditioned conjugated gradient (CG) algorithm with the default VASP’s convergence criteria. Finally, relaxed structures are examined using SGROUP program [133]; all resulting structures maintain the initial space-group.

3.1.3 Results and discussion

Defect type	Designation	Supercell*		SQS*
		16-atom	32-atom	
Cd vacancy	Va_{Cd}	1.40	1.44	2.48
Sc anti-site	Sc_{Cd}	1.32	1.12	0.90
Sc vacancy	Va_{Sc}	1.14	1.18	2.18
Cd anti-site	Cd_{Sc}	0.50	0.46	0.39
Triple Cd	$0 \rightarrow 2Va_{Cd} + Cd_{Sc}$	3.30	3.34	5.35
Schottky	$0 \rightarrow Va_{Cd} + Va_{Sc}$	2.54	2.62	4.66
Exchange	$0 \rightarrow Sc_{Cd} + Cd_{Sc}$	1.82	1.58	1.29
Triple Sc	$0 \rightarrow 2Va_{Sc} + Sc_{Cd}$	3.60	3.48	5.26
Interbranch Cd	$Cd_{Sc} \rightarrow 2Va_{Sc}$	1.78	1.9	3.97
Interbranch Sc	$Sc_{Cd} \rightarrow 2Va_{Cd}$	1.48	1.76	4.06

* Unit: *eV/defect*

(a) B2 CdSc

Defect type	Designation	Supercell*		SQS*
		16-atom	32-atom	
Ru vacancy	Va_{Ru}	0.17	0.75	0.90
Sc anti-site	Sc_{Ru}	0.98	0.27	0.62
Sc vacancy	Va_{Sc}	4.25	4.07	2.53
Ru anti-site	Ru_{Sc}	1.21	1.22	1.18
Triple Ru	$0 \rightarrow 2Va_{Ru} + Ru_{Sc}$	1.55	2.72	2.98
Schottky	$0 \rightarrow Va_{Ru} + Va_{Sc}$	4.42	4.82	3.43
Exchange	$0 \rightarrow Sc_{Ru} + Ru_{Sc}$	2.19	1.49	1.80
Triple Sc	$0 \rightarrow 2Va_{Sc} + Sc_{Ru}$	9.48	8.41	5.68
Interbranch Ru	$Ru_{Sc} \rightarrow 2Va_{Sc}$	7.29	6.92	3.88
Interbranch Sc	$Sc_{Ru} \rightarrow 2Va_{Ru}$	-0.64	1.23	1.18

* Unit: *eV/defect*

(b) B2 RuSc

Table 3.1 – First-principles calculated formation enthalpies of isolated point defects and complex composition-conserving defects in stoichiometric B2 TrSc[122]

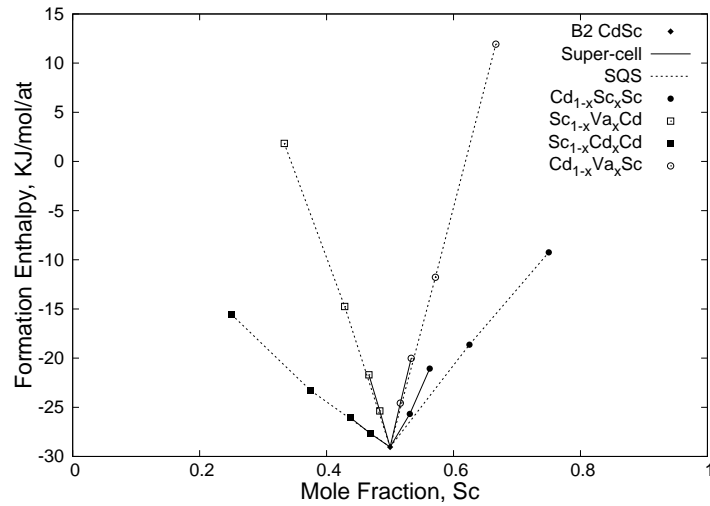
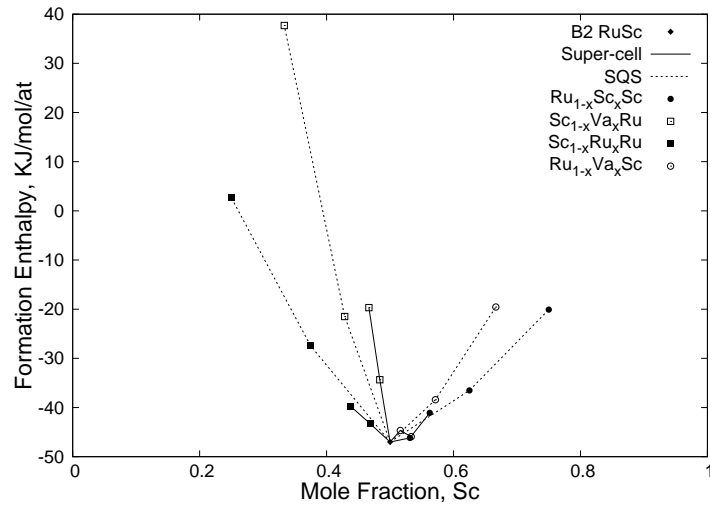
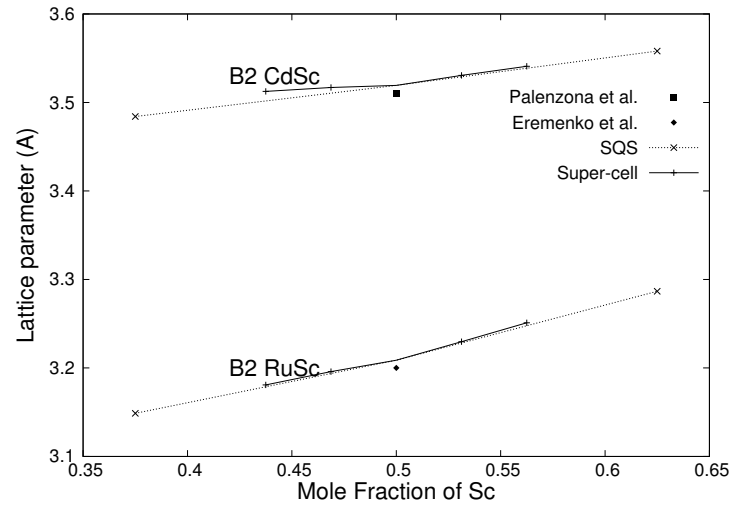
(a) $Tr = Cd$ (b) $Tr = Ru$

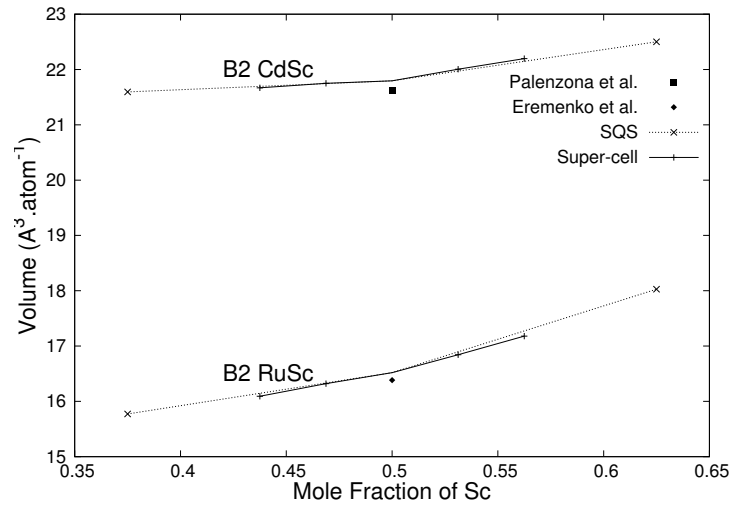
Figure 3.2 – Comparison between first-principles calculated formation enthalpies using supercell and SQS approaches for B2 $TrSc$ as a function of composition[122].

Fig. 3.2a and 3.2b show the formation energies of the B2 $CdSc$ and $RuSc$ as a function of composition, simulated with a 16-atom and a 32-atom supercells, compared to the formation energies obtained using the special quasi-random structure approach and the experimental ones [134]. As a result, calculations using supercell and SQS approaches are in good agreement, specifically in the Cd -rich and Ru -rich sides of the B2 $CdSc$ and $RuSc$ compounds, respectively. In Sc -rich side of B2 $CdSc$ and $RuSc$, the calculated alloy formation enthalpies using supercell and SQS approaches agree with each other and give the same prediction of the ascending order of the formation energies. Sometimes the supercell approach fails when determining the formation enthalpy in high defect concentration. The enthalpy of formation of the $RuSc$ compound in this work is in good agreement within the determined by direct synthesis calorimetry [134] within the expected uncertainty limits.

Fig. 3.2a shows that the lower branches of the alloy formation energy for Cd -rich and Sc -rich $CdSc$ correspond to constitutional anti-site Cd and anti-site Sc atoms, respectively. Similarly, figure 3.2b shows that branches containing the constitutional anti-site Ru



(a) Lattice parameter



(b) Volume

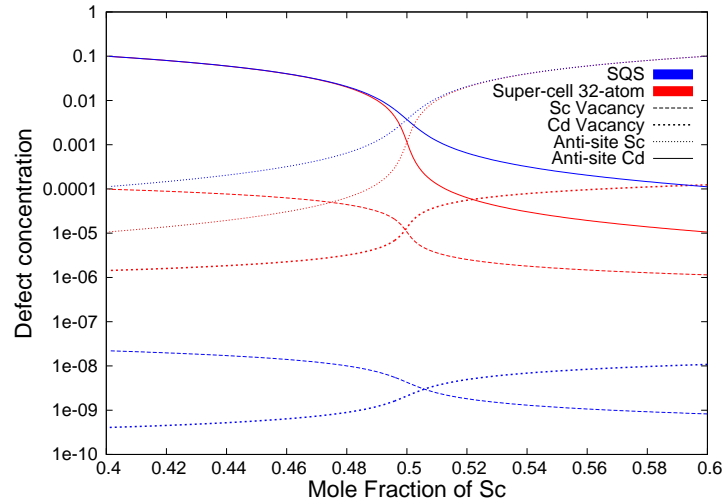
Figure 3.3 – Structural equilibrium of B2 *CdSc* and *RuSc* alloys as a function of composition[122].

and anti-site *Sc* atoms are the lower branches in *Ru*-rich and *Sc*-rich *RuSc*, respectively.

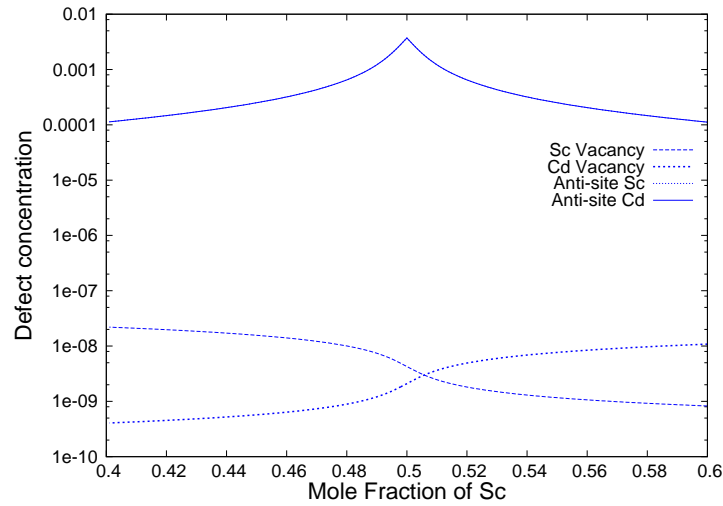
The calculated lattice parameter using supercell and SQS approaches of B2 *CdSc* and *RuSc* alloys are shown in Fig. 3.3a and compared to the available experimental data [124, 135], the calculated volume using supercell and SQS approaches of B2 *CdSc* and *RuSc* alloys are shown in figure 3.3b and compared to the available experimental data [124, 135]. The present results are consistent with the available experimental data.

The formation energies of different type of single point defects are listed in tables 3.1a and 3.1b for B2 *CdSc* and *RuSc*, respectively. All three sets of results are consistent with each other. There is only a numerical difference in defect formation energies using different sets of parameters for the supercell and SQS approaches. It is clear from the results that the enthalpies of supercell converge to the SQS enthalpies as the cell becomes larger.

B2 *TrSc* alloys become rich in *Sc* by introducing anti-site *Sc* atoms or *Tr* vacancies; where they become rich in *Tr* by introducing anti-site *Tr* atoms or *Sc* vacancies. From Table 3.1, in *sc*-rich region, anti-site *sc* defect have a minimal energy than the *Tr* vacancy, and in *Tr*-rich region, anti-site *Tr* have a minimal energy than the *Sc* vacancy. Calcu-



(a) Total defect

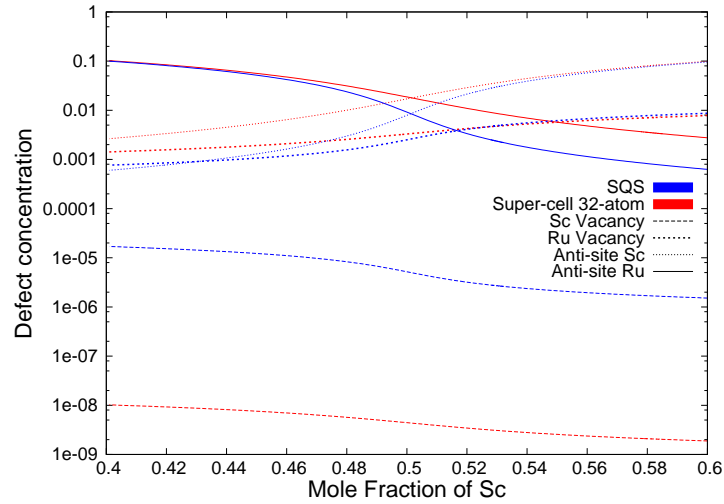


(b) Thermal defect

Figure 3.4 – Equilibrium defect concentrations in B2 $CdSc$ at $T = 1428$ K as a function of composition[122].

lated formation enthalpies of isolated point defects from Super-cell (16/32 atoms) and SQS approaches are in good agreement with results in Fig. 3.2a and 3.2b, where the lower branches are anti-site Sc and anti-sites Tr , in Sc -rich and Tr -rich regions, respectively.

At 1428K and zero external pressure, the calculated equilibrium atomic concentrations of defects x_d in $CdSc$ are shown in Fig. 3.4a as a function of composition. The main defects in Cd -rich $CdSc$ are anti-site Cd atoms, and in Sc -rich $CdSc$ are anti-site Sc atoms. It is useful to substitute constitutional defects that are present at ground state at $T = 0K$, to separate thermal defects which appear at a finite temperature. The concentrations of thermal defects x_d^t using SQS approach in $CdSc$ at 1428K are plotted in Fig. 3.4b. It can be observed that the dominant thermal defects are anti-sites Cd and anti-site Sc in all compositions with equal amounts, which are the constituents of an exchange defect. Additionally, one can observe in table 3.1a that exchange defect type presents the minimal energy in super-cell (32 atoms) and SQS approaches results; But super-cell (16 atoms) result shows that interbranch Sc defect presents the minimal energy, and this is due to failure of super-cell approach in high defect concentration, where we need a larger



(a) Total defect

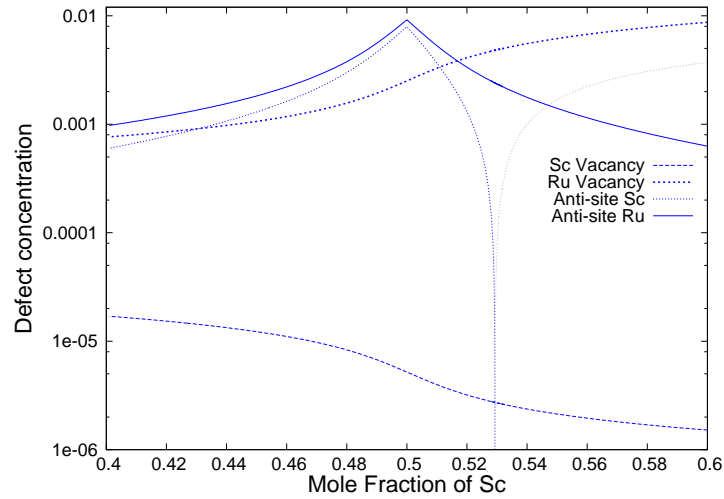

 (b) Thermal defect; anti-site *Sc* grey branch is negative.

Figure 3.5 – Equilibrium defect concentrations in B2 *RuSc* at $T = 2373\text{K}$ as a function of composition.

super-cells to get an accurate results.

The calculated equilibrium atomic concentrations of defects x_d in *RuSc* at 2373K and zero external pressure are shown in Fig. 3.5a as a function of composition. The main defects in *Ru*-rich *RuSc* are anti-site *Ru* atoms. However, the main defects in *Sc*-rich *RuSc* are anti-site *Sc* atoms, with small amounts of *Ru* Vacancies and anti-site *Sc* atoms. It is useful to substitute constitutional defects that are present in the ground state at $T = 0\text{K}$, to separate thermal defect which appears at a finite temperature. The concentration of thermal defects x_d^t using SQS approach in *RuSc* at 2373K are plotted in Fig. 3.5b. The dominant thermal defects in *Ru*-rich *RuSc* are anti-site *Ru*, anti-site *Sc* and *Ru* vacancies. However, in *Sc*-rich *RuSc*, the dominant thermal defects are *Ru* vacancies and anti-site *Ru*.

Apparently, the defect structures in the *Sc*-rich side are of complex nature, where the concentration of anti-site behaves even more interestingly and decreases rapidly with deviation from stoichiometry. The concentration of thermally formed anti-site *Sc* becomes negative when the composition exceeds the value of 0.53. Meyer and Fähnle [136] showed

that this kind of thermal behavior could be associated only with the interbranch Sc defect, in which two Ru vacancies replace one anti-site Sc .

Fig. 3.5b shows that: $x(Va_{Ru}) = 2.34x(Sc_{Ru})$ and $x(Ru_{Sc}) = 0.17x(Sc_{Ru})$. If we consider the concentration of anti-sites Sc as a unit, there are: one unit of anti-sites Sc is replaced by two units of Ru vacancies with an interbranch Sc defect type, and 0.34 units of Ru vacancies with 0.17 units of anti-site Ru are formed by triple Ru defect type. Consequently, the dominant defect type in Sc -rich $RuSc$ is interbranch Sc . As can be seen in table 3.1b the triple Ru and interbranch Sc have the minimal energy of formation. Therefore in Ru -rich $RuSc$, the defects will most likely be formed by a mixture of these two types of defects.

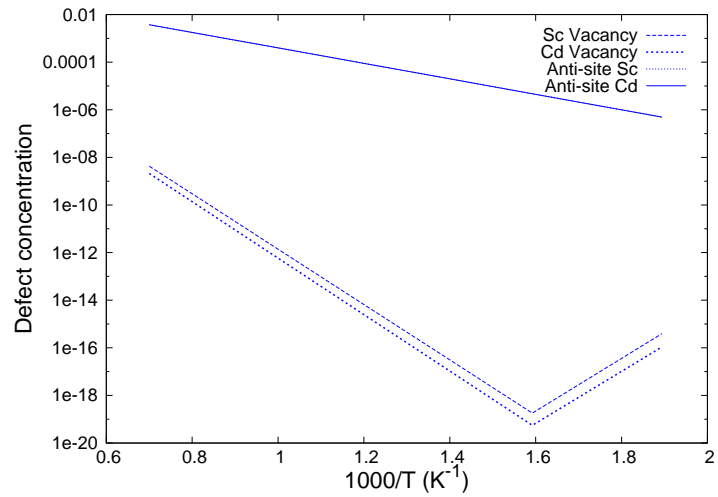
Fig. 3.6a and 3.6b show the predicted equilibrium point defect concentrations were plotted as a function of temperature in stoichiometric B2 $CdSc$ and $RuSc$, respectively. It can be observed that exchange defects dominate at all temperature in B2 $CdSc$, whereas the defects type in B2 $RuSc$ are of a complex nature.

Finally, in Fig. 3.7, the enthalpy of $RuSc$ phase was plotted as a function of molar fraction of Sc element using the Wagner-Schottky model, and compared with the enthalpy from theoretical study using CALPHAD (CALculation of PHase Diagram) method [125]. There is a reasonable agreement between our results and those using CALPHAD method [125]. The discrepancies of Wagner-Schottky and first principles regarding CALPHAD calculated enthalpy are probably due to the formation of vacancies which was not contemplated in CALPHAD method, where the $RuSc$ phase was modeled using the sublattice formalism based on B2 structure [125].

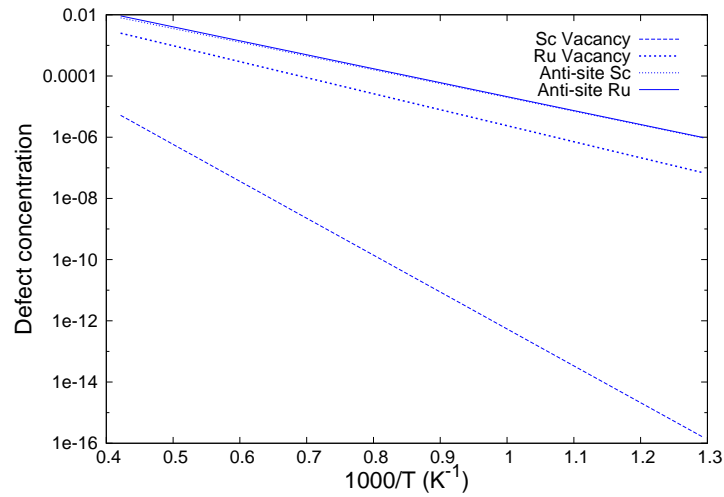
3.1.4 Conclusion

Point defect structure of B2 $TrSc$ ($Tr = Cd, Ru$) alloys was investigated using supercell and special quasi-random structure (SQS) approaches. According to our results, Tr and Sc anti-sites are the constitutional point defects in Tr -rich and Sc -rich B2 $TrSc$, respectively. To investigate the thermal defect concentrations at finite temperatures, we adopted the Wagner-Schottky model using point defect formation enthalpies obtained from supercell and SQS approaches. The present results suggest that the predominant thermal defects in B2 $CdSc$ are of exchange type, and in B2 $RuSc$ are of interbranch Sc type. The calculated results show an agreement with the available theoretical and experimental data.

In the present study, we have obtained the formation enthalpies of isolated point defects in stoichiometric B2 $CdSc$ and $RuSc$ utilizing the supercell and special quasi-random structure approaches. The present work shows that Cd anti-sites and Sc anti-sites are the constitutional point defects in Cd -rich and Sc -rich B2 $CdSc$, respectively. Moreover, Ru anti-sites and Sc anti-sites are the constitutional point defects in Ru -rich and Sc -rich B2 $RuSc$, respectively. Using the Wagner-Schottky model, we have also calculated the thermal defect concentrations at finite temperatures. Our results suggest that the predominant thermal defects in B2 $CdSc$ are of exchange type, and the predominant thermal defects in B2 $RuSc$ are interbranch of Sc type.



(a) B2 CdSc



(b) B2 RuSc.

Figure 3.6 – Equilibrium of defect concentration in stoichiometric B2 TrSc as a function of temperature.

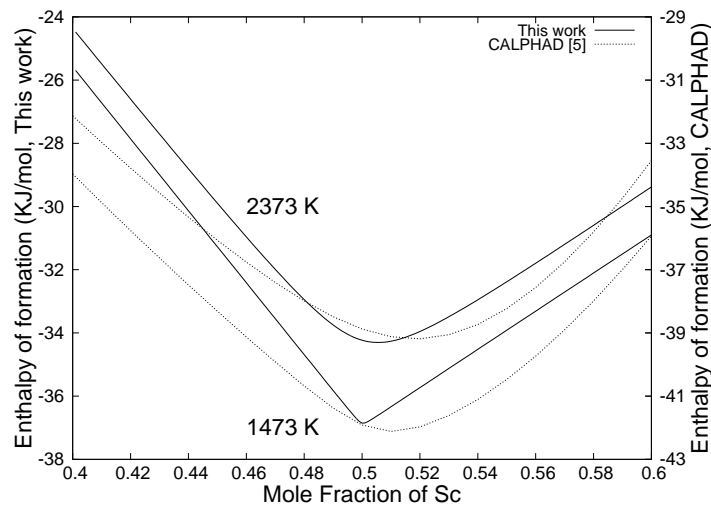


Figure 3.7 – Enthalpy of formation of RuSc phase as a function of molar fraction of Sc [122].

3.2 Thermodynamic and ab-initio investigations of the Os-Th and Os-Y systems

3.2.1 Introduction

In recent years, [Platinum-Group Metals \(PGMs\)](#) have attracted much attention as potential ultra-high-temperature structural materials, due to their unique high-temperature mechanical and corrosion resistant properties [137–139]. Solid solubilities as well as open lattice structures obtained by alloying PGMs with [Rare Earth Metals \(REM\)](#) have made these systems of great physical and metallurgical interest [140]. The strength of the Pt – Pd – Rh alloys, which are the main catalytic materials used for the preparation of nitric acid by the ammonia oxidation reaction, can be improved by rare earth additions; such as yttrium, cerium, gadolinium and thorium [140–142].

The PGMs have high melting points; for instance, Pt, Rh and Os melt at 2042K, 2239K and 3306K, respectively. They also have excellent corrosion resistance against a wide range of liquid and gaseous substances, and stable at high-temperatures under conditions where the base and refractory metals are easily oxidized [143]. According to the phase equilibria studies on the Os – RE systems, where RE is the lanthanide rare earth yttrium or the actinide rare earth thorium, only Os_2Th and Os_2Y melt above $T = 2500K$, and the remaining Os – RE compounds melt above $T = 1500K$. Obviously, these alloys are one of the most attractive candidate materials for ultra-high-temperature applications. However, thermodynamic properties of these alloys are poorly known. Therefore, the purpose of this work was to reveal ambiguities and contribute new data concerning the thermodynamic properties of alloys and compounds in the Os – RE (RE = Th, Y) systems. The thermodynamic properties of alloys in the Os – RE (RE = Th, Y) systems have been investigated by the first-principle methods. Thermodynamic assessments of the Os – RE systems have been done using the CALPHAD (CALculation of PHase Diagram) method.

We present in this chapter the thermodynamic evaluation we have performed on all the composition and temperature domains of the binary systems Os – Y and Os – Th employing the CALPHAD technique. The term excess Gibbs energy of the phases in solution present in this system (liquid, *bcc_A2*, *fcc_A1* et *hcp_A3*) was evaluated by the linear dependence of Temperature of the Redlich and Kister [103] polynomial equation using a [Solution Model \(SM\)](#). Intermetallic compounds are considered stoichiometric and therefore processed by a model involving [Two Sublattices Model \(TSM\)](#). As we have already indicated in section 2.2, the reference Gibbs energies of the pure elements used in this work are those published by Dinsdale [111].

The lack of experimental thermodynamic data on the systems Os – Y and Os – Th led us to calculate [Ab Initio](#) to estimate the enthalpy of formation of the stoichiometric compounds existing in this system, to enhance optimization.

3.2.2 Review of literature data

3.2.2.1 The binary system Os – Th

After studies by the metallographic and X-ray methods, Thomson [144] was first to report the Os – Th phase diagram in the temperature range from 1273 to 1773 K. This tentative phase diagram of Thomson [144] did not include data above $T = 1773K$, in which melting points of all alloys in the Os – Th system exist.

Kleykamp [145] has determined the Gibbs energies of formation for the intermediate phases in the Os – Th system by the electromotive force measurements (EMF) method.

In his studies, the rich osmium region of the phase diagram has been supplemented by determining the melting point of pyrometric. The results of both authors have been compiled by Moffatt [146] and later on by Massalski [147] to construct the complete phase diagram.

The Os–Th system is characterized by three intermetallic compounds (Os_2Th , Os_2Th_3 , and Os_3Th_7) and three terminal solution phases (HCP_A3 (Os), FCC_A1 (Th), and BCC_A2 (Th)). Os_2Th crystallizes congruently at $T = 2753K$, and forms an eutectic with osmium at $2493K$ and $25at.\%Th$ [145]. Os_3Th_7 crystallizes also congruently above $T = 1773K$ and forms an eutectic with thorium at $T = 1560K$ and $87at.\%Th$ [144]. Whereas the Os_2Th_3 compound forms peritectically and also melts above $T = 1773K$, it forms an eutectic with Os_3Th_7 at $T = 1755K$ and $64at.\%Th$ [144]. By using the metallographic examination, Thomson [144] found that the solubility of osmium in thorium is considerably less than $1at.\%Th$ at $T = 1373K$ and very low at $T = 873K$, and the allotropic transformation of thorium has been assumed to be $T = 1633K$. The crystallographic structures data of the pure elements, Os_2Th , and Os_3Th_7 were determined by several authors [144, 148–153] and they are listed in table 3.2.

^a Local Density Approximation refined by [50] (LDA-CA) (VASP), ^b Generalized Gradient Approximation as implemented by [54] (GGA-PBE) (VASP), ^c GGA-PBE (WIEN2k), ^d At 1723 K.

Thomson [144] reported difficulties with Os_2Th_3 alloys in the composition range from (50 to 65) $at.\%Th$, because the lumps of un-melted osmium which hindered the determination of the precise composition of the Os_2Th_3 compound. He designated it by $ThOs_x$ ($60at.\%Th$). However, Kleykamp [145] assumed that the composition of the compound to be Os_2Th_3 , without determining its crystal structure.

3.2.2.2 The binary system Os – Y

The Os – Y system consists of three terminal solution phases (HCP_A3 (Os), HCP_A3 (Y), and BCC_A2 (Y)) and two intermetallic compounds (Os_2Y and OsY_3). The Os_2Y compound crystallizes congruently at $T \approx 2773K$ [147], and form an eutectic with osmium at $T = 2373K$ and $6at.\%Y$ [158], whereas the OsY_3 compound crystallizes peritectically at $T = 1563K$, and forms an eutectic with yttrium at $T = 1423K$ and $\sim 88at.\%Y$ [158]. The crystal structures data of Os, Y, Os_2Y , and OsY_3 shown in table 3.2 were adopted from [148, 149, 154–157].

Savitskii and Polyakova [158] and Selhaoui and Kleppa [134] are the only authors who reported experimental data in the Os-Y system. Selhaoui and Kleppa [134] determined the standard enthalpy of formation of the compound Os_2Y by using high-temperature calorimetry. Massalski [147] compiled these experimental data and also estimated the allotropic transformation of yttrium to be at $T = 1751K$, which was not reported in the literature.

Savitskii and Polyakova [158] and Selhaoui and Kleppa [134] are the only authors who reported experimental data in the Os-Y system. Selhaoui and Kleppa [134] determined the standard enthalpy of formation of the compound Os_2Y by using high-temperature calorimetry. Massalski [147] compiled these experimental data and also estimated the allotropic transformation of yttrium to be at $T = 1751K$, which was not reported in the literature.

3.2. THE OS-TH AND OS-Y SYSTEMS

Phase	Comp. (at.%)	Pearson symbol and prototype	Space group	Lattice parameters (nm)			Ref.
Os	~ 0	<i>hP2</i> (Mg)	$P6_3/mmc$	0.27344	0.27344	0.43173	[148]
				0.27196	0.27196	0.42920	[142] ^a
				0.27552	0.27552	0.43358	[142] ^b
				0.27574	0.27574	0.43485	[142] ^c
Os_2Th	~ 33.3	<i>cF24</i> (MgCu ₂)	$Fd-3m$	0.7715	0.7715	0.7715	[144]
				0.7705	0.7705	0.7705	[149]
				0.7703	0.7703	0.7703	[150]
				0.7602	0.7602	0.7602	[142] ^a
				0.7725	0.7725	0.7725	[142] ^b
Os_3Th_7	70	<i>hP20</i> (Th ₇ Fe ₃)	$P6_3mc$	1.0031	1.0031	0.6296	[151]
				0.9835	0.9835	0.6179	[142] ^a
				1.0044	1.0044	0.6333	[142] ^b
<i>Th(rt)</i>	~ 100	<i>cF4</i> (Cu)	$Fm-3m$	0.50863	0.50863	0.50863	[144]
				0.50842	0.50842	0.50842	[152]
				0.49047	0.49047	0.49047	[142] ^a
				0.50548	0.50548	0.50548	[142] ^b
				0.50508	0.50508	0.50508	[142] ^c
<i>Th(ht)</i>	~ 100	<i>cI2</i> (W)	$Im-3m$	0.411	0.411	0.411	[153] ^d
Os_2Y	~ 33.3	<i>hP12</i> (MgZn ₂)	$P6_3/mmc$	0.5308	0.5308	0.8794	[149]
				0.5307	0.5307	0.8786	[154]
				0.5231	0.5231	0.8750	[142] ^a
				0.5311	0.5311	0.8881	[142] ^b
				0.5278	0.5278	0.8803	[142] ^c
OsY_3	75	<i>oP16</i> (Fe ₃ C)	$Pnma$	0.7418	0.9108	0.6317	[155]
				0.7425	0.9132	0.6337	[156]
				0.7274	0.8892	0.6209	[142] ^a
				0.7412	0.9097	0.6351	[142] ^b
Y	~ 100	<i>hP2</i> (Mg)	$P6_3/mmc$	0.36474	0.36474	0.5730	[157]
				0.35388	0.35388	0.55202	[142] ^a
				0.36423	0.36423	0.56190	[142] ^b
				0.36658	0.36658	0.56725	[142] ^c

^a LDA-CA (VASP), ^b GGA-PBE (VASP), ^c GGA-PBE (WIEN2k), ^d At 1723 K

Table 3.2 – The crystal structure data of the Os-Y and Os-Th systems.

3.2.3 Ab-Initio details

In this work, first-principles calculations based on DFT [49] were performed by using VASP [159, 160] and WIEN2k package [161] to get the energy of formation of intermetallic compounds in the Os – Th and the Os – Y systems.

The energy of formation at T = 0K (which also corresponds to the enthalpy of formation) for the compounds (Os₂Th, Os₂Th₃, Os₃Th₇, Os₂Y, and OsY₃) is obtained by the equation (1.59), with SER HCP_A3 (Os), FCC_A1 (Th), and HCP_A3 (Y).

3.2.3.1 VASP calculations

With VASP, calculations were performed using the PAW pseudo-potentials [129, 130] with the LDA-CA and the GGA-PBE. A plane wave cut off energy of 300eV was used. K-point meshes were compiled using the fully automatic scheme [131], which generates Γ centered Monkhorst-Pack grids [132], where the numbers of subdivisions N₁, N₂, and N₃ along reciprocal lattice vectors \vec{b}_1 , \vec{b}_2 , and \vec{b}_3 , respectively, are given by:

$$N_i = \max\left(1, l \left| \vec{b}_i \right| + 0.5\right), i = 1, 2, 3 \quad (3.4)$$

Where $\left| \vec{b}_i \right|$ is the norm of the reciprocal lattice vector \vec{b}_i . According to Kresse et al. [131], useful values for the length l vary between 10 (large gap insulators) and 100 (d -metals). In this work, we found that $l = 60$ is sufficient to achieve convergence to a precision less than 1 meV/atom atom for all compounds of both Os – Th and Os – Y systems. In addition to Monkhorst-Pack k-point meshes, Brillouin-zone integrations are performed using the Methfessel-Paxton technique with the smearing parameter of 0.1 eV. All calculations were performed using the “Accurate” setting within VASP, and all degrees of freedom of the crystal structures were allowed to relax, including cell shape, volume, and atom positions with a preconditioned Conjugated Gradient (CG) algorithm with the default VASP’s convergence criteria.

The phonon spectra were calculated by Phonopy [162], using the finite displacement method [163] on VASP’s minimized structures that had the lowest ground state energy. The force constants were extracted from VASP’s calculations, and the corresponding vibrational frequencies and entropies of the compounds (Os₂Th, Os₂Y, and OsY₃) are achieved. In fact, we have calculated the Helmholtz energy, which can be approximated to the Gibbs energy at zero stress.

Firstly, we re-minimized the crystal structures of the compounds (Os₂Th, Os₂Y, and OsY₃) using the value 10 – 8eV as accuracy for the electronic ground-state calculation. Then, different 2 × 2 × 2 super-cell structures with 0.01Å displacements were created. In the present cases, the Monkhorst–Pack grids were 2 × 2 × 1, 4 × 4 × 4, and 1 × 1 × 2 for these supercells of the compounds Os₂Th, Os₂Y, and OsY₃, respectively, and the other calculation parameters were kept the same.

3.2.3.2 WIEN2k calculations

The PAW method is almost as fast as the usual Ultra Soft Pseudo Potential (US-PP) method [132, 164, 165], and gives very close energies to the best Full-Potential Linearized Augmented Plane Wave (FP-LAPW) calculations [166]. All-electron DFT calculations using the FP-LAPW method are considered to give the most accurate results apart from the errors associated with the exchange-correlation functional, but they are computationally intensive. In this work, all-electron DFT calculations are limited to the Os₂Th and Os₂Y

compounds, where the other compounds are excluded, due to their complex structures and many degrees of freedom, which require a larger computational capacity than our computing abilities.

WIEN2k calculations are based on the Full-Potential (Linearized) Augmented Plane Wave plus local orbitals (FP-(L)APW+lo) [167] method. The GGA-PBE [54] was employed for the exchange and correlation potential. Muffin-tin radii of 2.32, 2.50, and 2.38 *a.u* were assumed for Os, Th, and Y, respectively. The value of RK_{max} was fixed at 9.0, which almost corresponds to the 15.05 Ry (204.67eV) cut off energy. The modified tetrahedron method [167, 168] was adopted for the k-space integration. The numbers of irreducible k-points were 104 and 165 for Os_2Th and Os_2Y , respectively. The convergence of total energy was carefully checked by 0.001 *mRy/(formulaunit)*. Firstly, *c/a* ratio of the Os_2Y compound and the pure elements (Os and Y) was optimized using the 2D-optimize package [169]. Then, the total energy of the intermetallic compounds (Os_2Th and Os_2Y) and the pure elements (Os, Th, and Y) was calculated as a function of volume and was fitted to the second order Birch-Murnaghan [170] state equation. Atom positions of Os_2Y compound were allowed to relax using the Multi Secant Rank One A (MSR1a) [167] algorithm in all calculations, and the forces were converged to less than 1 *mRy/au*. An energy convergence criterion of 10^{-4} Ry for electronic structure self-consistency was used in all calculations.

3.2.4 Optimization procedure

Optimizations of the model parameters of Gibbs energies were done by the CALPHAD method [29][45]. In both Os – Th and Os – Y binary systems thermodynamic interaction parameter optimization is based on the available experimental data and our enthalpies and entropies of formation determined by the first-principles and phonon calculations.

The set of thermodynamic parameters of the Os – Th and Os – Y systems were optimized using the PARROT module of the Thermo-Calc software developed by Jansson [31] and Sundman et al. Sundman et al. [30], Sundman and Ågren [119]. This program works by minimizing an error sum where each of the selected values is given a specific weight. The weight is chosen by personal judgment and changed by trial and error during the work until most of the selected experimental and first-principles, and phonon calculations are reproduced within the expected uncertainty limits.

The modeling of the Os – Th and the Os – Y systems was made in two main steps. Firstly, all thermodynamic parameters were optimized in one operation by using all available enthalpies and entropies of formation for the intermetallic compounds with the same weighting but higher than the weight of other experimental equilibrium data, than changing the weight step by step to achieve a good agreement. We observed that higher weight for first-principles results leads to a better agreement. For melt temperatures of Os_2Th_3 and Os_3Th_7 we used the predicted values by dashed lines [144, 147] as alternative values with the smallest weight, and then we suspended these alternative values from optimization. In the second step, a global optimization was performed by unfixing the enthalpies of formation for the intermetallic compounds, where the entire thermodynamic parameters of all phases are adjusted simultaneously to ensure the best fit.

3.2.5 Results and discussion

In the first attempt, we have calculated the enthalpy of formation for the Os_2Th_3 compound in several crystal structures, in the hope that we will find a crystal structure that

fits well in the convex hull of the ground state of the Os – Th system.

We found 14 crystal structures in the literature for the A_2B_3 compounds [171–184]. The calculated lattice parameters and their enthalpies of formation are listed in table 3.3. The crystal structure $tI140$ (Y_3Rh_2) have the smallest enthalpy among the 14 structures, which makes the Os_2Th_3 compound firmly a ground state, this value was used as the initial enthalpy for this compound in the optimization.

Pearson symbol and prototype	Space group	Lattice parameters (nm)			ΔH_f [142] ^a	Ref. ^b
		[142] ^a				
$tI140(Y_3Rh_2)$	$I4/mcm$	0.1123	0.1123	0.2552	-28.911	[171]
$hR45(Er_3Ni_2)$	$R-3$	0.7492	0.7492	0.7492	-28.195	[172]
$mS20(Dy_3Ni_2)$	$C2/m$	0.7188	0.7188	0.9563	-25.063	[173]
$tP20(Zr_3Al_2)$	$P4_2/mnm$	0.7675	0.7675	0.7820	-24.329	[174]
$pP20(Gd_3Al_2)$	$P4_2nm$	0.7678	0.7678	0.7816	-24.329	[175]
$tP10(U_3Si_2)$	$P4/mbm$	0.7677	0.7677	0.3939	-22.607	[176]
$hP10(Pt_2Sn_3)$	$P6_3/mmc$	0.4277	0.4277	1.6086	-20.910	[177]
$oP20(Pt_2Ge_3)$	$Pnma$	2.0918	0.4136	0.5794	-19.386	[178]
$hP30(Al_2O_3)$	$Ia-3$	0.7464	0.7464	0.7464	-15.800	[179]
$cI80((Mn_{0.5}Fe_{0.5})_2O_3)$	$Ia-3$	1.1346	1.1346	1.1346	-12.444	[180]
$oP40(Pt_3Ge_2)$	$Pnma$	1.5625	0.8799	0.7078	-0.272	[181]
$oS20(La_2Ni_3)$	$Cmca$	0.5311	0.5311	0.8553	1.847	[182]
$oS20(V_2B_3)$	$Cmcm$	0.3026	1.8115	0.2954	16.694	[183]
$hP20(Tl_2Pt_3)$	$P6_3/mmc$	0.6943	0.6943	1.3502	27.109	[184]

^a LDA-CA(VASP).

^b Reference of the initial crystal structure used in VASP calculation for the Os_2Th_3 compound.

Table 3.3 – The crystal structure data and the enthalpy of formation at 0 K of the Os_2Th_3 compound with the composition 60% at. thorium.

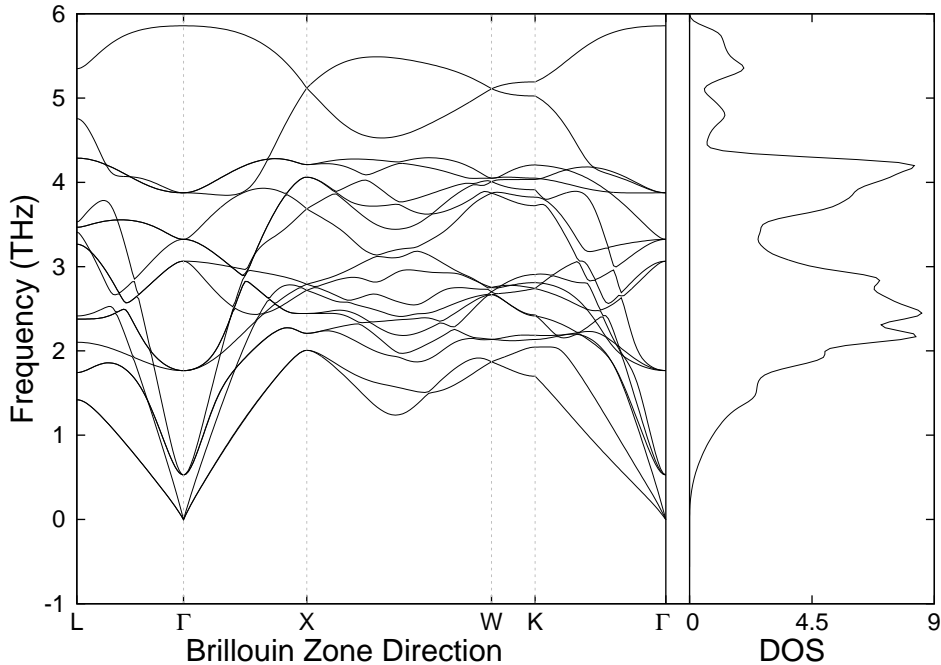


Figure 3.8 – Phonon dispersion curves along high symmetry directions and total DOS for Os_2Th .

Figures 3.8 to 3.10 show the phonon spectra for the compounds Os_2Th , Os_2Y , and OsY_3 , respectively. All of the frequencies estimated by Phonopy were positive, and therefore all of the structures are stable.

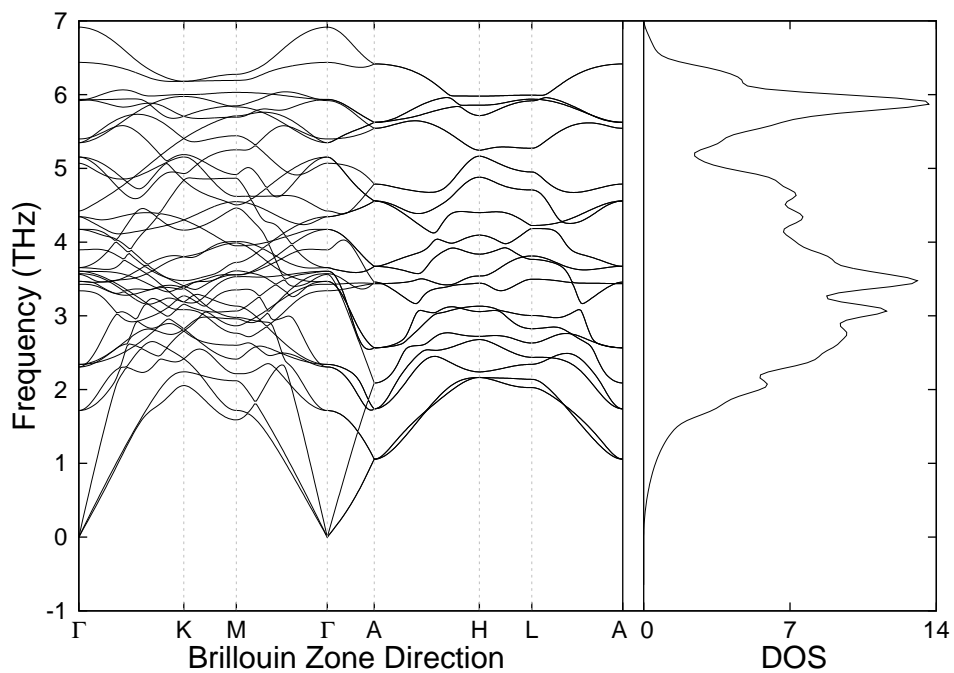


Figure 3.9 – Phonon dispersion curves along high symmetry directions and total DOS for Os_2Y .

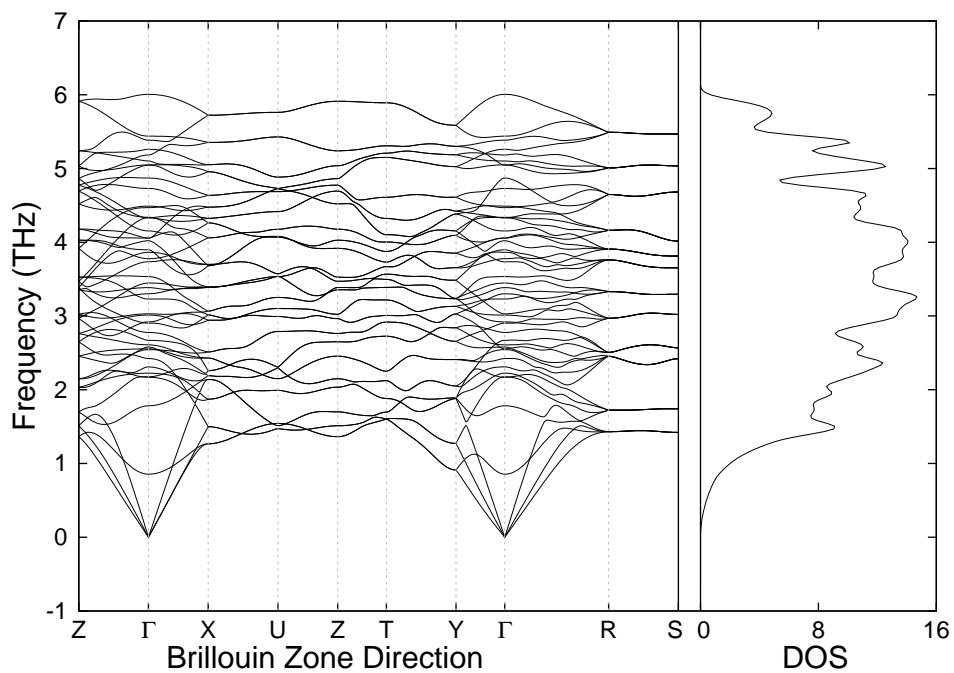


Figure 3.10 – Phonon dispersion curves along high symmetry directions and total DOS for OsY_3 .

The calculated enthalpies of formation using first-principle method for the stoichiometric compounds (Os_2Th , Os_2Th_3 , Os_3Th_7 , Os_2Y , and OsY_3) are presented in table 3.4, where the reference states are (HCP_A3) Os, (FCC_A1) Th, and (HCP_A3) Y. These calculated enthalpies of formation were used in the thermodynamic modeling of the Os – Th and the Os – Y systems.

Compound	ΔH_f KJ/mol	ΔS_f J/K/mol	Method	Ref.
Os_2Th	-53.5 ± 4.2	-16.6 ± 4.9	EMF (1200 K)	[145]
	-55		Miedema model	[185]
	-21.720		VASP (LDA)	[142]
	-24.989		VASP (GGA-PBE)	[142]
	-23.380		WIEN2k	[142]
	-25.929	-2.179	CALPHAD	[142]
Os_2Th_3	-67 ± 3.4	-28 ± 3.9	EMF (1200 K)	[145]
	-41		Miedema model	[185]
	-28.911		VASP (LDA)	[142]
	-32.468		VASP (GGA-PBE)	[142]
	-30.749	-2.724	CALPHAD	[142]
Os_3Th_7	-62.5 ± 2.8	-26.7 ± 3.2	EMF (1200 K)	[145]
	-36		Miedema model	[185]
	-28.168		VASP (LDA)	[142]
	-33.029		VASP (GGA-PBE)	[142]
	-29.203	-2.858	CALPHAD	[142]
Os_2Y	-24.8 ± 2.8		Calorimetry	[134]
	-38		Miedema model	[185]
	-28.430		VASP (LDA)	[142]
	-31.183		VASP (GGA-PBE)	[142]
	-28.754		WIEN2k	[142]
	-31.731	-1.489	CALPHAD	[142]
OsY_3	-30		Miedema model	[185]
	-22.685		VASP (LDA)	[142]
	-24.892		VASP (GGA-PBE)	[142]
	-23.030	-5.794	CALPHAD	[142]

Table 3.4 – The enthalpies of formation of compounds in the Os-Y and Os-Th systems.

The obtained thermodynamic description for the Os – Th and the Os – Y systems in this work is shown in table 3.5. The calculated phase diagrams of the Os – Th and the Os – Y systems are shown in figures 3.11 and 3.12, respectively, and compared with the available experimental data from Thomson [144] and Kleykamp [145] for Os – Th system and from Savitskii and Polyakova [158] and Chiotti et al. [153] for Os – Y system. As it can be seen in figures 3.11 and 3.12, a reasonable agreement between our calculated and the experimental liquidus lines [144, 145, 153, 158] of the Os – Y and Os – Th systems, especially in the Th – rich and Y – rich corners, were observed.

The calculated compositions and temperatures of the invariant reactions are listed in table 3.6 and compared with the experimental data. Some differences are noticeable:

System	Phase	Thermodynamic parameters
Os-Th	Liquid	$\theta_L^{Liq} = -103875 + 1.008T$
	Os ₂ Th	$G_{Os:Th}^{Os_2Th} - 0.667G_{Os}^{SER} - 0.333G_{Th}^{SER} = -25929.68 + 0.159T - 0.349T \ln(T)$
	Os ₂ Th ₃	$G_{Os:Th}^{Os_2Th_3} - 0.4G_{Os}^{SER} - 0.6G_{Th}^{SER} = -30749 + 2.724T$
	Os ₃ Th ₇	$G_{Os:Th}^{Os_3Th_7} - 0.3G_{Os}^{SER} - 0.7G_{Th}^{SER} = -29203 + 2.858T$
Os-Y	Liquid	$\theta_L^{Liq} = -81688.69 + 3.139T$
	Os ₂ Y	$G_{Os:Y}^{Os_2Y} - 0.667G_{Os}^{SER} - 0.333G_Y^{SER} = -31731.42 + 2.654T - 0.174T \ln(T)$
	OsY ₃	$G_{Os:Y}^{OsY_3} - 0.25G_{Os}^{SER} - 0.75G_Y^{SER} = -23029.866 + 9.833T - 0.603T \ln(T)$

Table 3.5 – The optimized parameters of Os – Y and Os – Th systems.

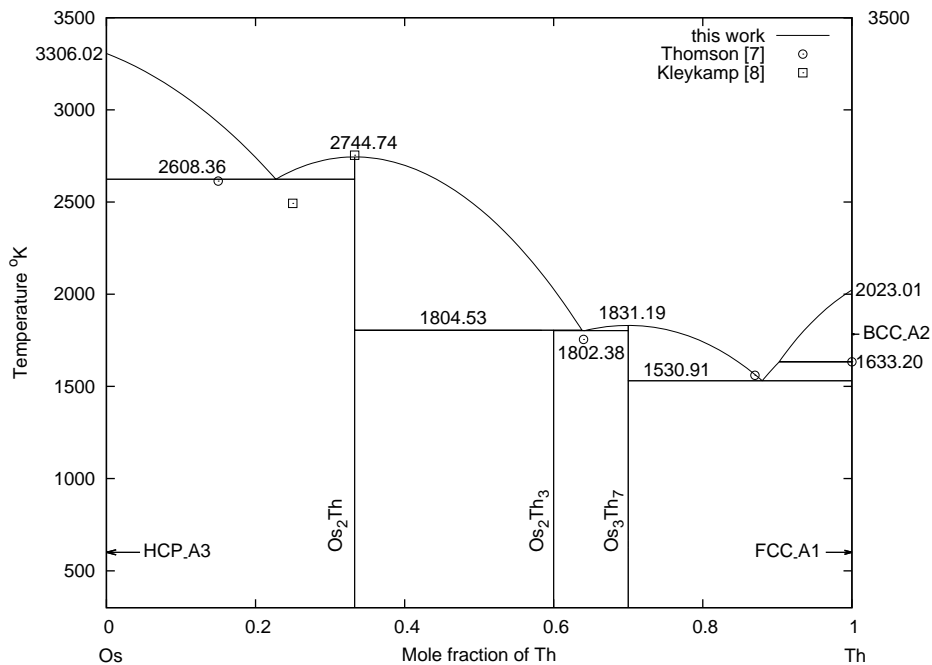


Figure 3.11 – Calculated phase diagram of the Os – Th system compared with that of Thomson [144], Kleykamp [145].

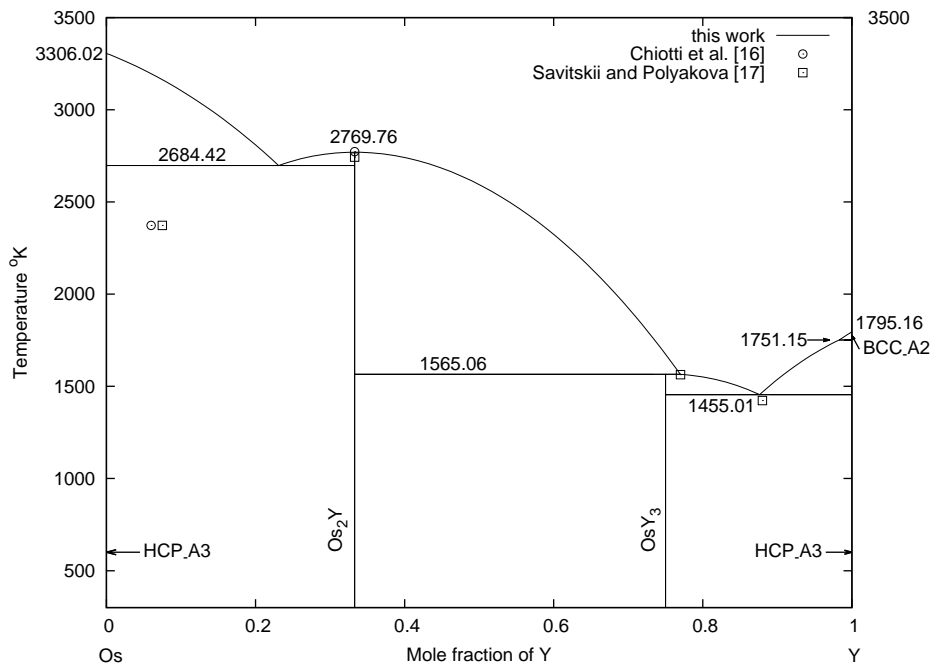


Figure 3.12 – Calculated phase diagram of the Os – Y system compared with that of Chiotti et al. [153], Savitskii and Polyakova [158].

The temperature of the $Liq \longleftrightarrow HCP_A3(Os) + Os_2Th$ and the $Liq \longleftrightarrow Os_2Th_3 + Os_3Th_7$ invariant reactions are in good agreement with the result of Thomson [144], but slightly higher than the ones determined by Kleykamp [145], respectively. The temperature of the $Liq \longleftrightarrow HCP_A3(Os) + Os_2Y$ invariant reaction is also higher than the one determined by Savitskii and Polyakova [158]. We estimate that the calculated eutectic is more credible because it is often difficult to determine the correct parts of the phase diagram in the temperature range from 2400 to 3000 K experimentally.

Optimized and calculated enthalpies of formation by using CALPHAD and first principle methods are reported in table 3.4, and are also reported in figures 3.13 and 3.14, respectively, experimental enthalpies of formation using the EMF method [145] and the predicted ones using the Miedema's semi empirical model [185] are also listed. FP-LAPW (WIEN2k), PAW (VASP), and optimized results are in good agreement. Also, EMF values [145] for Os_2Th compound, Miedema's values [185] for Os_3Th_7 , Os_2Y , and OsY_3 compounds, and optimized results in this work are in good agreement, but for other compounds of Os – Th system, the calculated enthalpies of formations in this work are higher than those of semi-empirical model of Miedema [185] and are lower than those of EMF method [145]. whereas, the only available experimental value using the calorimetry from the literature relative to the Os_2Y compound [134] is very close to our *Ab Initio* calculations and consistent with the performed CALPHAD modeling.

The calculated entropies for Os_2Th , Os_2Y , and OsY_3 compounds that can be observed in figures 3.15 to 3.17, respectively, are in excellent agreement with the entropies calculated using first principles and phonon calculations. The discrepancies of CALPHAD regarding first principles and phonon computed entropy found at higher temperatures are probably due to the formation of vacancies which was not contemplated in our calculations.

3.2. THE OS-TH AND OS-Y SYSTEMS

Reaction	Compositions of the respective phase <i>at.%RE</i> (RE = Th, Y)			T(K)	Type of reaction	Reference
$Liq \leftrightarrow Os_2Th$	0.333	0.333		2744.74	Congruent	[142]
	0.333	0.333		2753.15 ± 80		[145]
$Liq \leftrightarrow Os_3Th_7$	0.700	0.700		1831.19	Congruent	[142]
$Liq \leftrightarrow Os_{HCP_A3} + Os_2Th$	0.227	0.000	0.333	2608.36	Eutectic	[142]
	0.25 ± 0.02	0.000	0.333	2493.15 ± 50		[145]
$Os_2Th + Liq \leftrightarrow Os_2Th_3$	0.333	0.634	0.600	1804.53	Peritectic	[142]
$Liq \leftrightarrow Os_2Th_3 + Os_3Th_7$	0.644	0.600	0.700	1802.38	Eutectic	[142]
	0.640	0.600	0.700	1755.15 ± 12		[144]
$Liq + Th_{BCC_A2} \leftrightarrow Th_{FCC_A1}$	0.901	1.000	1.000	1633.20	Peritectic	[142]
		1.000	1.000	1633.15 ± 10		[144]
$Liq \leftrightarrow Os_3Th_7 + Th_{FCC_A1}$	0.877	0.700	1.000	1530.91	Eutectic	[142]
	0.870	0.700	1.000	1560.15 ± 12		[151]
$Liq \leftrightarrow Os_2Y$	0.333	0.333		2769.76	Congruent	[142]
	0.333	0.333		~ 2773.15		[147]
$Liq \leftrightarrow Os_{HCP_A3} + Os_2Y$	0.229	0.000	0.333	2684.42	Eutectic	[142]
	0.060	0.000	0.333	2373.15		[158]
$Liq + Y_{BCC_A2} \leftrightarrow Y_{HCP_A3}$	0.984	1.000	1.000	1751.15	Peritectic	[142]
		1.000	1.000	1751.15		[147]
$Os_2Y + Liq \leftrightarrow OsY_3$	0.333	0.770	0.750	1565.06	Peritectic	[142]
	0.333	0.660	0.750	1563.15		[158]
$Liq \leftrightarrow OsY_3 + Y_{HCP_A3}$	0.877	0.750	1.000	1455.01	Eutectic	[142]
	~ 0.880	0.750	1.000	1423.15		[158]

Table 3.6 – The invariant reactions in the Os – Y and Os – Th systems

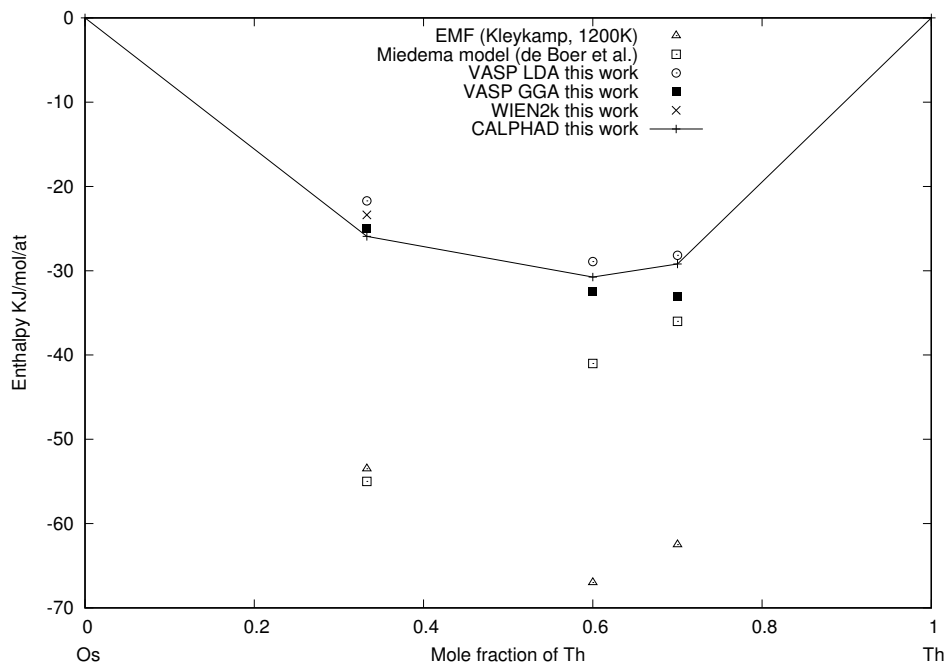


Figure 3.13 – Standard enthalpies of formation of intermediate phases in the Os – Th system.

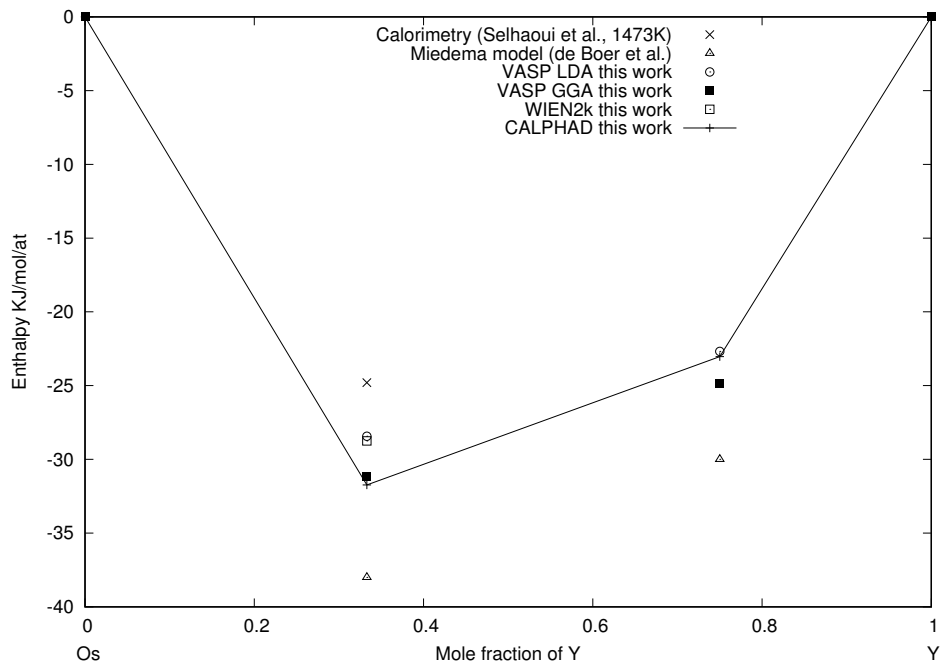


Figure 3.14 – Standard enthalpies of formation of intermediate phases in the Os – Y system.

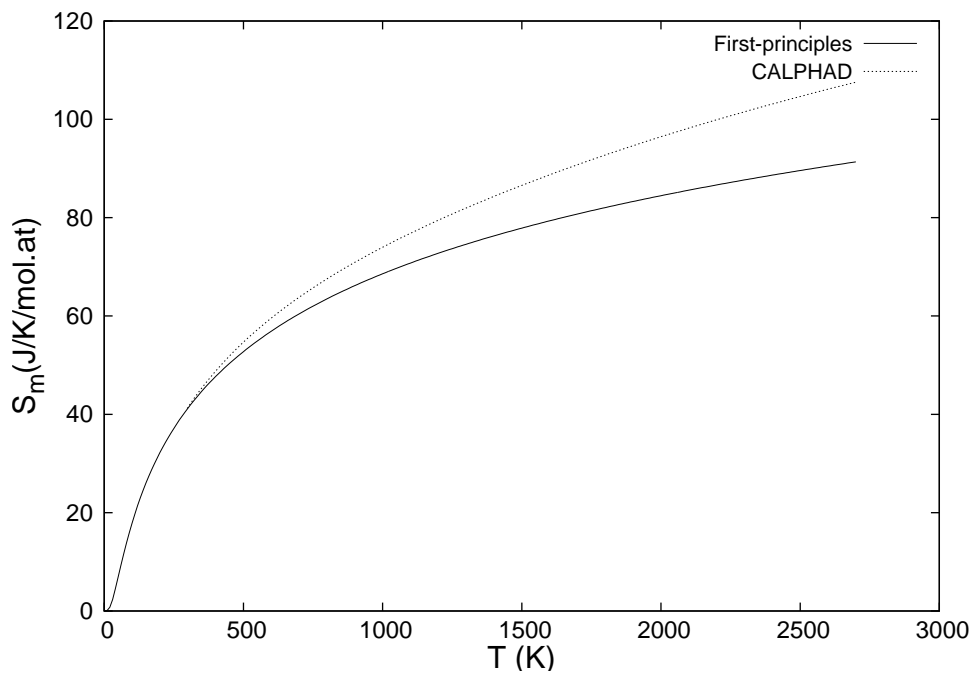


Figure 3.15 – Normalized entropy for the number of moles of atoms for Os₂Th.

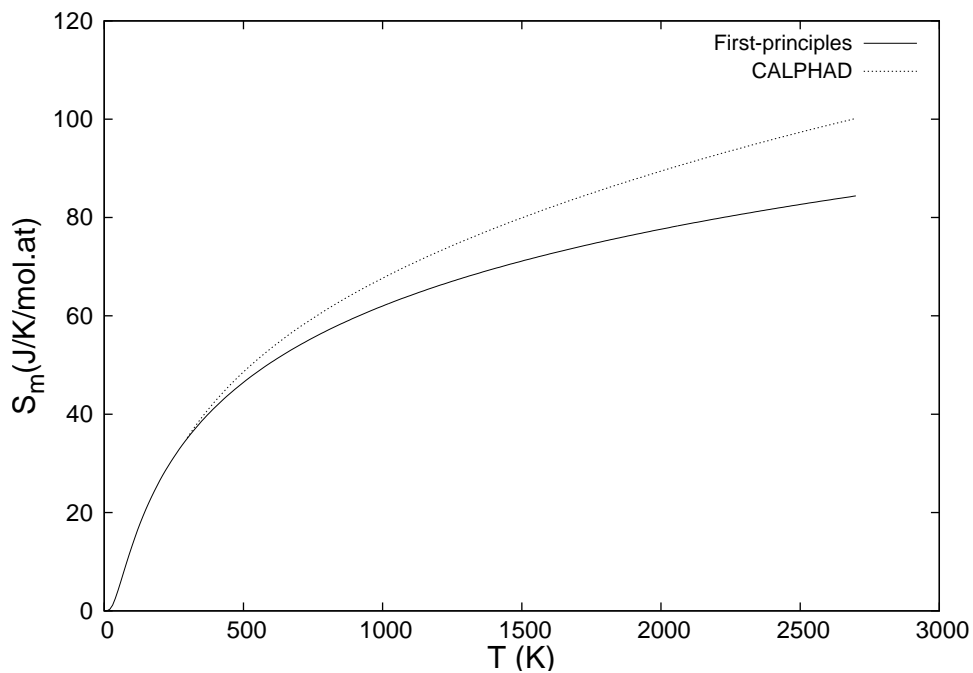


Figure 3.16 – Normalized entropy for the number of moles of atoms for Os_2Y .

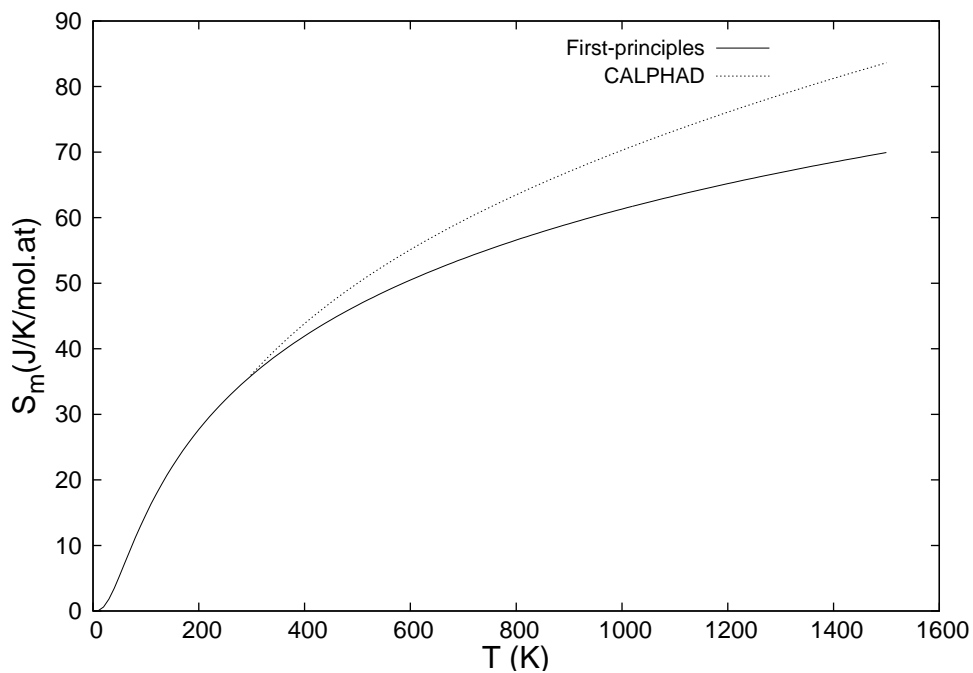


Figure 3.17 – Normalized entropy for the number of moles of atoms for OsY_3 .

3.2.6 Conclusion

Thermodynamic optimization of the Os – Th and the Os – Y systems has been performed utilizing the CALPHAD method combined with first-principles calculations. Enthalpies of formation for the compounds (Os_2Th , Os_2Th_3 , Os_3Th_7 , Os_2Y and OsY_3) were computed by ab-initio method based on DFT. Phonon calculations were performed to attain the thermodynamic data at $T > 0K$ for the compounds (Os_2Th , Os_2Y , and OsY_3). The liquid phase was modeled with the Redlich-Kister polynomial, and the five intermetallic compounds were described as stoichiometric phases. The Gibbs energy functions for individual phases in the Os – Th and the Os – Y systems were evaluated by considering the first-principles computed enthalpies of formation, vibrational entropies computed via phonon, and the experimental phase equilibria data. A set of self-consistent thermodynamic parameters for each system has been obtained, and the calculated results show a reasonable agreement with the available experimental data.

All phase equilibria and thermodynamic data available in the literature concerning the Os – Th and the Os – Y systems were critically evaluated. The enthalpies of formation for the four intermetallic compounds Os_2Th , Os_3Th_7 , Os_2Y and OsY_3 in the two binary systems have been computed via first-principles calculations and used in the present thermodynamic assessment. The crystal structure and the enthalpy of formation of the Os_2Th_3 were also predicted.

A consistent set of thermodynamic parameters were optimized for the Os – Th and the Os – Y systems which had not been previously thermodynamically assessed. In spite of the lack of experimental data for both Os – Th and Os – Y systems, the comprehensive comparison shows that the calculated phase diagrams and thermodynamic properties are in good agreement with the first-principles calculations.

3.3 Thermodynamic and ab-initio investigations of the Dy-Zn system

3.3.1 Introduction

Multi-component alloys of the transition metal with rare-earths form an exciting group of magnetic materials and are essential for making permanent magnets [186]. Especially those alloys of rare-earth with 3d transition elements, which have received much attention in the last few decades, because of their interesting crystal structures, promising physical properties, and potential application as, for example, magnetic materials [187, 188] and hydrogen storage devices [189]. Despite this interest, many of these systems remain poorly understood and their thermodynamic description undetermined, including those containing zinc element. The present work is devoted to the investigation of Dy-Zn binary system.

Saccone et al. [190] has reviewed the Dy-Zn phase diagram and related phase equilibria, but no self-consistent thermodynamic was given. CALPHAD (CALculation of PHase Diagram) is a successful and widely applied technique to facilitate material development [79]. It is necessary to investigate this binary system, and thereby offer new contents to the thermodynamic database of rare-earth-zinc alloys. This paper is dedicated to providing self-consistent and reliable thermodynamic descriptions for the Dy-Zn binary system based on the experimental data and the enthalpies of formation computed via the ab-initio method.

3.3.2 Review of literature data

The schematic Dy-Zn phase diagram shown in Massalski was as speculated by Moffatt on the sparse information that was available on this system [191]. Saccone et al. [190] has investigated the Dy-Zn system through differential thermal analysis (DTA), metallographic analysis, X-ray powder diffraction, and electron probe microanalysis (EPMA).

The Dy-Zn system is characterized by seven compounds and three terminal solutions (HCP_A3 (Dy), BCC_A2 (Dy), and HCP_ZN (Zn)). DyZn, DyZn₂, Dy₁₃Zn₅₈, and Dy₂Zn₁₇ melt congruently at 1368 K, 1323 K, 1203 K, and 1203 K, respectively. DyZn₃, Dy₃Zn₁₁, and DyZn₁₂ form through peritectic reactions at 1168 K, about 1173 K and 685 K, respectively. Four eutectic reactions occur at 1123 K and 30% zinc (between (Dy) and DyZn), 1263 K and 60% zinc (between DyZn and DyZn₂), 1158 K and 76% Zn (between DyZn₃ and Dy₃Zn₁₁), and 1148 K and 85% Zn (involving Dy₁₃Zn₅₈ and Dy₂Zn₁₇). The Dy-rich region end presents a catatectic equilibrium, and a degenerate invariant in the Zn-rich region. Dy-Zn crystal structure data shown in Table 3.7 were adopted from [192].

3.3.3 Ab initio details

In this work, first-principles calculations based on density functional theory (DFT) [49] were carried out using Vienna Ab-initio Simulation Package (VASP) [159, 160] to get formation energy of involved compounds.

The energy of formation at 0 K of the DyZn, DyZn₂, DyZn₃, Dy₃Zn₁₁, Dy₁₃Zn₅₈, βDy₂Zn₁₇, and DyZn₁₂ compounds is obtained by the equation (1.59). Where E(Dy_xZn_y), E(Dy_x), and E(Zn_y) are the total energy for Dy_xZn_y, pure HCP_A3 Dy, and pure HCP_A3 Zn at 0 K, respectively. The energy of formation corresponds also to the enthalpy of formation at 0 K.

3.3. THE DY-ZN SYSTEM

Phase	Comp. (at.%)	Pearson symbol and prototype	Space group	Lattice parameters (nm)			Ref.
Dy	~ 0	hP2 (Mg)	P6 ₃ /mmc	0.3589	0.3589	0.5646	[193]
				0.359	0.359	0.565	[194]
				0.3592	0.3592	0.5655	[195, 196]
				0.35915	0.35915	0.56501	[197]
				0.359	0.359	0.564	[198]
				0.3593	0.3593	0.56537	[199]
				0.3593	0.3593	0.5653	[200]
				0.35903	0.35903	0.56475	[157]
			0.36177	0.36177	0.56504	[201]	
Dy	~ 0	cI2 (W)	Im-3m	0.3982	0.3982	0.3982	[202]
DyZn	50	cP2 (CsCl)	Pm-3m	0.3563	0.3563	0.3563	[173, 203]
				0.3562	0.3562	0.3562	[204]*
				0.3555	0.3555	0.3555	[205]
				0.3560	0.3560	0.3560	[190]
				0.3563	0.3563	0.3563	[201]
DyZn ₂	~ 66.67	oI12 (KHg ₂)	Imma	0.4481	0.7107	0.7619	[206]
				0.4481	0.7151	0.7577	[190]
				0.4464	0.7064	0.7540	[201]
DyZn ₃	75	oP16 (Zn ₃ Y)	Pnma	0.67	0.4398	1.006	[192, 207]*
				0.6731	0.4440	1.0159	[190]
				0.6667	0.4368	1.0050	[201]
Dy ₃ Zn ₁₁	~ 78.57	oI28 (La ₃ Al ₁₁)	Immm	0.4395	0.883	1.2922	[206]
				0.4405	0.8805	1.3041	[190]
				0.4395	0.8830	1.2922	[192]*
				0.4380	0.8755	1.2852	[201]
Dy ₁₃ Zn ₅₈	~ 81.69	hP142 (Zn ₅₈ Dy ₁₃)	P6 ₃ /mmc	1.426	1.426	1.401	[190]
				1.424	1.424	1.399	[192]
				1.4198	1.4198	1.3849	[201]
βDy ₂ Zn ₁₇	~ 89.47	hP38 (Th ₂ Ni ₁₇)	P6 ₃ /mmc	0.8956	0.8956	0.8776	[208]*
				0.8959	0.8959	0.8725	[190]
				0.8919	0.8919	0.8698	[201]
βDy ₂ Zn ₁₇	~ 89.47	hR57 (Zn ₁₇ Th ₂)	R-3m	0.89658	0.89658	1.31339	[209, 210]
				0.8967	0.8967	1.3139	[208]*
				0.8973	0.8973	1.3141	[190]
				0.89089	0.89089	1.30796	[201]
DyZn ₁₂	~ 92.31	tI26 (ThMn ₁₂)	I4/mmm	0.8877	0.8877	0.5198	[208]*
				0.888	0.888	0.5199	[211]
				0.8868	0.8868	0.5184	[190]
				0.8801	0.8801	0.5188	[201]
Zn	~ 100	hP2 (Mg)	P6 ₃ /mmc	0.2665	0.2665	0.4947	[212, 213]
				0.26655	0.26655	0.49488	[214]
				0.26655	0.26655	0.49488	[215]
				0.26644	0.26644	0.4945	[216]
				0.26642	0.26642	0.49454	[217]
				0.26645	0.26645	0.49446	[217]
			0.26469	0.26469	0.49390	[201]	

* References used by Saccone et al. [190]

Table 3.7 – The crystal structure data of the Dy-Zn system.

Calculations were performed using the projected-augmented wave (PAW) pseudo-potentials [129, 130] with the generalized gradient approximation as implemented by [Perdew, Burke, and Ernzerhof](#) (GGA-PBE) [54]. A plane wave cutoff energy of 300 eV is used. K-point meshes are compiled using the fully automatic scheme [131], which generates Γ centered Monkhorst-Pack grids [132], where the numbers of subdivisions N_1 , N_2 , and N_3 along reciprocal lattice vectors \vec{b}_1 , \vec{b}_2 , and \vec{b}_3 , respectively, are given by:

$$N_i = \max\left(1, l \left| \vec{b}_i \right| + 0.5\right), i = 1, 2, 3 \quad (3.5)$$

Where $\left| \vec{b}_i \right|$ is the norm of the reciprocal lattice vector \vec{b}_i . According to [Kresse et al.](#) [131], useful values for the length l vary between 10 (large gap insulators) and 100 (d-metals). In this work, we found that $l = 60$ is sufficient to achieve convergence to a precision less than 1 meV/atom for all compounds of both Dy-Zn system. In addition to Monkhorst-Pack k-point meshes, Brillouin-zone integrations are performed using the Methfessel-Paxton technique with the smearing parameter of 0.1 eV. All calculations were performed using the ‘‘Accurate’’ setting within VASP, and all degrees of freedom of the crystal structures were allowed to relax, including cell shape, volume and atom positions with a preconditioned conjugated gradient (CG) algorithm with the default VASP’s convergence criteria.

Compound	ΔH_f KJ/mol	ΔS_f J/K/mol	Method	Ref.
DyZn	-33.889		GGA-PBE	[201]
	-32.369	-3.8	CALPHAD	[201]
	-30.929	-2.02	CALPHAD	[218]
DyZn ₂	-38.387		GGA-PBE	[201]
	-37.555	-5.9	CALPHAD	[201]
	-36.186	-3.79	CALPHAD	[218]
DyZn ₃	-35.087		GGA-PBE	[201]
	-35.343	-6.4	CALPHAD	[201]
	-35.614	-5.75	CALPHAD	[218]
Dy ₃ Zn ₁₁	-32.465		GGA-PBE	[201]
	-33.581	-6	CALPHAD	[201]
	-34.727	-6.16	CALPHAD	[218]
Dy ₁₃ Zn ₅₈	-30.574		GGA-PBE	[201]
	-31.718	-5.38	CALPHAD	[201]
	-33.222	-6.04	CALPHAD	[218]
β Dy ₂ Zn ₁₇	-22.715		GGA-PBE	[201]
	-25.767	-1.14	CALPHAD	[201]
	-21.816	-4.33	CALPHAD	[218]
DyZn ₁₂	-17.244		GGA-PBE	[201]
	-18.274	-2.8	CALPHAD	[201]
	-19.766	-4.36	CALPHAD	[218]

Table 3.8 – The formation enthalpies of the Dy-Zn system compounds.

3.3.4 Optimization procedure

The thermodynamic optimization of the Gibbs energy parameters is an application of the CALPHAD technique [Kaufman and Bernstein](#) [29], using both the experimental data of the phase diagram and the enthalpies of formation determined by the first-principles calculations in this work.

The set of thermodynamic parameters of the Dy-Zn system were optimized using the [PARROT](#) module of the [Thermo-Calc](#) software developed by [Jansson](#) [31] and [Sundman](#)

et al. Sundman et al. [30], Sundman and Ågren [119]. This program works by minimizing an error sum where each of the selected values is given a certain weight. The weight is chosen by personal judgment and changed by trial and error during the work until most of the selected experimental and first-principles calculations are reproduced within the expected uncertainty limits.

The modeling of the Dy-Zn was made in three main steps. Firstly, HCP_A3 and BCC_A2 phases are suspended, where all remaining thermodynamic parameters are optimized in one operation by assuming the enthalpies of formation of the intermetallic compounds to be fixed with these values determined from first-principle calculations of this work. In the second step, we have fixed the thermodynamic parameters obtained from the first step and restored the suspended phases previously; then optimisation is performed to get their thermodynamic parameters. Finally, a global optimization was performed by unfixing all thermodynamic parameters, which are adjusted simultaneously by taking into account all of the selected data to ensure the best fit.

System	Phase	Thermodynamic parameters
Dy-Zn	Liquid	${}^0L^{Liq} = -1205823 + 38.49T$
		${}^1L^{Liq} = 65419 - 16.97T$
		${}^2L^{Liq} = -35168 + 9.43T$
	DyZn	$G_{Dy:Zn}^{DyZn} - 0.5G_{Dy}^{SER} - 0.5G_{Zn}^{SER} = -32369 + 3.8T$
	DyZn ₂	$G_{Dy:Zn}^{DyZn_2} - 0.3333G_{Dy}^{SER} - 0.6667G_{Zn}^{SER} = -37555 + 5.9T$
	DyZn ₃	$G_{Dy:Zn}^{DyZn_3} - 0.25G_{Dy}^{SER} - 0.75G_{Zn}^{SER} = -35343 + 6.4T$
	Dy ₃ Zn ₁₁	$G_{Dy:Zn}^{Dy_3Zn_{11}} - 0.2143G_{Dy}^{SER} - 0.7857G_{Zn}^{SER} = -33581 + 6T$
	Dy ₁₃ Zn ₅₈	$G_{Dy:Zn}^{Dy_{13}Zn_{58}} - 0.1831G_{Dy}^{SER} - 0.8169G_{Zn}^{SER} = -31718 - 5.38T$
	βDy ₂ Zn ₁₇	$G_{Dy:Zn}^{βDy_2Zn_{17}} - 0.1053G_{Dy}^{SER} - 0.8947G_{Zn}^{SER} = -22767 + 2.8T$
DyZn ₁₂	$G_{Dy:Zn}^{DyZn_{12}} - 0.0769G_{Dy}^{SER} - 0.9231G_{Zn}^{SER} = -18274 + 2.8T$	

Table 3.9 – The optimized parameters of Dy-Zn system.

3.3.5 Results and discussion

We participated in JEEP2014 [201] with the partial results of this work, where we hoped to send the complete article to a scientific journal with an excellent reputation; unfortunately, the work has been published by [Zhu and Pelton](#) [218]. So, we haven't submitted the work for publication, as our work doesn't contain a new contribution in comparison with the work of [Zhu and Pelton](#) [218]. However, the results are in good agreement with those of [Zhu and Pelton](#)..

Results from first-principle calculations of the enthalpies of formation of the stoichiometric DyZn, DyZn₂, DyZn₃, Dy₃Zn₁₁, Dy₁₃Zn₅₈, βDy₂Zn₁₇ and DyZn₁₂ compounds are presented in [Table 3.8](#), where the reference states are (HCP_A3) Dy and Zn. Those enthalpies of formation calculated with the ab-initio method were used in the thermodynamic modeling of the Dy-Zn system.

Thermodynamic description obtained of the Dy-Zn system in this work is shown in [Table 3.9](#). The calculated phase diagram of the Dy-Zn system is shown in [Figure 3.18](#), compared with the available experimental data [190]. It can be seen an excellent agreement with the liquidus line between the calculated values and the experimental ones [190], within the expected uncertainty limits, for the Dy-Zn system, especially in the Zn-rich part.

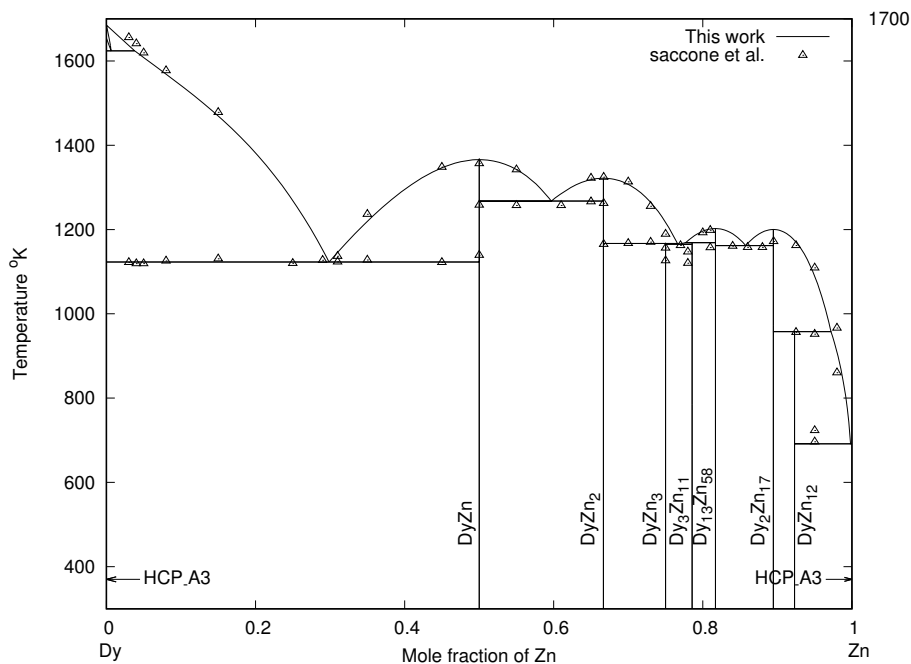


Figure 3.18 – Calculated phase diagram of the Dy-Zn system compared with that of **Saccone et al. [190]**.

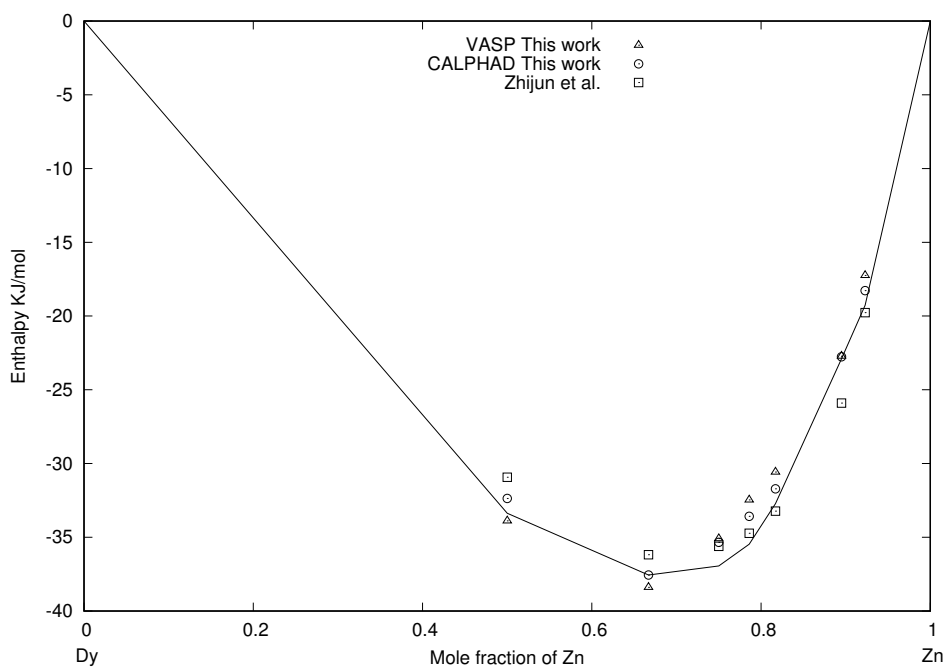


Figure 3.19 – Standard enthalpies of formation of intermediate phases in the Dy-Zn system.

The details of calculated compositions and temperatures for the invariant reactions compared with the experimental data are listed in Table 3.10. Some differences are noticeable:

Optimized and calculated via first-principle calculations enthalpies of formation are reported in Table 3.8 and Figure 3.19. Good agreement is obtained between PAW (VASP) and optimized results.

Reaction	Compositions of the respective phase <i>at.%Zn</i>			T(K)	Type of reaction	Reference
$Dy_{BCC_A2} \leftrightarrow Dy_{HCPA3}$		0		1654	allotropic	[191]
		0		1654		[201]
$Dy_{BCC_A2} \leftrightarrow Dy_{HCPA3} + Liq$	~ 2	< 0.5	~ 5	~ 1623	catatectic	[190]
	3.78	0.63	5.33	1624.05		[201]
$Liq \leftrightarrow Dy_{HCPA3} + DyZn$	30	< 0.5	50	1123	etectic	[190]
	29.87	0.67	50	1122.88		[201]
$Liq \leftrightarrow DyZn$		50		1368	Congruent	[190]
		50		1365.85		[201]
$Liq \leftrightarrow DyZn + DyZn_2$	60	50	66.7	1263	etectic	[190]
	59.68	50	66.7	1267.55		[201]
$Liq \leftrightarrow DyZn_2$		66.67		1323	Congruent	[190]
		66.67		1321.89		[201]
$Liq + DyZn_2 \leftrightarrow DyZn_3$	75.5	66.67	75	1168	peritectic	[190]
	76.59	66.67	75	1167.03		[201]
$Liq \leftrightarrow DyZn_3 + Dy_3Zn_{11}$	76	75	78.57	1158	etectic	[190]
	76.89	75	78.57	1165.15		[201]
$Liq + Dy_{13}Zn_{58} \leftrightarrow Dy_3Zn_{11}$	77.5	81.69	78.57	~ 1173	peritectic	[190]
	77.70	81.69	78.57	1169.00		[201]
$Liq \leftrightarrow Dy_{13}Zn_{58}$		81.69		1203	Congruent	[190]
		81.69		1202.38		[201]
$Liq \leftrightarrow Dy_{13}Zn_{58} + \beta Dy_2Zn_{17}$	85	81.69	89.47	1148	etectic	[190]
	85.76	81.69	89.47	1161.84		[201]
$Liq \leftrightarrow \beta Dy_2Zn_{17}$		89.47		1203	Congruent	[190]
		89.47		1200.24		[201]
$Liq \leftrightarrow DyZn_{12} + Zn_{HCPA3}$	> 99.5	92.31	~ 100	693	degenerate	[190]
	99.80	92.31	~ 100	691.50		[201]
or $Liq + DyZn_{12} \leftrightarrow Zn_{HCPA3}$	~ 100	92.31	> 99.5	693	degenerate	[190]
	~ 100	92.31	99.85	691.50		[201]

Table 3.10 – The invariant reactions in the Dy-Zn systems

3.3.6 Conclusion

The thermodynamic modeling of the Dy-Zn binary system was carried out with the help of ab-initio calculations and CALPHAD method. The enthalpies of formation of DyZn, DyZn₂, DyZn₃, Dy₃Zn₁₁, Dy₁₃Zn₅₈, β Dy₂Zn₁₇, and DyZn₁₂ are computed via density functional theory using the VASP code. The CALPHAD assessment of Dy-Zn system was then performed by considering both the first-principle computed enthalpies of formation and the experimental phase equilibrium data. The HCP_A3, BCC_A2, and liquid phases have been described with Redlich-Kister polynomial, and all compounds have been treated as stoichiometric. A set of self-consistent thermodynamic parameters has been obtained, where the obtained results are in satisfactory agreement with the experimental data.

All experimental phase diagram and thermodynamic data available in the literature for the Dy-Zn system are critically evaluated. The enthalpies of formation for the eight compounds DyZn , DyZn_2 , DyZn_3 , $\text{Dy}_3\text{Zn}_{11}$, $\text{Dy}_{13}\text{Zn}_{58}$, $\beta\text{Dy}_2\text{Zn}_{17}$, and DyZn_{12} have been computed via first-principle calculations, where they are used in the present thermodynamic assessment.

A consistent set of thermodynamic parameters were optimized for the Dy-Zn system. The comprehensive comparison shows that the calculated phase diagrams and thermodynamic properties are in good agreement with the first-principle calculations.

Conclusion

The CALPHAD method is a powerful tool for describing the thermodynamic properties of the equilibria of multi-component systems. It allows to determine and propose models to explain the different phases of equilibrium in a system from experimental and theoretical work. A database is then generated to store the parameters of these models for each system. These databases can be used with different thermodynamic calculation software (Thermo-Calc, Pandat, MTDATA, etc.) to plot phases diagrams and calculate the thermodynamic properties of these systems and explore them for higher order systems.

Using associated models with CALPHAD method requires knowledge of the crystallographic and experimental data of each phase taken into account in the calculation. This work enabled us to introduce the various useful models for the thermodynamic description of the studied systems during the thesis and to understand the relation between the thermodynamic stability of a phase and its free enthalpy.

Constructing a phase diagram from experimental data is a laborious, expensive, and sometimes even practically unfeasible job. However, computational thermodynamics can minimize the effort involved to obtain a thermodynamic description of a phase diagram by using thermodynamic data of phases obtained either experimentally or calculated theoretically, or both. First-principles methods allow us to get many thermodynamic data with low cost and gain of time comparatively with experimental techniques.

In the present work, we have used first-principles methods to obtain, the formation enthalpies of compounds, the configurational and electronic entropies of compounds and the formation enthalpies of intermediate phase along a range of composition, all those data are essential as input for the CALPHAD method to get a reliable description of a thermodynamic system.

One of the difficult tasks in CALPHAD method is getting the appropriate description of an intermediate phase, where defects type in this phase is needed to determine the proper sublattice, as their formation energies (formation enthalpy of each site in the sublattice). In this work, point defect structure of B2 $TrSc$ ($Tr = Cd, Ru$) alloys was investigated using supercell, and special quasi-random structure (SQS) approaches. According to our results, Tr and Sc anti-sites are the constitutional point defects in Tr -rich and Sc -rich B2 $TrSc$, respectively. To investigate the thermal defect concentrations at finite temperatures, we adopted the Wagner-Schottky model using point defect formation enthalpies obtained from supercell and SQS approaches. The present results suggest that the predominant thermal defects in B2 $CdSc$ are of exchange type, and in B2 $RuSc$ are of inter-branch Sc type, these results allow us to define the convenient sublattice and the species in each site, as they provide us with important input to CALPHAD method, which is formation energies of the phase and its members. The calculated results show an agreement with the available theoretical and experimental data.

Thermodynamic optimization of the $Os - Th$ and the $Os - Y$ systems has been performed employing the CALPHAD technique combined with first-principles calculations. Enthalpies of formation for the compounds (Os_2Th , Os_2Th_3 , Os_3Th_7 , Os_2Y and OsY_3)

were computed by ab-initio method based on [DFT](#). Phonon calculations were performed to attain the thermodynamic data at $T > 0\text{K}$ for the compounds (Os_2Th , Os_2Y , and OsY_3). The liquid phase was modeled with the Redlich-Kister polynomial, and the five intermetallic compounds were described as stoichiometric phases. The Gibbs energy functions for individual phases in the $\text{Os}-\text{Th}$ and the $\text{Os}-\text{Y}$ systems were evaluated by considering the first-principles computed enthalpies of formation, vibrational entropies computed via phonon, and the experimental phase equilibria data. A set of self-consistent thermodynamic parameters for each system has been obtained, and the calculated results show a reasonable agreement with the available experimental data.

The thermodynamic modeling of the $\text{Dy}-\text{Zn}$ binary system was carried out with the help of ab-initio calculations and [CALPHAD](#) method. The enthalpies of formation of DyZn , DyZn_2 , DyZn_3 , $\text{Dy}_3\text{Zn}_{11}$, $\text{Dy}_{13}\text{Zn}_{58}$, $\beta\text{Dy}_2\text{Zn}_{17}$, and DyZn_{12} are computed via density functional theory using the VASP code. The [CALPHAD](#) assessment of $\text{Dy}-\text{Zn}$ system was then performed by considering both the first-principle computed enthalpies of formation and the experimental phase equilibrium data. The HCP_A3, BCC_A2, and liquid phases have been described with Redlich-Kister polynomial, and all compounds have been treated as stoichiometric. A set of self-consistent thermodynamic parameters has been obtained, where the obtained results are in satisfactory agreement with the experimental data.

Bibliography

- [1] Khedidja Younsi. *Etude expérimentale et théorique des propriétés structurales et magnétiques des nanomatériaux Pr(Co,Fe)₃*. Ph.d. thesis, Paris Est, 2011. 3
- [2] Anton R. Chakhmouradian and Frances Wall. Rare earth elements: Minerals, mines, magnets (and more). *Elements*, 8(5):333–340, 2012. 3
- [3] Johan Schijf. *Aqueous geochemistry of the rare earth elements in marine anoxic basins*. Ph.d. dissertation no. 85, Rijksuniversiteit te Utrecht, 1992. 3
- [4] K.H.J. Buschow. Chapter 47 hydrogen absorption in intermetallic compounds. In Karl A. Gschneidner Jr. and LeRoy Eyring, editors, *Handbook on the physics and chemistry of rare earths*, volume 6 of *Handbook on the Physics and Chemistry of Rare Earths*, pages 1–111. Elsevier, 1984. 3
- [5] J. E. Geusic, H. M. Marcos, and L. G. Van Uitert. Laser oscillations in nd-doped yttrium aluminum, yttrium gallium and gadolinium garnets. *Applied Physics Letters*, 4(10):182–184, 1964.
- [6] K. Ohno and T. Abe. Bright green phosphor, $y_3al_{5-x}ga_xo_{12} : Tb$, for projection crt. *Journal of The Electrochemical Society*, 134(8):2072–2076, 1987.
- [7] N Sato, N Morishita, T Kimura, N Fujioka, O Takahashi, S Bito, Y Hattori, Y Dansui, and M. Ikoma. Nickel-metal hydride battery for hybrid electric vehicles. *Matsushita Techno*, 48:15–20, 2002. 3
- [8] J. J. Croat, J. F. Herbst, R. W. Lee, and F. E. Pinkerton. Pr-fe and nd-fe-based materials: A new class of high-performance permanent magnets (invited). *Journal of Applied Physics*, 55(6):2078–2082, 1984. 3
- [9] V Paul-Boncour, A Percheron-Guegan, M Diaf, and J.C Achard. Structural characterization of rni₂ (r= la, ce) intermetallic compounds and their hydrides. *Journal of the Less Common Metals*, 131(1):201–208, 1987.
- [10] Masato Sagawa. Development of the ndfeb magnets. *Materia Japan*, 40(11):943–946, 2001.
- [11] E.M Savitsky, E.I Klabunovskii, I.R Konenko, N.I Parfenova, V.P Mordovin, T.P Savostyanova, and D.E Bogatin. Intermetallic compounds $lnni_5$, $la_{1-x}pr_xni_5$ as sorbents and hydrogenation catalysts (ln= la, ce, pr, nd, sm, gd). *Journal of the Less Common Metals*, 89(2):528 –, 1983. 3
- [12] Gareth P. Hatch. Dynamics in the global market for rare earths. *Elements*, 8(5):341–346, 2012. 3
- [13] X. Q Bao, S. Z Zhou, and J. Zhu. *The Preparation of High-Performance Single-Phase NdFeB Nanocrystals and Related Mechanism*. University of Science and Technology Beijing, Beijing, 2008. 3
- [14] J. Hou. Characteristics of ndfeb electroplating equipment. *Plat. Finish.*, 27:21, 2005.
- [15] S. Z. Zhou and X. X. Gao. Sintered ndfeb permanent materials industry present situation and the challenges. *Plat. Finish.*, 5:9, 2011. 3

- [16] Régis Poisson. La guerre des terres rares. *L'Actualité Chimique*, 369:47–54, December 2012. 4
- [17] L. Bessais and C. Djéga-Mariadassou. Structure and magnetic properties of nanocrystalline $\text{Sm}(\text{Fe}_{1-x}\text{Co}_x)_{11}\text{Ti}$. *Physical Review B*, 63:054412, January 2001. 3
- [18] L. Bessais, S. Sab, C. Djéga-Mariadassou, and J. M. Grenéche. Crystallographic and hyperfine parameters of $\text{PrTi}(\text{Fe}, \text{Co})_{11}$ and their carbides. *Physical Review B*, 66:054430, August 2002.
- [19] L. Bessais, C. Djéga-Mariadassou, A. Nandra, M. D. Appay, and E. Burzo. Hard magnetic $\text{Sm}(\text{Fe}, \text{Si})_9$ carbides: Structure and magnetic properties. *Physical Review B*, 69:064402, February 2004.
- [20] Romulus Tetean, Emil Burzo, and Liviu Chioncel. Magnetic properties and electronic structures of $\text{gdco}_3\text{-xsix}$ compounds. *Journal of Alloys and Compounds*, 430(1-2):19–21, 2007. 3
- [21] Jinli Huang, Haichang Zhong, Xiuwen Xia, Wei He, Jinming Zhu, Jianqiu Deng, and Yinghong Zhuang. Phase equilibrium of the gd-fe-co system at 873 k. *Journal of Alloys and Compounds*, 471(1-2):74–77, 2009. 3
- [22] YuQi Yang, G.H. Rao, T. Wang, J.B. Li, J. Luo, G.Y. Liu, X.J. Chen, and J.L. Zhao. Effects of fe substitution on structural and magnetic properties of the $\text{nd}_2\text{co}_7\text{-xfex}$ compounds. *Journal of Alloys and Compounds*, 506(2):766–771, 2010. 3
- [23] E. Burzo. Magnetic behaviour of iron, cobalt and nickel in rare-earth (yttrium) compounds. *Journal of Magnetism and Magnetic Materials*, 196-197:901–903, 1999. 3
- [24] N.H. Duc, T.D. Hien, D. Givord, J.J.M. Franse, and F.R. de Boer. Exchange interactions in rare earth-transition metal compounds. *Journal of Magnetism and Magnetic Materials*, 124(3):305–311, 1993.
- [25] Jifan Hu, Bao gen Shen, Jianga Zhao, Wenshan Zhan, and Zhenxi Wang. Determination of magnetocrystalline anisotropy constants from a hard magnetic material with polycrystalline structure. *Solid State Communications*, 89(9):799–801, 1994.
- [26] Z. W. Li and A. H. Morrish. Negative exchange interactions and curie temperatures for $\text{Sm}_2\text{Fe}_{17}$ and $\text{Sm}_2\text{Fe}_{17}\text{N}_m$. *Physical Review B*, 55:3670–3676, February 1997.
- [27] R.J. Radwanski, J.J.M. Franse, and S. Sinnema. Effective anisotropy constants in rare earth-3d intermetallics. *Journal of Magnetism and Magnetic Materials*, 70(1):313–315, 1987. 3
- [28] J.J.M. Franse, F.E. Kayzel, and N.P. Thuy. Exchange and anisotropy in 3d-4f compounds. *Journal of Magnetism and Magnetic Materials*, 129(1):26–38, 1994. 3
- [29] L. Kaufman and H. Bernstein. *Computer Calculation of Phase Diagrams with Special Reference to Refractory Metals*. Refractory Materials. Academic Press, 1970. 4, 26, 41, 64, 76

- [30] Bo Sundman, Bo Jansson, and Jan-Olof Andersson. The thermo-calc databank system. *Calphad - Computer Coupling of Phase Diagrams and Thermochemistry*, 9(2): 153–190, 1985. [4](#), [31](#), [32](#), [33](#), [35](#), [64](#), [77](#)
- [31] B. Jansson. *Computer Operated Methods for Equilibrium Calculations and Evaluation of Thermodynamic Model Parameters*. Ph.d. dissertation, Royal Institute of Technology, Stockholm Sweden, 1984. [4](#), [64](#), [76](#)
- [32] M. Azzaoui. *Modélisation des liquides métalliques ternaires dans l'objectif du calcul des diagrammes d'équilibre, à partir des mesures ciblées calorimétriques et électrochimiques*. Ph.d. thesis, Université Henry Poincaré-Nancy I, 2000. [4](#)
- [33] Errol G. Lewars. *Introduction to Quantum Mechanics in Computational Chemistry*, pages 101–191. Springer International Publishing, Cham, 2016. [7](#)
- [34] Alexander Quandt. *Ab-Initio Approach to the Many-Electron Problem*, pages 415–436. Springer Berlin Heidelberg, Berlin, Heidelberg, 2008. [7](#), [8](#)
- [35] Errol G. Lewars. *Ab initio Calculations*, pages 193–419. Springer International Publishing, Cham, 2016. [7](#), [9](#), [10](#), [11](#)
- [36] Errol G. Lewars. *Ab initio Calculations*, pages 175–390. Springer Netherlands, Dordrecht, 2011. [7](#)
- [37] Fernando Nogueira, Alberto Castro, and Miguel A. L. Marques. *A Tutorial on Density Functional Theory*, pages 218–256. Springer Berlin Heidelberg, Berlin, Heidelberg, 2003.
- [38] William Paul Huhn. *Thermodynamics From First Principles: Prediction Of Phase Diagrams And Materials Properties Using Density Functional Theory*. PhD thesis, Carnegie Mellon University, 2014.
- [39] Virginie Trinite-Queque. *Etude ab initio et simulation à l'Echelle atomique des transitions de phase du titane*. PhD thesis, cole Polytechnique, Francais, 2006. [7](#), [14](#), [16](#)
- [40] P.W. Atkins, J. De Paula, and V. Walters. *Physical Chemistry*. Macmillan Higher Education, 2006. [8](#)
- [41] F. Jensen. *Introduction to Computational Chemistry*. Wiley, 2007. [8](#), [9](#)
- [42] R. Shankar. *Principles of quantum mechanics*. Kluwer Academic/Plenum Publishers, second edition, 1994. [8](#)
- [43] D.R. Hartree. The wave mechanics of an atom with a non-coulomb central field. part i. theory and methods. *Proc. Cambridge Phil. Soc.*, 24:89–110, 1928. [8](#)
- [44] D.R. Hartree. The wave mechanics of an atom with a non-coulomb central field. part ii. some results and discussion. *Proc. Cambridge Phil. Soc.*, 24:111–132, 1928. [8](#)
- [45] Pople John A and David L. Beveridge. *Approximate molecular orbital theory*. New York : McGraw-Hill, 1970. Includes bibliographical references. [10](#)
- [46] J. A. Pople and R. K. Nesbet. Self-consistent orbitals for radicals. *The Journal of Chemical Physics*, 22(3):571–572, 1954. [10](#)

- [47] John Lowe. *Quantum Chemistry*. Academic Press, New York, 1993. [10](#)
- [48] P. Hohenberg and W. Kohn. Inhomogeneous electron gas. *Physical Review*, 136: B864–B871, November 1964. [12](#)
- [49] W. Kohn and L. J. Sham. Self-Consistent Equations Including Exchange and Correlation Effects. *Physical Review*, 140(4A):A1133–A1138, November 1965. [12](#), [63](#), [74](#)
- [50] D. M. Ceperley. Ground State of the Electron Gas by a Stochastic Method. *Physical Review Letters*, 45(7):566–569, August 1980. [14](#), [61](#), [98](#)
- [51] R. O. Jones and O. Gunnarsson. The density functional formalism, its applications and prospects. *Reviews of Modern Physics*, 61:689–746, July 1989. [14](#)
- [52] J. Käbler and V. Eyert. Electronic structure calculations. In K. H. J. Buschow, editor, *Electronic and Magnetic Properties of Metals and Ceramics*, Materials Science and Technology, pages 1–145. VCH Verlagsgesellschaft, Weinheim, 1992. Volume 3A of the series: Materials Science and Technology, edited by R. W. Cahn, P. Haasen, and E. J. Kramer, VCH Verlagsgesellschaft, Weinheim 1991-1996. [14](#)
- [53] Aissa AOUADI. *Calcul ab initio des propriétés structurales, électroniques, élastiques et dynamiques des semiconducteurs III-V a base de phosphore*. Ph.d. thesis, Université Badji Mokhtar - Annaba, 2009. [14](#)
- [54] John P. Perdew, Kieron Burke, and Matthias Ernzerhof. Generalized gradient approximation made simple. *Physical Review Letters*, 77:3865–3868, October 1996. [14](#), [52](#), [61](#), [64](#), [76](#), [98](#)
- [55] Alberto García, Christian Elsässer, Jing Zhu, Steven G. Louie, and Marvin L. Cohen. Use of gradient-corrected functionals in total-energy calculations for solids. *Physical Review B*, 46:9829–9832, October 1992. [14](#)
- [56] Ale š Zupan, Peter Blaha, Karlheinz Schwarz, and John P. Perdew. Pressure-induced phase transitions in solid si, sio₂, and fe: Performance of local-spin-density and generalized-gradient-approximation density functionals. *Physical Review B*, 58: 11266–11272, November 1998. [14](#)
- [57] Hichem BOUDERBA. *COUPLAGE CALPHAD AB-INITIO POUR LE CALCUL DES DIAGRAMMES DE PHASES*. Ph.d. thesis, Université Hadj Lakhder BATNA, 2012. [15](#)
- [58] N.W. Ashcroft and N.D. Mermin. *Physique des solides*. EDP Sciences, 2002. [17](#), [23](#)
- [59] G. B. Bachelet, D. R. Hamann, and M. Schlüter. Pseudopotentials that work: From h to pu. *Physical Review B*, 26:4199–4228, October 1982. [17](#)
- [60] P. E. Blöchl. Projector augmented-wave method. *Physical Review B*, 50:17953–17979, December 1994. [18](#)
- [61] Michael Springborg. *Methods of Electronic-Structure Calculations: From Molecules to Solids*. John Wiley & Sons Ltd., 2000. [19](#)
- [62] Alex Zunger, S.-H. Wei, L. G. Ferreira, and James E. Bernard. Special quasirandom structures. *Physical Review Letters*, 65:353–356, July 1990. [21](#), [22](#), [51](#)

- [63] S.-H. Wei, L. G. Ferreira, James E. Bernard, and Alex Zunger. Electronic properties of random alloys: Special quasirandom structures. *Physical Review B*, 42:9622–9649, November 1990. [21](#)
- [64] Z. W. Lu, S.-H. Wei, and Alex Zunger. Large lattice-relaxation-induced electronic level shifts in random $\text{Cu}_{1-x}\text{Pd}_x$ alloys. *Physical Review B*, 44:3387–3390, August 1991. [21](#)
- [65] Z. W. Lu, S.-H. Wei, and Alex Zunger. Electronic structure of ordered and disordered Cu_3Au and Cu_3Pd . *Physical Review B*, 45:10314–10330, May 1992. [21](#), [22](#)
- [66] A. V. Ruban, S. I. Simak, S. Shallcross, and H. L. Skriver. Local lattice relaxations in random metallic alloys: Effective tetrahedron model and supercell approach. *Physical Review B*, 67:214302, June 2003. [21](#)
- [67] P. A. Korzhavyi, A. V. Ruban, A. Y. Lozovoi, Yu. Kh. Vekilov, I. A. Abrikosov, and B. Johansson. Constitutional and thermal point defects in $b2$ nial. *Physical Review B*, 61:6003–6018, March 2000. [23](#)
- [68] E. Flage-Larsen. Charge carrier passivating nitrogen–phosphorus defects in crystalline silicon. *Computational Materials Science*, 98(0):220–225, 2015. [23](#)
- [69] C. L. Fu, Y.-Y. Ye, M. H. Yoo, and K. M. Ho. Equilibrium point defects in intermetallics with the $B2$ structure: Nial and feal. *Physical Review B*, 48:6712–6715, September 1993. [23](#)
- [70] A.Yu. Lozovoi, K.V. Ponomarev, Yu.Kh. Vekilov, P.A. Korzhavyi, and I.A. Abrikosov. First-principles investigation of thermal point defects in $b2$ nial. *Physics of the Solid State*, 41(9):1494–1499, 1999. [23](#), [51](#)
- [71] W. Frank, C. Elsässer, and M. Fähnle. Ab initio force-constant method for phonon dispersions in alkali metals. *Physical Review Letters*, 74:1791–1794, March 1995. [24](#)
- [72] G J Ackland, M C Warren, and S J Clark. Practical methods in ab initio lattice dynamics. *Journal of Physics: Condensed Matter*, 9(37):7861, 1997. [24](#)
- [73] P.K. Kofstad. *Nonstoichiometry, Diffusion and Electrical Conductivity in Binary Metal Oxides (Science and Technology of Materials)*. John Wiley and Sons Inc, 1972. [24](#)
- [74] F. A. KRÖGER. *The chemistry of imperfect crystals*. North Holland publishing Company, Amsterdam, 1964. [24](#)
- [75] G. Boureau, C. Giaconia, and R. Tétot. Defect modelling in non-stoichiometric oxides. *Solid State Ionics*, 101-103(Part 1):397 – 401, 1997. [24](#)
- [76] Elisabetta Pizzi. *Influence de la pression partielle d'oxygene sur les concentrations en défauts et sur la diffusion de l'oxygene dans l'UO2+x*. Ph.d. thesis, École centrale des arts et manufactures « école centrale paris », 2013. [24](#)
- [77] N. Saunders and A.P. Miodownik. In N. Saunders and A.P. Miodownik, editors, *CALPHAD Calculation of Phase Diagrams A Comprehensive Guide*, volume 1 of *Pergamon Materials Series*, pages 1–479. Pergamon, 1998. [26](#), [38](#), [46](#), [48](#)

- [78] Hans Lukas, Suzana G. Fries, and Bo Sundman. *Computational thermodynamics : the Calphad method*. Cambridge university press Cambridge, 2007. 26, 29, 34
- [79] P.J. Spencer. A brief history of {CALPHAD}. *Calphad - Computer Coupling of Phase Diagrams and Thermochemistry*, 32(1):1–8, 2008. 26, 74
- [80] Matvei Zinkevich. *Computational Thermodynamics : Learning Doing and Using*. MaxPlanck-Institut für Metallforschung, Germany, 2003. 28, 29
- [81] A.R. Miedema, P.F. de Châtel, and F.R. de Boer. Cohesion in alloys — fundamentals of a semi-empirical model. *Physica B+C*, 100(1):1–28, 1980. 30
- [82] D. De Fontaine. Configurational thermodynamics of solid solutions. In Frederick Seitz Henry Ehrenreich and David Turnbull, editors, *Solid State Physics*, volume 34 of *Solid State Physics*, pages 73–274. Academic Press, 1979. 30
- [83] D. Gratias, J.M. Sanchez, and D. De Fontaine. Application of group theory to the calculation of the configurational entropy in the cluster variation method. *Physica A: Statistical Mechanics and its Applications*, 113(1):315–337, 1982.
- [84] Ryoichi Kikuchi and Didier de Fontaine. Theoretical calculation of phase diagrams using the cluster variation method. In G. C. Carter, editor, *Application of Phase Diagrams in Metallurgy and Ceramics*, pages 967–998. National Bureau of Standards, Gaithersburg, Maryland, 1978.
- [85] Ryoichi Kikuchi. A theory of cooperative phenomena. *Physical Review*, 81:988–1003, March 1951. 30
- [86] A. Walle and G. Ceder. Automating first-principles phase diagram calculations. *Journal of Phase Equilibria*, 23(4):348–359, 2002. 30
- [87] W. Cao, S.-L. Chen, F. Zhang, K. Wu, Y. Yang, Y.A. Chang, R. Schmid-Fetzer, and W.A. Oates. {PANDAT} software with panengine, panoptimizer and panprecipitation for multi-component phase diagram calculation and materials property simulation. *Calphad - Computer Coupling of Phase Diagrams and Thermochemistry*, 33(2):328–342, 2009. Tools for Computational Thermodynamics. 31, 32
- [88] S.-L. Chen, S. Daniel, F. Zhang, Y.A. Chang, X.-Y. Yan, F.-Y. Xie, R. Schmid-Fetzer, and W.A. Oates. The {PANDAT} software package and its applications. *Calphad - Computer Coupling of Phase Diagrams and Thermochemistry*, 26(2):175–188, 2002. 31, 32
- [89] C.W. Bale, P. Chartrand, S.A. Degterov, G. Eriksson, K. Hack, R. Ben Mahfoud, J. Melançon, A.D. Pelton, and S. Petersen. Factsage thermochemical software and databases. *Calphad - Computer Coupling of Phase Diagrams and Thermochemistry*, 26(2):189–228, 2002. 31, 32
- [90] RH Davies, AT Dinsdale, JA Gisby, JAJ Robinson, and SM Martin. {MTDATA} - thermodynamic and phase equilibrium software from the national physical laboratory. *Calphad - Computer Coupling of Phase Diagrams and Thermochemistry*, 26(2):229–271, 2002. 31

- [91] K.C. Hari Kumar and P. Wollants. Some guidelines for thermodynamic optimisation of phase diagrams. *Journal of Alloys and Compounds*, 320(2):189–198, 2001. Materials Constitution and Thermochemistry. Examples of Methods, Measurements and Applications. In Memoriam Alan Prince. 31, 34
- [92] R. Schmid-Fetzer, D. Andersson, P.Y. Chevalier, L. Eleno, O. Fabrichnaya, U.R. Kattner, B. Sundman, C. Wang, A. Watson, L. Zabdyr, and M. Zinkevich. Assessment techniques, database design and software facilities for thermodynamics and diffusion. *Calphad - Computer Coupling of Phase Diagrams and Thermochemistry*, 31(1):38–52, 2007. 31
- [93] Ursula R. Kattner, Gunnar Eriksson, Iris Hahn, Rainer Schmid-Fetzer, Bosse Sundman, Varghese Swamy, Armin Kussmaul, Philip J. Spencer, Tim J. Anderson, Tim G. Chart, André Costa da Silva, Bo Jansson, Byeong-Joo Lee, and Mikael Schalin. Joint Report from: Groups 4: Use of thermodynamic software in process modelling and Group 5: New applications of thermodynamic calculations. *Calphad: computer coupling of phase diagrams and thermochemistry*, 24(1):55–94, 2000. 31
- [94] Bo Sundman. *Scientific Group Thermodata Europe (SGTE) Solution Database Ver. 2*. Royal Institute of Technology, Stockholm, Sweden, 1994. 32
- [95] F. Sommer. Influence of associate formation in alloy-melts on the thermodynamic quantities. *Calphad - Computer Coupling of Phase Diagrams and Thermochemistry*, 2(4):319–324, 1978. 33
- [96] G Inden and Meyer W O. Approximate determination of the curie temperatures of bcc fe-co alloys. *Zeitschrift fuer Metallkunde*, 66(12):725–727, 1975. 33
- [97] Kenneth S. Pitzer. Thermodynamics of electrolytes. i. theoretical basis and general equations. *The Journal of Physical Chemistry*, 77(2):268–277, 1973. 33
- [98] ML Kapoor, GM Mehrotra, and MG. Frohberg. Calculation of thermodynamic values and structural-properties of liquid binary silicate systems. *ARCHIV FUR DAS EISENHUTTENWESEN*, 45(10):663–669, 1974. 33
- [99] M. Temkin. Mixtures of fused salts as ionic solutions. *Acta Physicochim. URSS*, 20(4):411–420, 1945. 33, 43
- [100] M Hillert and LI. Staffansson. Regular-solution model for stoichiometric phases and ionic melts. *Acta Chemica Scandinavica*, 24(10):3618–3626, 1970. v, 33, 43, 46, 47
- [101] Yves M Muggianu, Michele Gambino, and JP. Bros. Enthalpies of formation of liquid alloys bismuth–gallium–tin at 723 k–choice of an analytical representation of integral and partial thermodynamic functions of mixing for this ternary–system. *Journal de Chimie Physique et de Physico-Chimie Biologique*, 72(1):83–88, 1975. 33
- [102] F. Kohler. Zur berechnung der thermodynamischen daten eines ternären systems aus den zugehörigen binären systemen. *Monatshefte für Chemie und verwandte Teile anderer Wissenschaften*, 91(4):738–740, 1960. 33
- [103] Otto Redlich and AT. Kister. Algebraic representation of thermodynamic properties and the classification of solutions. *Industrial and Engineering Chemistry*, 40(2):345–348, 1948. 33, 34, 41, 48, 60

- [104] Claude HP. Lupis. *Chemical thermodynamics of materials*. Elsevier Science Publishing Co., Inc., 1983. 34, 39
- [105] George Kaptay. A new equation for the temperature dependence of the excess gibbs energy of solution phases. *Calphad - Computer Coupling of Phase Diagrams and Thermochemistry*, 28(2):115–124, 2004. 34
- [106] G. Kaptay. A calphad-compatible method to calculate liquid/liquid interfacial energies in immiscible metallic systems. *Calphad - Computer Coupling of Phase Diagrams and Thermochemistry*, 32(2):338–352, 2008. 34
- [107] G. Kaptay. A unified model for the cohesive enthalpy, critical temperature, surface tension and volume thermal expansion coefficient of liquid metals of bcc, fcc and hcp crystals. *Materials Science and Engineering: A*, 495(1–2):19–26, 2008. Fifth International Conference on High Temperature Capillarity HTC-2007, Alicante, Spain. 34
- [108] Mats Hillert. Some properties of the compound energy model. *Calphad - Computer Coupling of Phase Diagrams and Thermochemistry*, 20(3):333–341, 1996. 35
- [109] Mats Hillert. The compound energy formalism. *Journal of Alloys and Compounds*, 320(2):161–176, 2001. Materials Constitution and Thermochemistry. Examples of Methods, Measurements and Applications. In Memoriam Alan Prince. 35
- [110] I Ansara, TG Chart, A Fernandez Guillermet, FH Hayes, UR Kattner, DG Pettifor, N Saunders, and K Zeng. Workshop on thermodynamic modelling of solutions and alloys: Schloß ringberg, march 10 to march 16, 1996. *Calphad - Computer Coupling of Phase Diagrams and Thermochemistry*, 21(2):171–218, 1997. 35
- [111] A.T. Dinsdale. Sgte data for pure elements. *Calphad - Computer Coupling of Phase Diagrams and Thermochemistry*, 15(4):317–425, 1991. 35, 60
- [112] F. D. Murnaghan. The compressibility of media under extreme pressures. *Proceedings of the National Academy of Sciences of the United States of America*, 30(9):244–247, 1944. 35
- [113] Mats Hillert and Magnus Jarl. A model for alloying in ferromagnetic metals. *Calphad - Computer Coupling of Phase Diagrams and Thermochemistry*, 2(3):227–238, 1978. 35
- [114] G. Inden. the project meeting calphad v. Technical report, max-planck inst., Eisenforsch. Düsseldorf, 21-25 june 1976. 35
- [115] G. Inden. The role of magnetism in the calculation of phase diagrams. *Physica B+C*, 103(1):82–100, 1981. 35
- [116] Göran Grimvall. Appendix f - heat capacity contributions in a real solid—an overview. In Göran Grimvall, editor, *Thermophysical Properties of Materials*, pages 367–368. Elsevier Science B.V., Amsterdam, 1999. 37, 42
- [117] Joel H. Hildebrand. Solubility. xii. regular solutions1. *Journal of the American Chemical Society*, 51(1):66–80, 1929. 37

- [118] Mats Hillert and Mats Waldenström. Isothermal sections of the fe-mn-c system in the temperature range 873k/2-1373k. *Calphad - Computer Coupling of Phase Diagrams and Thermochemistry*, 1(2):97–132, 1977. 43
- [119] Bo Sundman and John Ågren. A regular solution model for phases with several components and sublattices, suitable for computer applications. *Journal of Physics and Chemistry of Solids*, 42(4):297–301, January 1981. 43, 64, 77
- [120] Mats Hillert. *Phase equilibria, phase diagrams and phase transformations : their thermodynamic basis*. Cambridge University Press, 2007. v, 47
- [121] S.H. Whang, D.P. Pope, and C.T. Liu. *High Temperature Aluminides and Intermetallics*. Elsevier Science Ltd, 1993. 51
- [122] Aissam Hidoussi, Aissa Belgacem-Bouzida, Maria Helena Braga, and Haroun Righi. Theoretical investigation of defect structure in b2 trsc (tr= cd, ru) alloys. *Modern Physics Letters B*, 29(35n36):1550234, 2015. v, vii, 51, 53, 54, 55, 56, 59
- [123] C. McQuarrie, D.A. McQuarrie, P.A. Rock, and P. Depovere. *Chimie générale*. Chimie générale. De Boeck Supérieur, 2000. 51
- [124] A. Palenzona and P. Manfrinetti. The phase diagram of the sc-cd system. *Journal of Alloys and Compounds*, 237(1-2):121–123, 1996. 51, 55
- [125] Zhenmin Du, Zhenquan Jiang, and Changrong Li. Thermodynamic optimization of the ru-sc system. *Journal of Alloys and Compounds*, 427(1–2):148–152, 2007. 51, 58
- [126] Chao Jiang, Long-Qing Chen, and Zi-Kui Liu. First-principles study of constitutional and thermal point defects in {B2} pdin. *Intermetallics*, 14(3):248–254, 2006. 51
- [127] C. Jiang, M.F. Besser, D.J. Sordelet, and B. Gleeson. A combined first-principles and experimental study of the lattice site preference of pt in {B2} nial. *Acta Materialia*, 53(7):2101–2109, 2005. 51, 52
- [128] Tanmoy Ghosh, Ambika Prasad Jena, Biplab Sanyal, Hirosuke Sonomura, Takashi Fukuda, Tomoyuki Kakeshita, P.K. Mukhopadhyay, and Abhijit Mookerjee. Effect of short range ordering on the magnetism in disordered fe:al alloy. *Journal of Alloys and Compounds*, 613(0):306–311, 2014. 51
- [129] P. E. Blöchl. Projector augmented-wave method. *Physical Review B*, 50(24):17953–17979, December 1994. 52, 63, 76
- [130] G. Kresse and D. Joubert. From ultrasoft pseudopotentials to the projector augmented-wave method. *Physical Review B*, 59:1758–1775, January 1999. 52, 63, 76
- [131] Georg Kresse, Martijn Marsman, and Jurgen Furthmüller. *VASP the GUIDE*. University of Vienna, Vienna/Austria, June 1, 2012. 52, 53, 63, 76
- [132] Hendrik J. Monkhorst and James D. Pack. Special points for brillouin-zone integrations. *Physical Review B*, 13:5188–5192, June 1976. 52, 63, 76

- [133] B.Z. Yanchitsky and A.N. Timoshevskii. Determination of the space group and unit cell for a periodic solid. *Computer Physics Communications*, 139(2):235–242, 2001. [53](#)
- [134] N. Selhaoui and O.J. Kleppa. Standard enthalpies of formation of scandium alloys, sc-me (me=fe, co, ni, ru, rh, pd, ir, pt), by high-temperature calorimetry. *Journal of Alloys and Compounds*, 191(1):145–149, 1993. [54](#), [61](#), [67](#), [69](#)
- [135] V.N. Eremenko, V.G. Khorujaya, P.S. Martsenyuk, and K.Ye. Korniyenko. The scandium-ruthenium phase diagram. *Journal of Alloys and Compounds*, 217(2): 213–217, 1995. [55](#)
- [136] B. Meyer and M. Fähnle. Atomic defects in the ordered compound b2-nial: A combination of ab initio electron theory and statistical mechanics. *Physical Review B*, 59:6072–6082, March 1999. [57](#)
- [137] David R. Lide. *CRC handbook of chemistry and physics : a ready-reference book of chemical and physical data*. Taylor & Francis, Boca Raton [etc.], 2005. ISBN 9780849304866. [60](#)
- [138] G. Bayer and H.G. Wiedemann. Formation, dissociation and expansion behavior of platinum group metal oxides (pdo, ruo₂, iro₂). *Thermochimica Acta*, 11(1):79–88, 1975.
- [139] Francesco L. Bernardis, Richard A. Grant, and David C. Sherrington. A review of methods of separation of the platinum-group metals through their chloro-complexes. *Reactive and Functional Polymers*, 65(3):205–217, December 2005. [60](#)
- [140] M. L. Doyle and I. R. Harris. Palladium-rare earth alloys: Their order-disorder transformations and behaviour with hydrogen. *Platin. Met. Rev.*, 32(3):130–140, 1988. [60](#)
- [141] Yuantao Ning and Xin Hu. Strengthening platinum-palladium-rhodium alloys by ruthenium and cerium additions: effects on mechanical properties at room and high temperature. *Platin. Met. Rev.*, 47(3):111–119, 2003.
- [142] Aissam Hidoussi, Aissa Belgacem Bouzida, Fiseha Tesfaye, and Saïd Kardellass. Thermodynamic and ab-initio investigations of the os-th and os-y systems. In *TMS Annual Meeting & Exhibition, Nashville, TN, USA*, volume 145, 2016. [60](#), [62](#), [65](#), [67](#), [70](#)
- [143] L.L. Shrier, R.A. Jarman, and G. T. Burstein. *Corrosion (3rd Edition) Volumes 1-2*. Elsevier, 1994. [60](#)
- [144] J.R. Thomson. Alloys of thorium with certain transition metals II. The systems thorium-osmium, thorium-iridium and thorium-platinum. *Journal of the Less Common Metals*, 6(1):3–10, January 1964. [v](#), [60](#), [61](#), [62](#), [64](#), [67](#), [68](#), [69](#), [70](#)
- [145] H Kleykamp. Thermodynamische untersuchungen in den systemen Thorium-Osmium und Thorium-Iridium. *Journal of the Less Common Metals*, 63(1):P25–P33, January 1979. [v](#), [60](#), [61](#), [67](#), [68](#), [69](#), [70](#)
- [146] William. G. Moffatt. *The handbook of binary phase diagrams*. Schenectady, N.Y. : General Electric, 1981. [61](#)

- [147] T. B. Massalski. *Binary alloy phase diagrams*, volume 3. Materials Information Soc, Materials Park, Ohio, second edition, 1990. 61, 64, 70
- [148] V. A. Finkel, M. I. Palatnik, and G. P. Kovtun, 1971. translated into English in *Phys. Met. Metallogr.*, 1972, 32, (1), 231. 61, 62
- [149] A. E. Dwight. *Trans. Am. Soc. Met.*, 53:479–500, 1961. 61, 62
- [150] J.R. Thomson. Alloys of thorium with certain transition metals V. The ThOs₂-ThIr₂ pseudo-binary system and some additional results on the thorium-iridium system. *Journal of the Less Common Metals*, 27(3):293–296, June 1972. 62
- [151] J.R. Thomson. Some New Intermetallic Compounds of Thorium of the Type Th₇X₃. *Nature*, 189(4760):217–217, January 1961. 62, 70
- [152] D.S. Evans and G.V. Raynor. The lattice spacing of thorium, with reference to contamination. *Journal of Nuclear Materials*, 1(3):281–288, October 1959. 62
- [153] P. Chiotti, V. V. Akhachinskij, I. Ansara, and M. H. Rand. The Os-Th (Osmium–Thorium) system. *Bulletin of Alloy Phase Diagrams*, 3(1):101–102, June 1982. v, 61, 62, 67, 69
- [154] V. B. Compton and B. T. Matthias. Laves phase compounds of rare earths and hafnium with noble metals. *Acta Crystallographica*, 12(9):651–654, September 1959. 61, 62
- [155] A Palenzona. The crystal structure of the rare-earth-rich osmium compounds R₃O_s and Y₃O_s. *Journal of the Less Common Metals*, 72(1):P21–P24, July 1980. 62
- [156] R. Sanjines-Zeballos, B. Chabot, and E. Parthé. Rare earth-osmium compounds R₃O_s and Y₃Ru, Y₃O_s and Y₃Pd with the Fe₃C structure. *Journal of the Less Common Metals*, 72(1):P17–P20, July 1980. 62
- [157] F. H. Spedding, A. H. Daane, and K. W. Herrmann. The crystal structures and lattice parameters of high-purity scandium, yttrium and the rare earth metals. *Acta Crystallographica*, 9(7):559–563, July 1956. 61, 62, 75
- [158] E.M. Savitskii and V.P. Polyakova. Physico-chemical research in noble metals. *Journal of the Less Common Metals*, 43(1-2):169–177, November 1975. v, 61, 67, 69, 70
- [159] G. Kresse. Efficient iterative schemes for ab initio total-energy calculations using a plane-wave basis set. *Physical Review B*, 54(16):11169–11186, October 1996. 63, 74
- [160] G. Kresse and J. Furthmüller. Efficiency of ab-initio total energy calculations for metals and semiconductors using a plane-wave basis set. *Computational Materials Science*, 6(1):15–50, 1996. 63, 74
- [161] Karlheinz Schwarz and Peter Blaha. Solid state calculations using WIEN2k. *Computational Materials Science*, 28(2):259–273, October 2003. 63
- [162] Atsushi Togo, Fumiyasu Oba, and Isao Tanaka. First-principles calculations of the ferroelastic transition between rutile-type and CaCl₂-type SiO₂ at high pressures. *Physical Review B*, 78(13):134106, October 2008. 63

- [163] K. Parlinski, Z. Li, and Y. Kawazoe. First-Principles Determination of the Soft Mode in Cubic ZrO₂. *Physical Review Letters*, 78(21):4063–4066, May 1997. 63
- [164] John P. Perdew and Yue Wang. Accurate and simple analytic representation of the electron-gas correlation energy. *Physical Review B*, 45(23):13244–13249, June 1992. 63
- [165] E Sjöstedt, L Nordström, and D.J Singh. An alternative way of linearizing the augmented plane-wave method. *Solid State Communications*, 114(1):15–20, March 2000. 63
- [166] Y. Wang, S. Curtarolo, C. Jiang, R. Arroyave, T. Wang, G. Ceder, L.-Q. Chen, and Z.-K. Liu. Ab initio lattice stability in comparison with CALPHAD lattice stability. *Calphad - Computer Coupling of Phase Diagrams and Thermochemistry*, 28(1):79–90, March 2004. 63
- [167] P. Blaha, K. Schwarz, K. H.G. Madsen, D. Kvasnicka, and J. Luitz. *WIEN2k An Augmented Plane Wave + Local Orbitals Program for Calculating Crystal Properties*. Vienna University of Technology, Vienna/Austria, 2012. 64
- [168] Peter E. Blöchl. Improved tetrahedron method for Brillouin-zone integrations. *Physical Review B*, 49(23):16223–16233, June 1994. 64
- [169] Ali H. Reshak and Morteza Jamal. Calculation of the lattice constant of hexagonal compounds with two dimensional search of equation of state and with semilocal functionals a new package (2D-optimize). *Journal of Alloys and Compounds*, 555:362–366, April 2013. 64
- [170] Francis Birch. Finite Elastic Strain of Cubic Crystals. *Physical Review*, 71(11):809–824, June 1947. 64
- [171] J.-M. Moreau, D. Paccard, and E. Parthé. The tetragonal crystal structure of R₃Rh₂ compounds with R = Gd, Tb, Dy, Ho, Er, Y. *Acta Crystallographica Section B*, 32(6):1767–1771, Jun 1976. doi: 10.1107/S0567740876006365. URL <https://doi.org/10.1107/S0567740876006365>. 65
- [172] A. Iandelli and A. Palenzona. The crystal structure of the intermetallic compound Eu₃Pd₂. *Journal of the Less Common Metals*, 40(2):263–264, April 1975. 65
- [173] J. M. Moreau, D. Paccard, and E. Parthé. The monoclinic, CrB-related, crystal structure of Tb₃Ni₂, Dy₃Ni₂ and Ho₃Ni₂. *Acta Crystallographica Section B Structural Crystallography and Crystal Chemistry*, 30(11):2583–2586, November 1974. 65, 75
- [174] N.J. Clark and E. Wu. Hydrogen absorption in the Zr-Al system. *Journal of the Less Common Metals*, 163(2):227–243, October 1990. 65
- [175] K.H.J. Buschow. Rare earth-aluminium intermetallic compounds of the form RAl and R₃Al₂. *Journal of the Less Common Metals*, 8(3):209–212, March 1965. 65
- [176] T. Miyadai, H. Mori, T. Oguchi, Y. Tazuke, H. Amitsuka, T. Kuwai, and Y. Miyako. Magnetic and electrical properties of the U-Si system (part II). *Journal of Magnetism and Magnetic Materials*, 104-107:47–48, February 1992. 65

- [177] Ph. Durussel, R. Massara, and P. Feschotte. Le système binaire Pt-Sn. *Journal of Alloys and Compounds*, 215(1-2):175–179, November 1994. 65
- [178] Ingvar Engström and Hans-Ulrich Pfeifer. The Crystal Structure of Pt₂Ge₃. *Acta Chemica Scandinavica*, 22:3137–3145, 1968. 65
- [179] H. Sawada. Residual electron density study of α -aluminum oxide through refinement of experimental atomic scattering factors. *Materials Research Bulletin*, 29(2): 127–133, February 1994. 65
- [180] C. Boulesteix, P. E. Caro, M. Gasgnier, Ch. Henry la Blanchetais, B. Pardo, and G. Schiffmacher. La structure cubique C des sesquioxides de terres rares. Diagrammes de diffraction électronique et groupe d'espace. *Physica Status Solidi (a)*, 23(2):597–604, June 1974. 65
- [181] S. Heinrich and K. Schubert. Kristallstruktur von Pt₃Ge₂. *Journal of the Less Common Metals*, 45(1):125–135, February 1976. 65
- [182] J.H.N. Van Vucht and K.H.J. Buschow. The crystal structure of La₂Ni₃. *Journal of the Less Common Metals*, 46(1):133–138, April 1976. 65
- [183] Shigeru Okada, Tetsuzo Atoda, and Iwami Higashi. Structural investigation of cr₂b₃, cr₃b₄, and crb by single-crystal diffractometry. *Journal of Solid State Chemistry*, 68(1):61 – 67, 1987. ISSN 0022-4596. doi: [https://doi.org/10.1016/0022-4596\(87\)90285-4](https://doi.org/10.1016/0022-4596(87)90285-4). URL <http://www.sciencedirect.com/science/article/pii/0022459687902854>. 65
- [184] S. Bhan and K. Schubert. Über die struktur von phasen mit kupfer unterstruktur in einigen t-b legierungen (T= Ni, Pd, Pt; B = Ga, In, Tl, Pb, Sb, Bi). *Journal of the Less Common Metals*, 17(1):73–90, January 1969. 65
- [185] F.R. de Boer, R. Boom, W.C.M. Mattens, A.R. Miedema, and A.K. Niessen. *Cohesion in metals : transition metal alloys*. North-Holland, Amsterdam, 1988. 67, 69
- [186] P.C.M. Gubbens, A.M. Kraan, and K.H.J. Buschow. Magnetic properties of rare earth-transition metal compounds. *Hyperfine Interactions*, 53(1-4):37–57, 1990. 74
- [187] Alex Goldman. Hmaterials for permanent magnet applications. In *Handbook of Modern Ferromagnetic Materials*, volume 505 of *The Springer International Series in Engineering and Computer Science*, pages 75–106. Springer US, 1999. 74
- [188] A. Szytula and J. Leciejewicz. *Handbook of Crystal Structures and Magnetic Properties of Rare Earth Intermetallics*. CRC Press, Boca Raton, 1994. 74
- [189] T. Sakai, M. Matsuoka, and C. Iwakura. Chapter 142 Rare earth intermetallics for metal-hydrogen batteries. In Jr. Karl A. Gschneidner and LeRoy Eyring, editors, *Handbook on the Physics and Chemistry of Rare Earths*, volume 21 of *Handbook on the Physics and Chemistry of Rare Earths*, pages 133–178. Elsevier, 1995. 74
- [190] A. Saccone, S. Delfino, A.M. Cardinale, and R. Ferro. The Dy-Zn phase diagram. *Metallurgical and Materials Transactions A*, 34(3):743–750, 2003. vi, 74, 75, 77, 78, 79

- [191] H. Okamoto. Dy-Zn (Dysprosium-Zinc). *Journal of Phase Equilibria and Diffusion*, 28(5):492–493, 2007. 74, 79
- [192] G. Bruzzone, M.L. Fornasini, and F. Merlo. Rare-earth intermediate phases with zinc. *Journal of the Less Common Metals*, 22(3):253–264, 1970. 74, 75
- [193] V.N. Eremenko, M.V. Bulanova, and P.S. Martsenjuk. The dysprosium-tin phase diagram. *Journal of Alloys and Compounds*, 189(2):229–233, 1992. 75
- [194] J.J. Bara, A.T. Pedziwiatr, and W. Zarek. Investigations of crystal and magnetic properties of Dy-Fe intermetallic compounds. *Journal of Magnetism and Magnetic Materials*, 27(2):168–174, 1982. 75
- [195] Hana Krizek and K.N.R. Taylor. Crystal structure of lanthanum-dysprosium alloys. *Journal of the Less Common Metals*, 38(2–3):263–265, 1974. 75
- [196] D Chatterjee and K N R Taylor. Magnetic and structural properties of the neodymium-dysprosium alloy system. *Journal of Physics F: Metal Physics*, 2(1):151, 1972. 75
- [197] F.H. Spedding, B. Sanden, and B.J. Beaudry. The Er-Y, Tb-Ho, Tb-Er, Dy-Ho, Dy-Er and Ho-Er phase systems. *Journal of the Less Common Metals*, 31(1):1–13, 1973. 75
- [198] R. Wang. Formation of metastable low temperature allotropic solid solutions in rare earth-zirconium systems. *Metallurgical Transactions*, 3(5):1213–1221, 1972. 75
- [199] I.R. Harris and G.V. Raynor. Some observations on the crystal structures of the rare-earth metals and alloys. *Journal of the Less Common Metals*, 17(3):336–339, 1969. 75
- [200] F. J. Darnell and E. P. Moore. Crystal structure of dysprosium at low temperatures. *Journal of Applied Physics*, 34(4):1337–1338, 1963. 75
- [201] A. B. Bouzida, Benhafid R., and A. Hidoussi. Ab-initio calculations and calphad approach for the assessment of the dy-znsystem. In *Poster presented at 40 conference on phase equilibria JEEP2014, 2014, Universite Claude Bernard Lyon 1, Villeurbanne, France, 2014.* 75, 76, 77, 79
- [202] J.W. Herchenroeder, P. Manfrinetti, and K.A. Gschneidner. Physical metallurgy of metastable bcc lanthanide-magnesium alloys for R = La, Gd, and Dy. *Metallurgical Transactions A*, 20(9):1575–1583, 1989. 75
- [203] C. C. Chao, H. L. Luo, and P. Duwez. CsCl-Type Compounds in Binary Alloys of Rare-Earth Metals with Zinc and Copper. *Journal of Applied Physics*, 35(1):257–258, 1964. 75
- [204] A. Iandelli and A. Palenzona. Atomic size of rare earths in intermetallic compounds. MX compounds of CsCl type. *Journal of the Less Common Metals*, 9(1):1–6, 1965. 75
- [205] E. Laube and J.B. Kusma. Über einige Y-und Dy-haltige Legierungsphasen. *Monatshefte für Chemie und verwandte Teile anderer Wissenschaften*, 95(6):1504–1513, 1964. 75

- [206] M. Ohashi, T. Kitai, T. Kaneko, H. Yoshida, Y. Yamaguchi, and S. Abe. Neutron diffraction study of magnetic transition in DyZn₂. *Journal of Magnetism and Magnetic Materials*, 90–91(0):585–586, 1990. 75
- [207] D. J. Michel and E. Ryba. The crystal structure of HoZn₃. *Acta Crystallographica Section B*, 24(9):1267–1269, September 1968. 75
- [208] A. Iandelli and A. Palenzona. Zinc-rich phases of the rare-earth-zinc alloys. *Journal of the Less Common Metals*, 12(5):333–343, 1967. 75
- [209] T. Siegrist and Y. Le Page. Crystal chemistry of some Th₂Zn₁₇-type rare-earth-zinc phases. *Journal of the Less Common Metals*, 127(0):189–197, 1987. 75
- [210] M. Olivier, T. Siegrist, and S.P. McAlister. Magnetic susceptibility and electrical resistivity of some Th₂Zn₁₇-type rare-earth zinc phases. *Journal of Magnetism and Magnetic Materials*, 66(2):281–290, 1987. 75
- [211] E. Laube. Strukturen von neuen SE-Verbindungen, 1. Mitt. *Monatshefte für Chemie und verwandte Teile anderer Wissenschaften*, 97(3):722–732, 1966. 75
- [212] S. Popović, B. Gržeta, V. Ilakovac, R. Kroggel, G. Wendrock, and H. Löffler. Lattice constant of the F.C.C. Al-rich α -Phase of Al-Zn alloys in equilibrium with GP zones and the β (Zn)-Phase. *physica status solidi (a)*, 130(2):273–292, 1992. 75
- [213] R.W. Lynch and H.G. Drickamer. The effect of pressure on the resistance and lattice parameters of cadmium and zinc. *Journal of Physics and Chemistry of Solids*, 26(1):63–68, 1965. 75
- [214] R.A. Farrar and H.W. King. Axial ratios and solubility limits of H.C.P. η and ϵ phases in the systems Cd-Mn and Zn-Mn. *Metallography*, 3(1):61–70, 1970. 75
- [215] R.A. Farrar and H.W. King. Axial ratios and solubility limits of H.C.P. η phases in the systems Cd-Au, Cd-Li, and Zn-Li. *Metallography*, 1(1):79–90, 1968. 75
- [216] E A Owen and D A Davies. An x-ray study of the mutual solid solubilities of zinc and cadmium. *British Journal of Applied Physics*, 16(9):1291, 1965. 75
- [217] D A Davies and E A Owen. An x-ray investigation on the solid solutions of certain elements in zinc. *British Journal of Applied Physics*, 15(11):1309, 1964. 75
- [218] Zhijun Zhu and Arthur D. Pelton. Critical assessment and optimization of phase diagrams and thermodynamic properties of re–zn systems – part {II} – y–zn, eu–zn, gd–zn, tb–zn, dy–zn, ho–zn, er–zn, tm–zn, yb–zn and lu–zn. *Journal of Alloys and Compounds*, 641:261–271, 2015. 76, 77

Appendix A

List of acronyms

CALPHAD CALculation of PHase Diagram. v, 4, 5, 26, 28, 29, 32, 34, 36, 49, 60, 64, 67, 69, 73, 81, 82

CG Conjugated Gradient. 63

CVM Cluster Variation Method. 30

DFT Density Functional Theory. 1, 5, 7, 12, 15, 20, 21, 30, 63, 73, 82

DGM Driving force per mole component. 27, 28

DTA Thermomechanical Analysis. 29

EMF Electromotive Force Measurements. 30, 60, 67, 69

EPMA Electron Probe Micro Analysis. 29

FP-(L)APW+lo Full-Potential (Linearized) Augmented Plane Wave plus local orbitals. 64

FP-LAPW Full-Potential Linearized Augmented Plane Wave. 63, 69

GGA Generalized Gradient Approximation. 4, 14, 15, 101

GGA-PBE Generalized Gradient Approximation as implemented by [54]. 61–64, 67

KTH Royal Institute of Technology in Stockholm. 32

LDA Local Density Functional. 4, 14, 67, 101

LDA-CA Local Density Approximation refined by [50]. 61–63, 65

MSR1a Multi Secant Rank One A. 64

PAW Projected-Augmented Wave. 18, 19, 63, 69

PES potential energy surface. 8

PGM Platinum-Group Metals. 60

RE Rare earths. v, 2–4

REM Rare Earth Metals. 60

SCF Self Consistent Field. ii, 6, 8, 9

SEM Scanning Electron Microscopy. 29

SER Stable Element Reference. 21, 35, 36, 42, 63

SGTE Scientific Group Thermodata Europe. 32, 35

SM Solution Model. 60

SOM Scanning Optical Microscopy. 29

SQS Special Quasirandom Structure. 4, 5, 21, 22, 51, 52

STA Simple Thermal Analysis. 29

TDB Thermo DataBase. 33

TEM Transmission Electron Microscopy. 29

TM Transition metal. 2–5

TSM Two Sublattices Model. 60

US-PP Ultra Soft Pseudo Potential. 63

VASP Vienna Ab initio Simulation Package. iii, 50, 61–63, 65, 67, 69

Appendix B

Glossary

Ab Initio The term ab initio was first used in quantum chemistry by Robert Parr and coworkers, including David Craig in a semiempirical study on the excited states of benzene. In its modern meaning ('from first principles of quantum mechanics') the term was used by Chen (when quoting an unpublished 1955 MIT report by Allen and Nesbet), https://en.wikipedia.org/wiki/Ab_initio_quantum_chemistry_methods. 2, 4, 5, 7, 8, 21, 28, 30, 60, 69

Factsage is a set of thermochemical software and database developed jointly by Thermfact / CRCT (Montreal, Canada) www.crct.polymtl.ca and GTT-Technologies (Aachen, Germany) www.gtt-technologies.de. 31, 32

MTDATA Phase Diagram Software from the National Physical Laboratory. 31, 34, 81

Pandat an integrated calculation tool developed on the basis of the gls calphad approach for property simulation and phase diagram calculation of multi-component materials. It has a robust thermodynamic calculation engine, a user-friendly graphical user interface, and a flexible post-calculation table editing function that allows the user to plot types of variety diagrams. The software is designed to create a working environment that allows various computing modules integrated into the same work area. It currently consists of three modules: PanPhaseDiagram (phase diagram and calculation of thermodynamic properties), Pan Precipitations (Precipitation simulation) and PanOptimizer (property optimization). 31, 32, 34, 81

PARROT Parameter optimizations. 4, 33, 64, 76

Phonopy Phonopy is an open source package for phonon calculations at harmonic and quasi-harmonic levels.. 63, 65

POLY Equilibrium Calculations. 33, 34

POST Processing of various phase diagrams (module du logiciel Thermo-Calc). 33

Thermo-Calc is a product that is used by customers around the world in academia, government and industry to make calculations that predict or help to understand complex multicomponent alloys and nonmetallic systems, as well as relevance processes Industrial and scientific. v, 4, 31–35, 64, 76, 81, 100

WIEN2k program package allows to perform electronic structure calculations of solids using density functional theory (DFT). iii, 50, 61–64, 67, 69

Appendix C

List of symbols

- a_i Activity of the specie i , $a_i = \exp[\mu_i / (R \times T)]$. 30, 42
- α Alpha spin function. 9, 10, 103
- a^s The site fraction corresponding to the sub-lattice s . 45, 46, 48
- β_0 Average magnetic moment per atom. 35, 37, 38
- β Beta spin function. 9, 10, 103
- c The number of species. 44, 45
- C_p Heat capacity at constant pressure. 30, 37, 42
- E The average energy. 8, 10–13
- E_0 The smallest eigenvalue of the Hamiltonian. 8
- E_H Hartree Energy. 13
- ϵ_{xc} The exchange and correlation energy of a free electron gas. 14
- E_{xc} The exchange and correlation energy and the difference between the kinetic energy of the independent Kohn-Sham electrons and that of the real system. 13
- E_{xc}^{GGA} The exchange and correlation energy in the approximation GGA. 15
- E_{xc}^{LDA} The exchange and correlation energy in the approximation LDA. 14
- F An universal functional independent of the external potential which makes it possible to obtain the energy of the system from the density $n_0(r)$. 12, 13
- G Gibbs Free Energy. v, 26–30, 32–43, 45–49, 101, 102
- ${}^0G_{ms}^\Phi$ The Gibbs free energy of one mole of sites of the phase Φ . 45, 48
- GES Gibbs Energy System. 32, 33
- ${}^{ex}G^\Phi$ Excess free enthalpy of mixing. 37, 45, 47, 48
- ${}^{id}G^\Phi$ Ideal mixing free enthalpy. 37, 38, 45, 46, 49

${}^{ref}G^{\Phi}$ Free Enthalpy Reference of phase Φ . 37, 45–47, 49

H Formation Enthalpy. 30, 33, 35, 37, 40, 42

\hat{H} The Hamiltonian of the system. 7, 8, 10–12, 18

H_p Partial Enthalpy. 30

k Wave Vector. 15, 16

k_b The Boltzmann constant. 45, 46

m Electronic spin variable. 8

μ_i Chemical potential of component i . 30

N The number of electrons. 12, 13

n_0 The charge density of the ground state. 12, 101

N_{av} Avogadro's number. 40

n_i^s The number of species i of sub-lattice s . 44–46

n The total number of moles in the phase. 27, 33, 34, 36, 44–46, 102

n_i The number of moles of elements i . 27, 33, 34, 36, 44, 45

n_j The number of moles of elements j . 44

n_p The total number of phases in the system. 36

n The charge density. 12–15

n^s The total number of sites in the sublattice s . 44–46

n_{va}^s The total number of vacancies sites in the sub-lattice s . 44

ω_p The total number of possible arrangements on all sites. 45

P Pressure. 26, 27, 33, 34, 37

v_{eff} Effective Potential. 13

v_{ext} External potential. 12, 13

Φ Phase : liquide, fcc_A1 , bcc_A2 , hcp_A3 , ... v, 35–39, 41, 42, 45–49, 101–103

v_{KS} Kohn-Sham potential. 13, 15

ψ The wave function. 7–13, 15, 16, 18, 19

$\tilde{\psi}$ The pseudo-wave function. 18, 19

q Refers to the total number of sublattices. 45, 46, 48

- r Position vector of electron. 7–16, 101
- R Perfect gas constant. 35, 39, 41, 42, 46, 48
- R Position vector of nucleus. 7, 8, 11, 15, 16
- S Entropy. 26, 33, 45, 46
- s Refers to the sublattice s . 44–46, 48, 101–103
- ξ Variable of spin function (α or β). 9
- T Thermodynamic temperature, such as : $T(\text{K}) = \theta(^{\circ}\text{C}) + 273.15^{\circ}\text{C}$ where $\theta(^{\circ}\text{C})$ being the Celsius scale. 26, 27, 33–35, 37, 39, 41–43, 46, 48
- \hat{T}_N Kinetic energy of ions. 7, 8
- τ Curie temperature T_C for the ferromagnetic phases bcc_A2 and Neel temperature T_N for the phases fcc_A1 . 35
- T_C Curie temperature. 35, 37
- \hat{T}_e Kinetic energy of electrons. 7, 8, 12
- T^* The critical magnetic temperature. 35
- T_N Neel temperature. 35, 37
- T The kinetic energy of Kohn-Sham electrons. 13
- U Internal Energy. 26
- V Volume. 26
- Va Vacancy site. 44, 45, 48, 102, 103
- \hat{V}_{e-e} The electron-electron coulomb interaction. 7, 8, 12
- \hat{V}_{e-N} The Coulomb electron-nucleus interaction. 7, 8
- \hat{V}_{N-N} The Coulomb interaction Nucleus-Nucleus. 7, 8
- v_{xc} The potential of exchange and correlation. 13
- x Mole fraction of component B in the binary phase diagrams. 37–39, 41, 44, 45, 103
- x_i Mole fraction of component i . 38, 39, 41, 44
- $x_i^{\bar{\Phi}}$ The molar fraction of the element i in the phase $\bar{\Phi}$. 45
- y Fraction of sites. 44–48, 103
- y_i^s Fraction of sites of the species i of the sub-lattice s . 44–46, 48
- y_{Va}^s The total fraction of vacancies sites in the sub-lattice s . 44, 45, 48
- Z Atomic number. 8, 10, 11